REPORT DOCUMENTATION PAGE

Form Approved
OMB No. 0704-0188

1. AGENCY USE ONLY (Leave blank)	2. REPORT DATE	3. REPORT TYPE AND DATES COVERED
	June 1996	Final, 1 April 95 – 1 April 96

4. TITLE AND SUBTITLE
The Effect of Solid Propellant Binder on the Formation and Evolution of Aluminum Combustion Products

5. FUNDING NUMBERS
PE – 61102F
PR – 2508
SA – AS
G – AFOSR-95
   –1-0268

6. AUTHOR(S)
V.E. Zarko, O. G. Glotov, V. V. Karasev, M. W. Beckstead

7. PERFORMING ORGANIZATION NAME(S) AND ADDRESS(ES)
Brigham Young University
Provo, Utah, U.S.A.
and
Institute of Chemical Kinetics and Combustion
Russian Academy of Sciences, Novosibirsk, 630090, Russia

AFOSR-TR-96

0392

9. SPONSORING/MONITORING AGENCY NAME(S) AND ADDRESS(ES)
AFOSR/NA
110 Duncan Avenue Suite B115
Bolling AFB Washington DC 20332-0001

NA

10. SPONSORING/MONITORING AGENCY REPORT NUMBER
95-1-0268

19960726 025

11. SUPPLEMENTARY NOTES

12a. DISTRIBUTION/AVAILABILITY STATEMENT
Approved for public release; distribution is unlimited

13. ABSTRACT (Maximum 200 words)

Novel particle collection and high speed photography techniques have been used to study the combustion behavior of an inert binder (IB) propellant and an energetic binder (EB) propellant. Both contained 18% aluminum and 37% coarse AP in order to provide very similar geometrical structures, and both propellants had essentially common burning rates. The aluminum combustion efficiency is higher and the characteristic agglomerate size is significantly smaller for the EB propellant than for the IB propellant (at 43 atm the agglomerate size, D_{43}, was 190 μm for the EB propellant and 670 μm for the IB propellant). At 7.5 atm the characteristic roughness of the burning surface is about 300 μm for the EB propellant and about 800 μm for the IB propellant. X-ray photography and visual observations of quenching particles show that similar sized agglomerates can differ significantly in structure and aluminum content, and there is some indication of internal voids (i.e. low density). This appears to be a result of the different initial conditions that the agglomerates are exposed to when they inially form at the surface. The size distribution of fine oxide particles was not dependent on either pressure or the propellant binder (or on the size of agglomerates). The fine particle mass size distribution (i.e. the smoke) was observed to have 3 modal sizes, ~1, 3.5, and 7 μm.

14. SUBJECT TERMS Solid propellant combustion, energetic binder, aluminum, agglomeration, condensed combustion products, aluminum oxide, quenching, sampling, particle size distribution, aluminum combustion efficiency, high speed photography.

15. NUMBER OF PAGES
81

16. PRICE CODE

17. SECURITY CLASSIFICATION OF REPORT	18. SECURITY CLASSIFICATION OF THIS PAGE	19. SECURITY CLASSIFICATION OF ABSTRACT	20. LIMITATION OF ABSTRACT
Unclassified	Unclassified	Unclassified	UL

NSN 7540-01-280-5500

DTIC QUALITY INSPECTED 1

Standard Form 298 (Rev. 2-89)
Prescribed by ANSI Std. Z39-18
298-102

GENERAL INSTRUCTIONS FOR COMPLETING SF 298

The Report Documentation Page (RDP) is used in announcing and cataloging reports. It is important that this information be consistent with the rest of the report, particularly the cover and title page. Instructions for filling in each block of the form follow. It is important to *stay within the lines* to meet *optical scanning requirements.*

Block 1. Agency Use Only *(Leave blank).*

Block 2. Report Date. Full publication date including day, month, and year, if available (e.g. 1 Jan 88). Must cite at least the year.

Block 3. Type of Report and Dates Covered. State whether report is interim, final, etc. If applicable, enter inclusive report dates (e.g. 10 Jun 87 - 30 Jun 88).

Block 4. Title and Subtitle. A title is taken from the part of the report that provides the most meaningful and complete information. When a report is prepared in more than one volume, repeat the primary title, add volume number, and include subtitle for the specific volume. On classified documents enter the title classification in parentheses.

Block 5. Funding Numbers. To include contract and grant numbers; may include program element number(s), project number(s), task number(s), and work unit number(s). Use the following labels:

C	- Contract	PR	- Project
G	- Grant	TA	- Task
PE	- Program Element	WU	- Work Unit Accession No.

Block 6. Author(s). Name(s) of person(s) responsible for writing the report, performing the research, or credited with the content of the report. If editor or compiler, this should follow the name(s).

Block 7. Performing Organization Name(s) and Address(es). Self-explanatory.

Block 8. Performing Organization Report Number. Enter the unique alphanumeric report number(s) assigned by the organization performing the report.

Block 9. Sponsoring/Monitoring Agency Name(s) and Address(es). Self-explanatory.

Block 10. Sponsoring/Monitoring Agency Report Number. *(If known)*

Block 11. Supplementary Notes. Enter information not included elsewhere such as: Prepared in cooperation with...; Trans. of...; To be published in.... When a report is revised, include a statement whether the new report supersedes or supplements the older report.

Block 12a. Distribution/Availability Statement. Denotes public availability or limitations. Cite any availability to the public. Enter additional limitations or special markings in all capitals (e.g. NOFORN, REL, ITAR).

DOD	- See DoDD 5230.24, "Distribution Statements on Technical Documents."
DOE	- See authorities.
NASA	- See Handbook NHB 2200.2.
NTIS	- Leave blank.

Block 12b. Distribution Code.

DOD	- Leave blank.
DOE	- Enter DOE distribution categories from the Standard Distribution for Unclassified Scientific and Technical Reports.
NASA	- Leave blank.
NTIS	- Leave blank.

Block 13. Abstract. Include a brief *(Maximum 200 words)* factual summary of the most significant information contained in the report.

Block 14. Subject Terms. Keywords or phrases identifying major subjects in the report.

Block 15. Number of Pages. Enter the total number of pages.

Block 16. Price Code. Enter appropriate price code *(NTIS only).*

Blocks 17. - 19. Security Classifications. Self-explanatory. Enter U.S. Security Classification in accordance with U.S. Security Regulations (i.e., UNCLASSIFIED). If form contains classified information, stamp classification on the top and bottom of the page.

Block 20. Limitation of Abstract. This block must be completed to assign a limitation to the abstract. Enter either UL (unlimited) or SAR (same as report). An entry in this block is necessary if the abstract is to be limited. If blank, the abstract is assumed to be unlimited.

ABSTRACT

Condensed combustion products collection and high speed photography techniques were used to study the difference in combustion behavior of two aluminized propellant, one with inert binder(IB) and one with energetic binder(EB). The aluminum content and size distribution of the product particles were measured for pressures from 1 to 85 atm. Both propellants contained the same mass fractions of aluminum (18%) and coarse AP (37%) in order to provide very similar geometrical structures, and both propellants had essentially common burning rates. The aluminum combustion efficiency is higher and the characteristic agglomerate size is significantly smaller for the EB propellant than for the IB propellant (at 43 atm the agglomerate size, D_{43}, was 190 μm for the EB propellant and 670 μm for the IB propellant). The difference in combustion behavior also manifests itself in the shape of the burning surface. At 7.5 atm the characteristic roughness of the burning surface is about 300 μm for the EB propellant and about 800 μm for the IB propellant. X-ray photography and visual observations of quenched particles show that agglomerates of the same size may differ significantly in structure and aluminum content, and some indicate internal voids (i.e. loss density). This appears to be a result of the different initial conditions that the agglomerates are exposed to when they inially form at the burning surface. Size distribution of fine oxide particles does not depend on either pressure or the propellant binder (or on the size of the agglomerates). Mass size distribution of the fine particles (i.e. the somke) was observed to have 3 modal size in the ranges 1, 3.5, and 7 μm. The existence of these three modal sizes should be checked further with independent experimental methods. The mass fraction of fine oxide particles from both propellants, corresponds directly to the amount of aluminum burned. Observations in movies shows that the behavior of the burning agglomerates correlates well with the shadow diameter of the particles in flame and does not correlate with "halo" diameter (or the flame surrounding the particle).

Keywords

1. INTRODUCTION

1.1. Background

The advantages and disadvantages of using aluminum as fuel in composite solid propellants have been discussed broadly in the literature [1-4]. In practice, the efficiency of use of aluminized propellants in solid rocket motors is determined not only by conversion of chemical energy in the heat of combustion but also by formation of condensed combustion products that cause two-phase loss of specific impulse, slagging in the combustion chamber and erosion of the nozzles. The additional peculiarity of metal combustion in solid rocket motors is in damping of acoustic waves in combustion chamber.

It has been established in numerous studies that virgin aluminum particles merge in a subsurface layer and form so called agglomerates that burn out in flame generating oxide particles. The behavior of aluminum in a combustion wave can be picturized in a following simplified manner. The component formulation of the propellant determines its geometry structure and burning rate depending on the chemical and physical properties of components. The external factors like as pressure, initial temperature, acceleration, blowing, strains and deformation may make significant effect on the burning rate. The agglomeration of metal and agglomerates behavior (geometrical structure, completeness of metal consumption) depend both on propellant formulation and combustion conditions [5-8].

Condensed combustion products consist of carbonaceous residue, metal agglomerates with partly non-consumed metal, and pure oxide particles which form during combustion of metal on the surface of propellant and in agglomerates moving away from the surface. Some portion of pure oxide particles may deposit on the surface of agglomerates moving with less than gas flow velocity that changes the agglomerate structure and density [4]. The evolution of agglomerates occurs, assumably, mainly due to the vapor combustion of metal and deposition of certain portion of the oxide formed [9, 10] with following interaction of aluminum and Al_2O_3 that results in formation of vapor of aluminum and Al_2O leaving agglomerate [4]. The agglomerate burning rate depends on beforementioned external factors and oxidizer content in the environment. Besides, it depends on gasdynamics and gas flow geometry that may affect the ejection of agglomerates from the burning surface [11, 13]. Flow geometry in combustion chamber makes effect on the deposition of agglomerates on the interior walls (slagging) [14]. To simulate the agglomerates behavior one needs to know information about size distribution and structure of initial and final agglomerates and the laws of conversion of metal on the burning surface and during transport of agglomerates in the gas flow. A comprehensive model of agglomerate behavior should consider different stages of its evolution which are still not known in detail. In reality only separate stages are studied in the most of the works: agglomeration on the surface [1-5, 7, 8, 15-19, 27], formation of oxide particles [11, 20-22, 35], modeling of aluminum combustion in agglomerates [25, 28]. There are few works [6, 27, 35] devoting to studying both agglomeration and oxide particles formation that provides valuable information for substantiation of the model of agglomerate behavior.

1.2. Objectives

The goal of this study was to characterize condensed combustion products of two propellants, combusted at pressure 1-80 atm in dependence on the distance from the burning surface (0-10 cm). The original sampling technique and high speed movies provided information about size distribution and chemical composition of particles with sizes in 1-1000 μm range. The propellants under study contained the same fractions of aluminum and coarse ammonium perchlorate and had close values of burning rate. However, the propellants were based on inert and energetic binder that allowed to investigate the effect of binder nature on combustion of aluminum in flame of composite propellant.

2. MANUFACTURING AND CHARACTERIZATION OF THE MODEL PROPELLANTS

The metalized propellants were designated in this work as IB and EB in accordance with the nature of binder (IB-inert binder, EB-energetic binder). Some experiments were also conducted with non-metalized propellants IBN and EBN which are the analogues of IB and EB formulations.

The composition of the propellants is presented in Table 2.1. The results of particle size analysis of aluminum (Al) and ammonium perchlorate (AP) powders are shown in Figs 2.1, 2.2, 2.3. The content of metal in virgin aluminum particles amounts 99.5%.

The mixing of components was performed in mortar made of inert plastics by portions of 80 g total weight. Curing of cylindrical slab of propellant was made in air at 80°C during 120 hours. The samples for combustion tests were cutted from the cured material in form of cylinder with diameter 11.5 mm and height about 7 mm. The lateral surface of the samples was prohibited with epoxy glue.

The burning rate vs pressure dependencies are presented in Fig. 2.4. It is seen that the pressure levels corresponding combustion tests in similar conditions are slightly differ. The limits of experimental errors shown by arrays in Fig. 2.4 correspond to maximum and minimum magnitude of measured parameters.

Table 2.1. Propellant formulations (% mass.)

Propel-lant	Energetic binder	Inert binder	Al $D_{30}=14\mu m$	AP 200-315 μm	AP $S=6000$ cm^2/g	Catalyst	Density, g/cm^3
IB	-	15	18	37	27	3	1.62
EB	30	-	18	37	15	-	1.73
IBN	-	18.3	-	45.1	32.9	3.7	1.70
EBN	36.6	-	-	45.1	18.3	-	1.60

Inert binder: isoprene rubber (26.4%), transformer oil (69.6%), additives (4%)
Energetic binder: nitryl rubber plasticized by DEGDN (98%), additives (2%).
Catalyst: 1'1-bis (dimethyloctoxylil) ferrocene
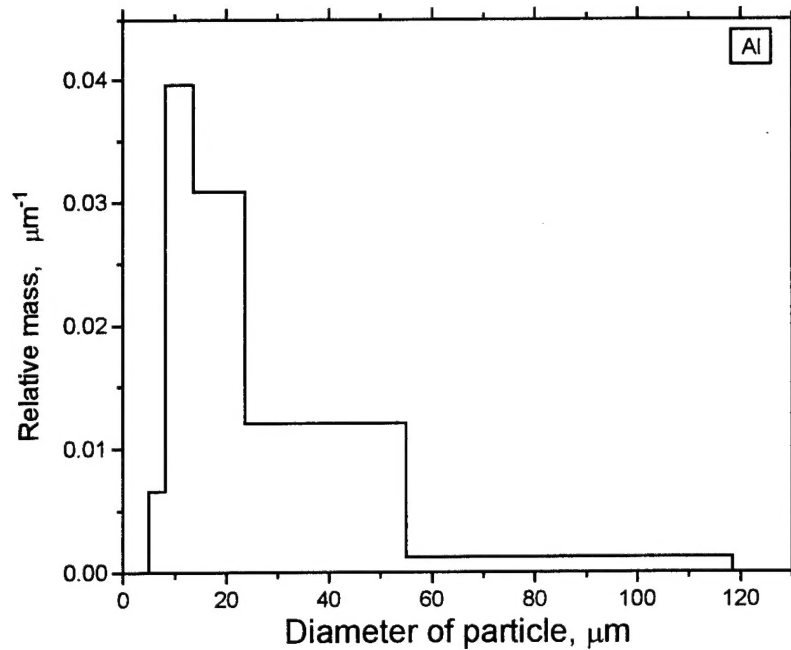
Fig. 2.1. Mass size distribution for aluminum used for manufacturing the model propellants. Measurements were made by Malvern 3600E in acetone after treatment by ultrasound during 5 min., mixer ON, size range 0.5-118 μm.

D_{mn}, μm: D_{10}=11.3, D_{20}=12.5, D_{30}=14.4, D_{21}=13.9, D_{32}=19.2, D_{43}=29.2, D_{53}=35.8.
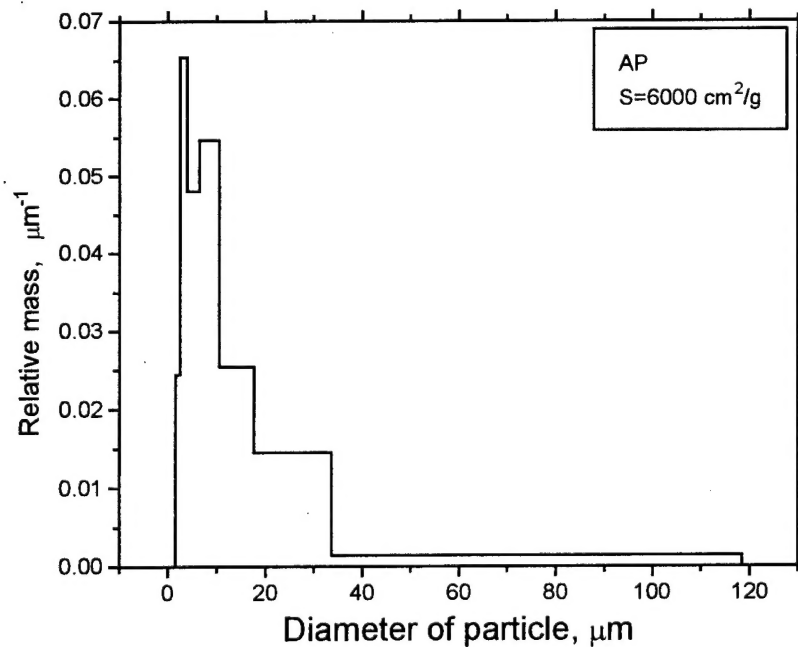
Fig. 2.2. Mass size distribution for fine AP with S = 6000 cm^2/g used to manufacture the model propellants. Measurements were made by Malvern 3600E in hexane, mixer ON, size range 0.5-118 μm.

D_{mn}, μm: D_{10}=4.3, D_{20}=4.0, D_{30}=5.1, D_{21}=4.8, D_{32}=8.4, D_{43}=17.1, D_{53}=22.9.
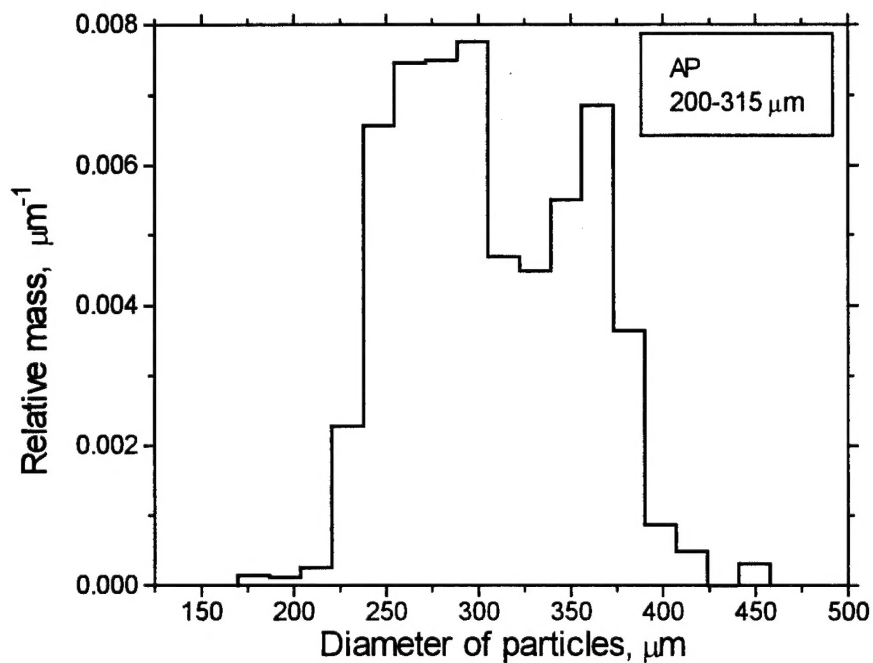
Fig. 2.3. Mass size distribution for coarse AP 200-315 μm used in manufacturing the model propellants.

Measurements were made by optical microscope.

D_{mn}, μm: D_{10}=284, D_{20}=288, D_{30}=292, D_{21}=292, D_{32}=299, D_{43}=306, D_{53}=310.

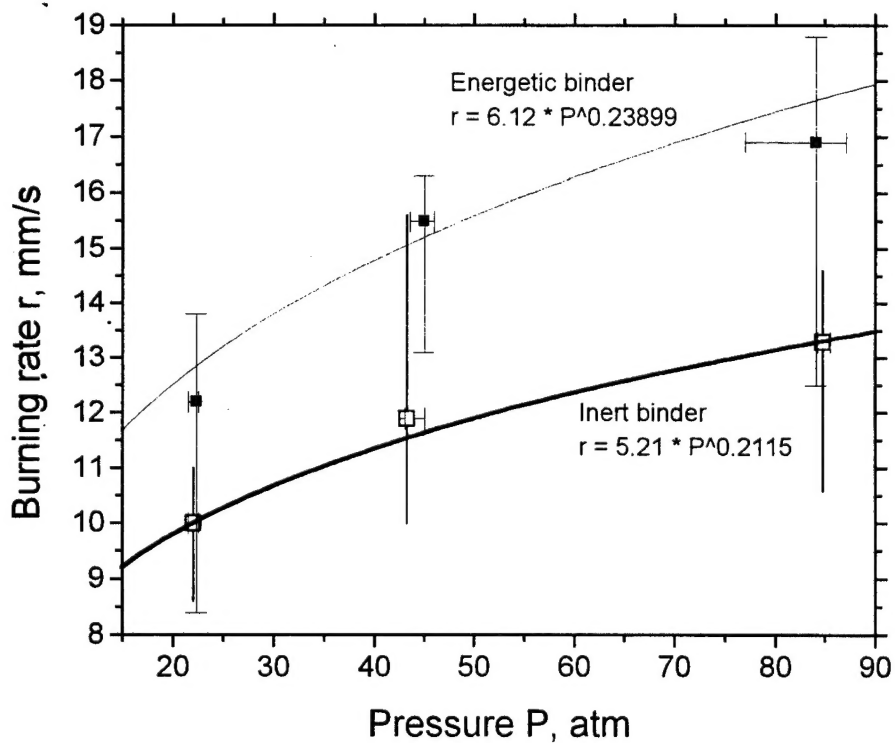

Fig. 2.4. Burning rate vs pressure.

3. METHOD OF SAMPLING THE CONDENSED COMBUSTION PRODUCTS

3.1. The setup and experimental procedure

The original technique designed in the Institute for sampling and analyses of condensed combustion products (CCP) in wide size range (agglomerates and oxide particles are collected in one run) has been described previously [6, 24]. Below we describe briefly the particular features of the technique options used in this study.

The blow through bomb (Fig. 3.1) consists of massive case *1* supplied with gas inlet *12* and outlet *7* valves which allow to maintain an appropriate gas flow rate in the bomb. Inside the bomb there is a steel cylinder *3* of 50 mm in diameter with propellant specimen *10* mounted in the top cover *2* (inner part) of cylinder. The bottom of a cylinder is supplied with a set *5* of metallic grids and aerosol analytical filter AFA *6*. The propellant specimen is ignited by nichrome wire *9* and the flame torch is directed downward. The protecting tube *8* is slipped over a specimen providing protection of combustion products against mixing with environmental gas. After leaving the tube the combustion products mix with cold nitrogen filling the bomb and cylinder interior through the top ring slot *11* ($\varnothing 40 - \varnothing 30$) mm and lateral surface holes 4. Mass flow of nitrogen through the bomb was 3.2 g/s in all runs.

Using protecting tube of different length allow to vary the residence time of CCP particles in flame environment. In the present work:

• protecting tubes with wall thickness 3 mm were made of plexiglass with length L being equal 3 and 10 cm; in additional, the propellant samples were prepared without tube (L=0) with ignited surface being mounted flush with the edge of inhibitor layer;

• the diameter of specimens was 11.5 mm, height was 6-8 mm, weight was 1.3-1.5 g. The lateral surface was inhibited with epoxy glue that was cured after insertion of the specimens into mounting cup made of teflon.

• at identical conditions (pressure, gas flow, initial temperature) 3-4 propellant samples were combusted that provided total propellant mass burnt 3-4 g and generated 1-2 g of CCP used for subsequent analysis;

• the maximum rise of pressure during combustion run was 12 atm in the experiments with propellant EB at pressure 80 atm. The characteristic pressure in the individual run was taken as a half of sum of initial and final pressures. The characteristic pressure and burning rate for a given series were chosen as arithmetical mean values of characteristic pressure and burning rate for individual runs;

• the nominal mesh sizes of grids in the set installed inside the bomb were 80, 160, 280, 480, 590, 880 and 1060 μm;

• the CCP particles kept by grids in the bomb were divided on fraction via wet sieving in acetone by using grids with the same mesh sizes. After that the fractions of CCP particles were weighed with accuracy no less than 0.00015 g and were subjected to size and chemical analysis. The latter was made by permanganatometric method [26] that allows to determine a free aluminum content;

• particle size analysis was made for coarse (> 80 μm) particles using optical microscope. The accuracy of size measurement can be estimated as a half of histogram sub-range. It was equal 9 μm for fraction 80-280 μm, 22 μm for fraction 280-590 μm and 27-42 μm for fraction with size exceeding 590 μm.

• fine (< 80 μm) particles were analyzed with commercial sizer Malvern 3600E using acetone as carrier liquid after 3 minute treatment by ultrasound and with continuous mechanical mixing of suspension;

• the density of fine particles was assumed to be equal 3.71 g/cm^3 while that of coarse particles was determined individually as mean in each fraction.
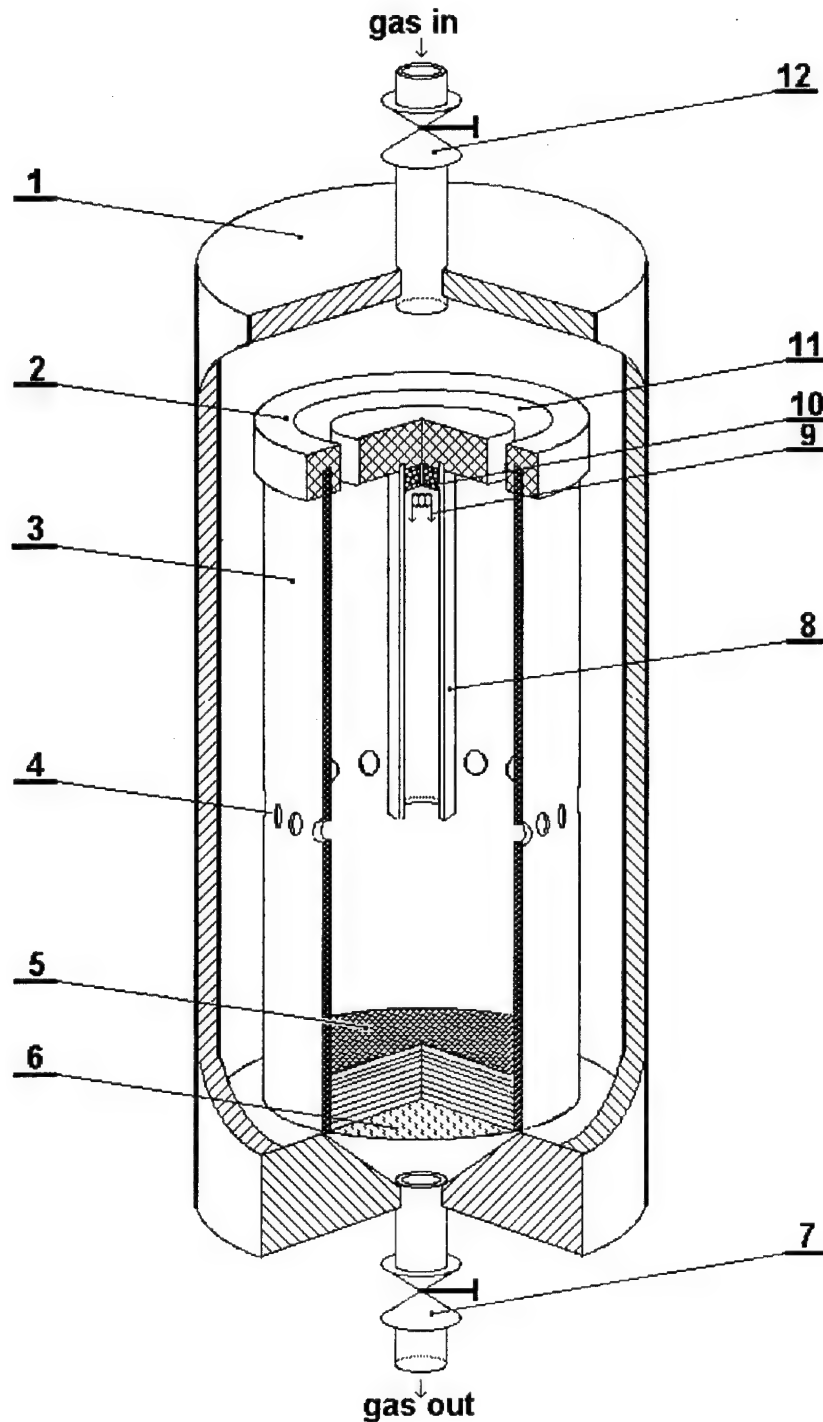
Fig. 3.1. Chart of the bomb for CCP sampling.

1	-	bomb body,	7	-	gas outlet valve,
2	-	top cover of the cylinder 3,	8	-	protecting tube,
3	-	thin wall cylinder,	9	-	ignition wire,
4	-	holes for the gas input to cylinder 3,	10	-	propellant specimen,
5	-	set of grids,	11	-	ring slot for blowing the cylinder 3,
6	-	filter,	12	-	gas inlet valve.

3.2. Treatment of the experimental data and parameters used to characterize CCP particles.

Size distribution function for the entire population of CCP particles has been defined on the basis of original computer code taking into account:

- mass contribution of individual fractions and their size distribution;
- mean density of particles in particular fractions of the CCP;
- overlapping of the histograms corresponding to separate fractions.

The results of particle size analysis were picturized in the form of histograms of the relative mass of CCP $f_i(D)$ defined as

$$f_i = \frac{m_i}{m_p \cdot \Delta D_i}.$$

Here m_i is the mass of CCP in the i-th size interval, m_p is the total mass of propellant burnt, ΔD_i is the width of i-th size interval. In other words the value f_i is the density distribution of the mass of CCP related to the total mass of propellant. Hence, the total mass of CCP m_c can be calculated by

$$m_c = m_p \int_{D_{min}}^{D_{max}} f(D)dD.$$

The results of chemical analysis on aluminum content were presented in the form of histograms $f_i^{Al}(D)$ defined as

$$f_i^{Al} = f_i \cdot \varepsilon_j^{Al},$$

where ε_j^{Al} is the mass content of aluminum in the j-th fraction which contains i-th size interval.

Any size distribution function can be characterized statistically by its moments. If one defines $N(D)$ as size distribution function by number that meet condition

$$\int_{D_{min}}^{D_{max}} N(D)dD = N_{\Sigma}$$

where N_{Σ} is the overall number of particles, the initial moment (or simply moment) M_r is determined by

$$M_r = \frac{1}{N_{\Sigma}} \int_{D_{min}}^{D_{max}} D^r N(D)dD$$

Here r is the order of the moment. If $r = 1$ then M_1 is the first initial moment which is called expected mean value.

Similarly, the central moments are defined as

$$M_r^{center} = \frac{1}{N_{\Sigma}} \int_{D_{min}}^{D_{max}} (D - M_1)^r N(D)dD.$$

If $r = 2$ then second central moment $M_2^{center} = \sigma^2$ that called dispersion (variance).

When constructing a histogram, the particle sizes change discretely and all particles in the i-th size interval have conventionally effective size $D_i = D_{il} + \Delta D/2$, where D_{il} is the left bound of the i-th size interval.

Consequently, calculated on the basis of histograms initial moments are

$$M_r = \frac{1}{N_\Sigma} \sum_{i=1}^{k} D_i^r N_i = \sum_{i=1}^{k} D_i^r \left(\frac{N_i}{N_\Sigma} \right),$$

where k is the number of intervals.

In analysis of polydisperse powders more convenient is to use the <u>mean sizes</u> D_{mn}.[31, 32]. Mean size (diameter) D_{mn}. with order (m, n) is associated with the moments by formula

$$D_{mn} = \sqrt[m-n]{\frac{M_m}{M_n}}.$$

There are several useful properties of mean sizes definition:

$$D_{mn} = D_{nm}; \quad D_{30} = (D_{10} \cdot D_{21} \cdot D_{32})^{1/3} \text{ [20]}; \quad \sigma^2 = D_{20}^2 - D_{10}^2.$$

In the present work, to calculate mean size D_{mn} on the basis of experimentally determined mass size distribution we used following formula to obtain effective number of particles N_i in a given i-th size interval:

$$N_i = \frac{m_i}{\frac{\pi}{6} D_i^3 \rho_p},$$

where density of CCP particles was assumed to be the same in overall size range and equal 2.25 g/cm^3.

In a similar way the "mean size" for aluminum can be calculated on the basis of experimental data on aluminum content in CCP particles, D_{mn}^{Al}. In this case the density was taken to be equal 2.7 g/cm^3 and calculated value N_i^{Al} has a conventional meaning. The mean sizes D_{mn}^{Al} characterize size distribution function only and should not be associated directly with an agglomerate structure, i.e. they don't correspond to equivalent size of metal core within the agglomerate shell.

<u>In-completeness of aluminum combustion</u> η was characterized by the ratio of mass of metallic aluminum in CCP particles with size exceeding 60 μm (m_c^{Al}) and mass of metal in the propellant samples (m_p^{Al}):

$$\eta = \frac{m_c^{Al}}{m_p^{Al}}$$

There are some reasons for choosing such definition of η.

1. The chemical analysis data show that the main portion of aluminum is contained in coarse CCP particles and from the point of view of practice the burn out of aluminum in agglomerates is the most important characteristic of combustion behavior of metallized propellant.

2. The error in determination of true aluminum content in fine particles of CCP is relatively high due to small absolute magnitude (less than 1%) of that value. It may cause significant error in determination of overall aluminum content in CCP because of relative high contribution of fine particles into total mass of CCP. Besides, in many cases there were uncontrolled losses of fine particles due to damage of collecting filters (see discussion below).

3. The above definition of η coincides with commonly used in the literature that allows to compare appropriate experimental data obtained by different researchers.

Let define three additional <u>parameters</u> used to characterize the mass of CCP as:

$$R_< = \frac{\text{mass of CCP with size less than 60 micron}}{\text{mass of propellant}},$$

$$R_> = \frac{\text{mass of CCP with size more than 60 micron}}{\text{mass of propellant}},$$

$$R_\Sigma = \frac{\text{total mass of CCP}}{\text{mass of propellant}}.$$

3.3. The reproducibility test as the method for estimation of experimental error

Traditional methods to estimate the experimental error can not be applied in the most of our experiments due to complex and multistage procedure for deriving the experimental results. To avoid these difficulties and to get reliable estimation of errors we used procedure called a reproducibility test. To this end, two series of experiments were conducted at identical conditions. The magnitudes of parameters determined in such a way were treated as random variables and they were used to calculate expected mean value and mean square deviation σ. The confidence interval was estimated as $\pm 2\sigma$, where 2 is the Student coefficient corresponding to the confidence level of 70%. This coefficient was used to characterize reproducibility of both the experimental procedure and data treatment.

Let demonstrate this approach in particular case of determining error on η - relative aluminum content in coarse CCP particles.

Assume that in each of the j-th CCP fraction the mass content of aluminum amounts ε_j^{Al} with absolute experimental error $\Delta \varepsilon_j^{Al}$. The instrumental error of permanganatometric method was shown [26] to be negligible as compared with experimental data scatter. Unfortunately, in real conditions the latter could not be determined for some fractions of coarse CCP particles due to their relatively small mass. In this case only single measurements are available. To obtain upper estimate for error, these data should be characterized by the maximum experimental error known for series of runs at identical conditions. Finally, the error in determining a relative mass of non-consumed aluminum in CCP coarse particles can be estimated as

$$\Delta\eta = \frac{\sum_j \Delta m_j^{Al}}{m_p}, \tag{*}$$

where $\Delta m_j^{Al} = \Delta \varepsilon_j^{Al} \cdot m_j$ and m_j is the mass of CCP j-th fraction (for particles > 60 μm).

For example, in case of propellant IB combusted at P = 85 atm and L=0, $\sum_j \Delta m_j^{Al} = 0.024$ g

and m_p=3.97 g that gives value $\Delta\eta$ =0.006.

At the same time, according to the result of reproducibility test for two series of experiments conducted at identical conditions $\eta_1 = 0.20$ and $\eta_2 = 0.23$, i.e. $\eta_{mean} = 0.215$ and

$$\sigma = \sqrt{\frac{(\eta_1 - \eta_{mean})^2 + (\eta_2 - \eta_{mean})^2}{2}} = 0.015.$$

The value $\Delta\eta$ estimated as 2σ was found as $\Delta\eta =0.03$. Hence, in the case under discussion the reproducibility of the experimental data appeared to give figure higher than the estimated by Eq (*) experimental error. Therefore it was recommended to use in further calculations the maximum value of $\Delta\eta$ (i.e. derived in the reproducibility test).

This approach was also applied to estimate the accuracy of experimental values $R_>$, $R_<$, R_Σ.

It was found that the reproducibility of mean sizes D_{mn} in different runs is better than the accuracy of measurement of particle sizes. Therefore, the last one may serve as an estimate for error in determination of mean sizes D_{mn}.

3.4. The estimation of particle residence time in flame.

The residence time of particles in flame (hot products of propellant combustion) was calculated, according [24], as the time which a particle spends to pass a distance which is equal to sum of tube length and characteristic length of mixing of the hot gases jet with cocurrent flow of nitrogen [30]. It is assumed that the initial velocity of particle is equal zero and the particle is accelerated due to gravity force and drag (Stokes law) force action. The velocity of gaseous combustion products is determined approximately by the continuity equation in the form

$$V_{gp} = \rho_{NM} \cdot r \cdot (1-\alpha)/\rho_{gp}$$

where ρ_{NM} is the density of nonmetalized part of metalized propellant (ρ_{NM} was taken equal to experimental density of nonmetalized propellants IBN, 1.70 g/cm^3 and EBN, 1.60 g/cm^3), r is the burning rate, α is the mass fraction of nongasified part of propellant, ρ_{gp} is the density of gaseous combustion products. The value α was calculated as

$$\alpha = \alpha_{Al} + \alpha_C$$

where $\alpha_{Al} = 0.18$ is the mass fraction of aluminum in the propellants IB and EB; α_C is the mass fraction of condensed combustion products formed from non-metalized part of propellants IB and EB. It was assumed that $\alpha_C = 0.82 \cdot R_\Sigma$, where R_Σ is the mass fraction of CCP for nonmetalized propellants IBN and EBN. Correspondingly, the value of α_C was taken as:

$\alpha_C=0.14$ for propellant IB at   P=22 atm,   L=0;
$\alpha_C=0.09$ for propellant IB at   P=84 atm   L=10 cm;
$\alpha_C=0.08$ for propellant EB at   P=22 atm   L=0;
$\alpha_C=0.28$ for propellant EB at   P=80 atm   L=10cm.

In other cases (different L and P) the residence time was calculated with extreme values of α_C for given propellant and obtained values of time were averaged. The density of particles was taken equal to experimentally determined for given size range. For propellant IB particles density changed in the range 0.9-2.9 g/cm^3 while for propellant EB it varied in the range 1.4-3.3.g/cm^3. The characteristic size of particles was taken as D_{43}^{Al} determined on the basis of mass size distributions obtained in the experiments with L = 0:

$D_{43}^{Al} =489$ μm   for propellant IB at   P=22 atm;
$D_{43}^{Al} =692$ μm   for propellant IB at   P=43 atm;
$D_{43}^{Al} =507$ μm   for propellant IB at   P=85 atm;
$D_{43}^{Al} =173$ μm   for propellant EB at   P=22 atm;
$D_{43}^{Al} =200$ μm   for propellant EB at   P=44 atm;
$D_{43}^{Al} =171$ μm   for propellant EB at   P=85 atm.

The molecular mass of gaseous combustion products was taken equal M=27, dynamic viscosity is described by [33]: $\mu=0.87 \cdot 10^{-7} \cdot M^{0.5} \cdot T_f^{0.65}$ (Pa·s). The flame temperature $T_f = T_{gp} = 3350$ K. Typical values of calculated parameters realized in experiments are as follows: velocity of gas combustion products is 2-3 m/s at P = 85 atm, 3-5 m/s at 44 atm and 5-8 m/s at 22 atm, the characteristic length for mixing of combustion products with environmental gas is 3 cm.

4. EXPERIMENTAL DATA ON CONDENSED COMBUSTION PRODUCTS

4.1. Experimental program

The experiments on collection of condensed combustion products (CCP) were conducted at pressure levels about 20, 40 and 80 atm with protecting tube length of 3 sizes: L=0, L=3 cm and L=10 cm. In order to evaluate the contribution of non-metallized part of propellant into the total mass of CCP for metallized propellant special experiments were conducted on combustion of propellants IBN and EBN (see Table 2.1 with component composition). These experiments were performed at P=20 atm with L=0 and at P=80 atm with L=10 cm that should correspond to the minimum and maximum magnitudes of contribution due to combustion of non-metallized part of propellant.

4.2. Overall characteristics of mass size distribution of CCP

The typical total (in the range from 0.5 μm to maximum) mass size distributions of CCP for the propellants IB and EB are shown in Figs. 4.1a and 4.1b. The relative mass of CCP was defined in Chapter 3 as

$$f_i = \frac{m_i}{m_p \Delta D_i}$$

where m_i is the mass of CCP in the i-th size range, m_p is the total mass of propellant combusted, ΔD_i is the width of the i-th size range.

In linear scale the magnitude of area beneath the curve f_i is proportional to the mass of CCP. Examining Fig. 4.1 one may conclude that

- the total range of CCP particle sizes is rather broad with maximum size for propellant IB (1300 μm) being higher than for propellant EB (300 μm);
- total size distribution can be divided to two intervals with local minimum corresponding to the size about 60-80 μm;
- propellant with energetic binder produces bigger mass fraction of small size (oxide particles) CCP that indicates more complete combustion of aluminum in the propellant EB.

Similar size distributions have been published in numerous papers. Based on the literature [4, 6, 16, 17, 27] and own data we will treat here the CCP with size higher than 60 μm as agglomerates while smaller size CCP at the total size distribution curve will be treated as pure oxide and carbon contained particles. Such division of CCP agrees well with the results of chemical analysis: the content of aluminum in CCP with size less than 80 μm does not exceed 0.7%, Table 4.1.

Thus, with a good accuracy one may determine depletion degree of aluminum through the ratio of mass of neat aluminum in coarse part of CCP and mass of aluminum in propellant.

To provide most clear description of experimental data we will discuss separately the results corresponding to the coarse and fine size CCP.
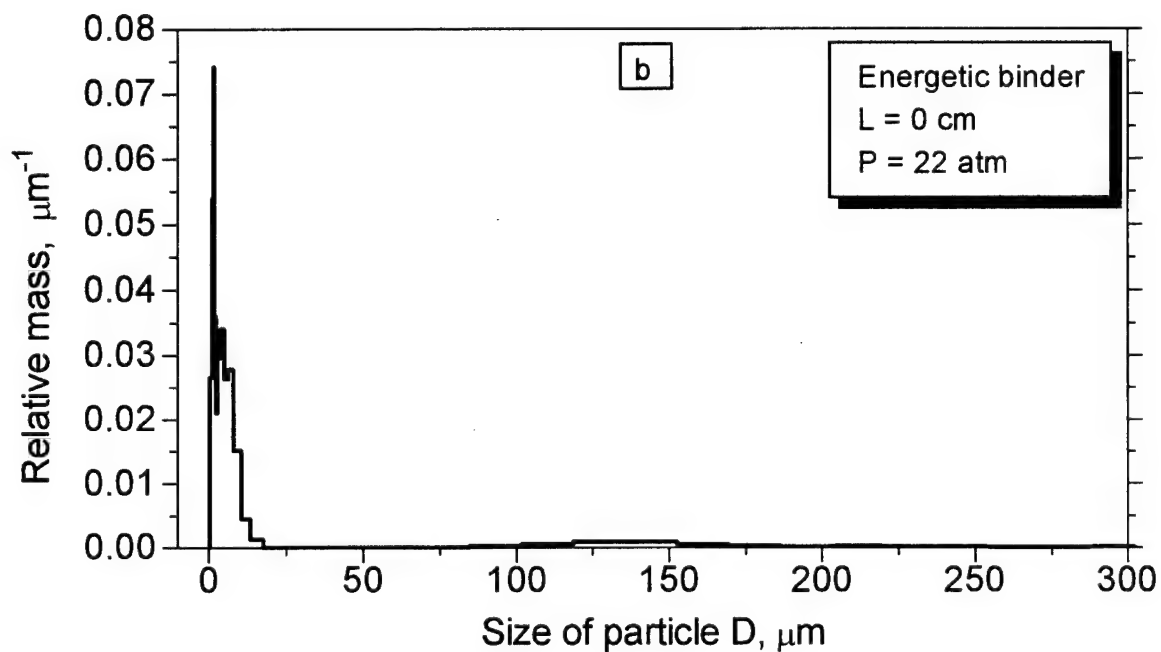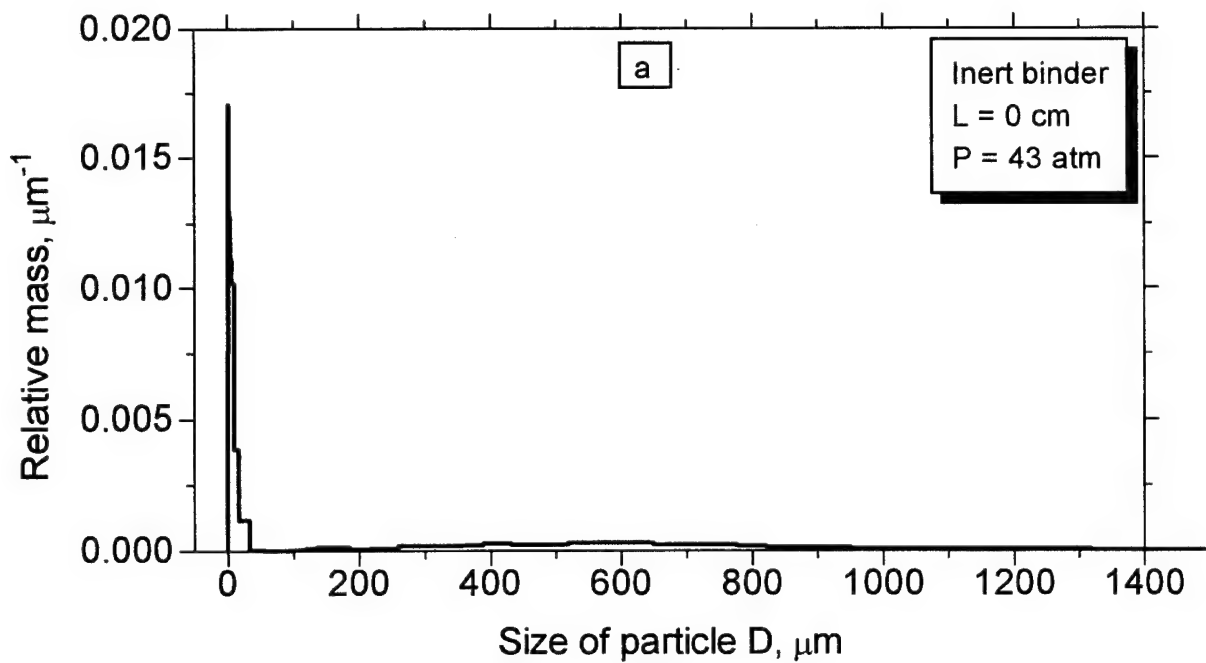
Fig. 4.1. Typical mass size distribution of CCP for metallized propellants with inert (a) and energetic (b) binder.

Tables 4.1a, 4.1b. Chemical analysis data on aluminum content (% mass.) in CCP individual fractions. (Combined data cells correspond to the joint fraction with small absolute mass)

a). Propellant IB

P, atm	L, cm	<80 μm	80-160 μm	160-280 μm	280-480 μm	480-590 μm	590-880 μm	880-1060 μm	>1060 μm
22	0	0.41±0.03	12.8±0.1	30.7±1.0	30.8±0.2	31.3	29.9±1.0	22.9	22.2
22	3	0.47±0.01	7.89	20.7±0.3	29.4±0.2	29.1±0.1	28.5±0.1	28.2	24.7
22	10	0.47±0.01	23.4±0.1	28.8±0.2	29.6±0.1	28.0±0.2	27.4±0.1	25.9	21.7
43	0	0.59±0.07	10.6	19.2	25.5	25.86±0.05	25.9±0.3	24.5±0.1	
44	3	0.26±0.02	7.74	23.5	27.3±0.5	27.6±0.2	26.2±0.2	25.4	25.7
43	10	0.52±0.14	16.0	22.8	21.9±0.3	22.8±0.1	23.0±0.1	23.15±0.05	22.7±1.0
85	0	0.67±0.03	11.9	18.28±0.05	22.45±0.05	24.8±0.4	26.1±0.5	20.9	13
84	3	0.57±0.04	12.8	21.2	24.2±0.2	25.1±0.1	25.9±0.3	13.8	
84	10	0.70±0.08	13.8	18.6	22.0±0.1	0	23.0±0.1	23.3±0.1	21.2

b). Propellant EB

P, atm	L, cm	<80 μm	80-160 μm	160-280 μm	280-480 μm	480-590 μm	590-880 μm	> 880 μm
22	0	0.40±0.04	23.5±0.1	28.1				
22	3	0.32±0.02	18.0±1.0	25.8±0.6	19			
22	10	0.36±0.03	23.1±0.1	23.2				
44	0	0.20±0.01	3.64±0.01	9.44	2.4			
46	3	0.20±0.03	3.14±0.09	9.92	6.08			
45	10	0.20±0.03	8.4±0.7	9.64	7.28			
85	0	0.44±0.04	10.1	6.5				
87	3	0.18±0.01	6.19	8.77			0	
81	10	0.27±0.01	4.35			0	3.4	

4.3. Reproducibility test for coarse (> 60 μm) CCP particles

The procedure to estimate the experimental error based on reproducibility test was described in Chapter 3.3. To this end two series of experiments were conducted in identical conditions.

Let demonstrate the results of the reproducibility of mass size distribution functions $f(D)$ and $f^{Al}(D)$ and their statistical parameters - mean diameters D_{mn} and D_{mn}^{Al}. Figure 4.2 presents the Data for two series of experiments with propellant IB at L=0 and pressure 85 atm. It is seen that casual differences in histogram form do not result in significant difference in values of D_{mn} and D_{mn}^{Al}. The differences in value η - relative aluminum content for coarse CCP particles for this data set are discussed above by estimation of experimental error on η. (The value of η=0.20 and η = 0.23 for Data "1" and "2", respectively).
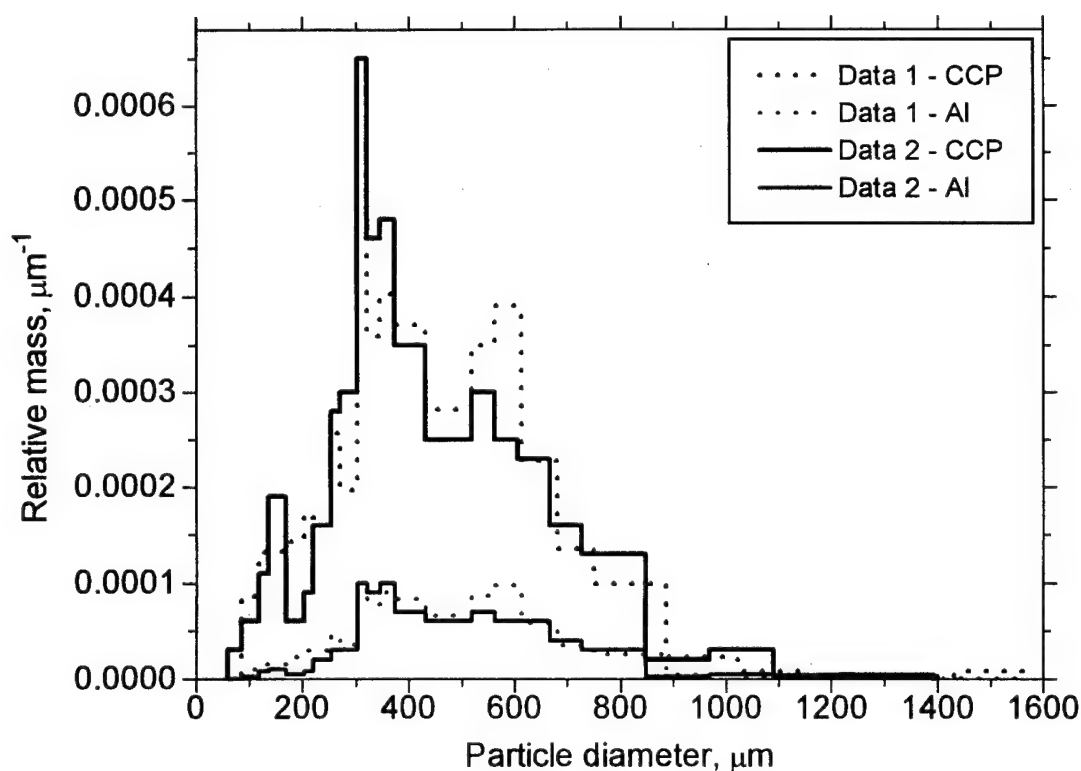

Fig. 4.2. Comparison of the results on relative mass distributions of coarse CCP and aluminum in coarse CCP in two series at the same firing conditions. Propellant IB, 85 atm, L=0.

D_{mn}, μm for CCP particles > 60 μm
Data 1: D_{10}=197, D_{20}=234, D_{30}=276, D_{21}=279, D_{32}=383, D_{43}=486, D_{53}=534.
Data 2: D_{10}=185, D_{20}=224, D_{30}=266, D_{21}=271, D_{32}=374, D_{43}=474, D_{53}=520.

D_{mn}^{Al}, μm for aluminum in CCP > 60 μm
Data 1: D_{10}=231, D_{20}=273, D_{30}=315, D_{21}=322, D_{32}=420, D_{43}=507, D_{53}=546.
Data 2: D_{10}=278, D_{20}=317, D_{30}=355, D_{21}=363, D_{32}=442, D_{43}=515, D_{53}=549.

4.4. Coarse size (> 60 μm) CCP of the propellant IB.

Figure 4.3 presents the dependence of relative mass of non-consumed aluminum in the agglomerates of propellant IB versus calculated residence time at different pressures. It is seen that the completeness of aluminum combustion is relatively uniform at all combustion conditions and equals $(1-\eta)$ = 0.73-0.78. Such behavior is not typical for similar propellants studied by us previously where the consumption degree changed under variation of environmental parameters by 1.5-2 times.

Figure 4.4 shows the behavior of the relative mass of CCP particles > 60 μm ($R_>$), < 60 μm ($R_<$) and R_Σ (in whole size range 0.5 μm -D_{max}) collected at different pressures and with varied length of protecting tube. Examining the behavior of parameter $R_>$ one may recognize that it varies in a very restricted range that corresponds to stagnation (strong retardation) of aluminum combustion in agglomerates. Weak variation of $R_>$ may be attributed to redistribution of mass between different fractions of CCP rather than to burn out of aluminum. To check this assumption we analyze mass size distribution for coarse CCP particles collected at various pressures.

4.4.1. Pressure 22 atm.

There are two modes in the mass size distribution (Fig. 4.5). The B-mode corresponds to 350 μm size and does not change its location under variation of protecting tube length. The A-mode at L=0 is about 3-times higher the B-mode and gradually decreases in height when L increases. The content of aluminum in A-mode is relatively small at L=0. Keeping in mind the trend of overall decrease of coarse CCP mass (Fig. 4.4, P=22 atm) with tube length, one may conclude that the mass of oxide corresponding to the A-mode transforms both to the mass of coarse particles and to the mass of particles lesser 60 μm. Mass size distribution becomes more uniform at long tube combustion conditions that manifests itself in increase of characteristic size D_{43} from 380 μm up to 510 μm. The Table 4.2 presents calculated characteristic sizes D_{mn} and D_{mn}^{Al}. It is seen that with long tube the mass size distributions for CCP and aluminum in CCP become similar, i.e. $D_{mn} \rightarrow D_{mn}^{Al}$. The cause of similarity is a weak dependence of aluminum content on particle size in the range of large sizes of CCP particles. At pressure 22 atm the aluminum content in CCP particles of 160-880 μm sizes changes in the limits of 26-31%. Note that these particles contain about 60% of mass of CCP with size exceeding 60 μm.

4.4.2. Pressure 43 atm.

There are A-mode at 100-200 μm and B-mode at 500-600 μm in mass size distribution (Fig. 4.6). In contrast to the previous case (22 atm) A-mode is less in amplitude than B-mode. However, the maximum of mass size distribution for aluminum in CCP coincides with B-mode for CCP particles as in case of 22 atm. This is provided by almost uniform content of aluminum (22-28%) in coarse fraction of CCP (280-1060 μm). The mass distribution functions at different tube lengths are similar geometrically and statistically. The latter is confirmed by only 20% difference in characteristic sizes D_{32}, D_{43}, D_{53} with variation of the tube length. It can be stated that not only aluminum depletion degree but also mass size distribution "freezes" at a relatively short distance above burning surface during combustion at 43 atm.

4.4.3. Pressure 85 atm.

There are B-mode at 400 μm and C-mode at 600 μm in mass size distribution (Fig. 4.7). The mode amplitudes are close in magnitude and characteristic sizes D_{32}, D_{43}, D_{53} change under tube length variation by 30% only. Hence, mass size distributions for CCP and aluminum in CCP are close that is the result of weak dependence (22 to 26%) of aluminum content in CCP fractions 200-880 μm. Mass size distribution at the longest tube length exhibits remarkable A-mode whose

appearance is not accompanied with increase of mass of non-consumed aluminum in the size range of 100 μm but is accompanied with increase of total mass of coarse CCP particles (cf. Fig. 4.4). These data indicate that A-mode appears due to supply of mass of oxide from the range of fine CCP particles. Thus, the experimental data for propellant IB show that an evolution of agglomerate size distribution functions occurs rather due to their "own" transformation and not due to the burn out of aluminum. In the range of residence times 60-150 ms (tube length 3-10 cm) a content of aluminum at different experimental conditions varies in narrow limits 22-26 % that is within the estimated error of experimental approach (±3 % abs.). Mass size distribution of CCP depends on pressure, e.g. D_{43}=380, 670 and 490 μm at L=0 and corresponding pressures 21, 43 and 85 atm. These distributions slightly vary under change of tube length, mainly due to transformations in the size range around 100 μm. The latter results in variation of D_{10} which is sensitive to variation of number of fine particles: D_{10} increases from 90 to 190 μm at 22 atm and decreases from 200 to 100 μm at 85 atm. It should be noted that the overall view of plots in Fig. 4.3, showing the aluminum content in CCP at different experimental conditions, may not change drastically under variation of characteristic size used for calculation of residence time. For example, a residence time for D=100 μm at tube length 0-10 cm is equal 36-74 ms but for D=700 μm it is equal 61-122 ms, i.e. the ratio of residence times remains approximately constant. Remember that according to experimental data the aluminum content in agglomerates is practically the same starting from the residence time 50 ms. It may mean that aluminum combustion has been stopped at less distance (less residence time) above beginning surface. Note that L=0 corresponds to finite residence time 50 ms and finite length of mixing with blowing the sample nitrogen stream. It is interesting that under rise of residence time due to both tube length or pressure the size distribution function becomes more uniform, or polymodal. As a result, there is no for the propellant IB agglomerates typical monotonous dependence of D_{43} on pressure or burning rate.
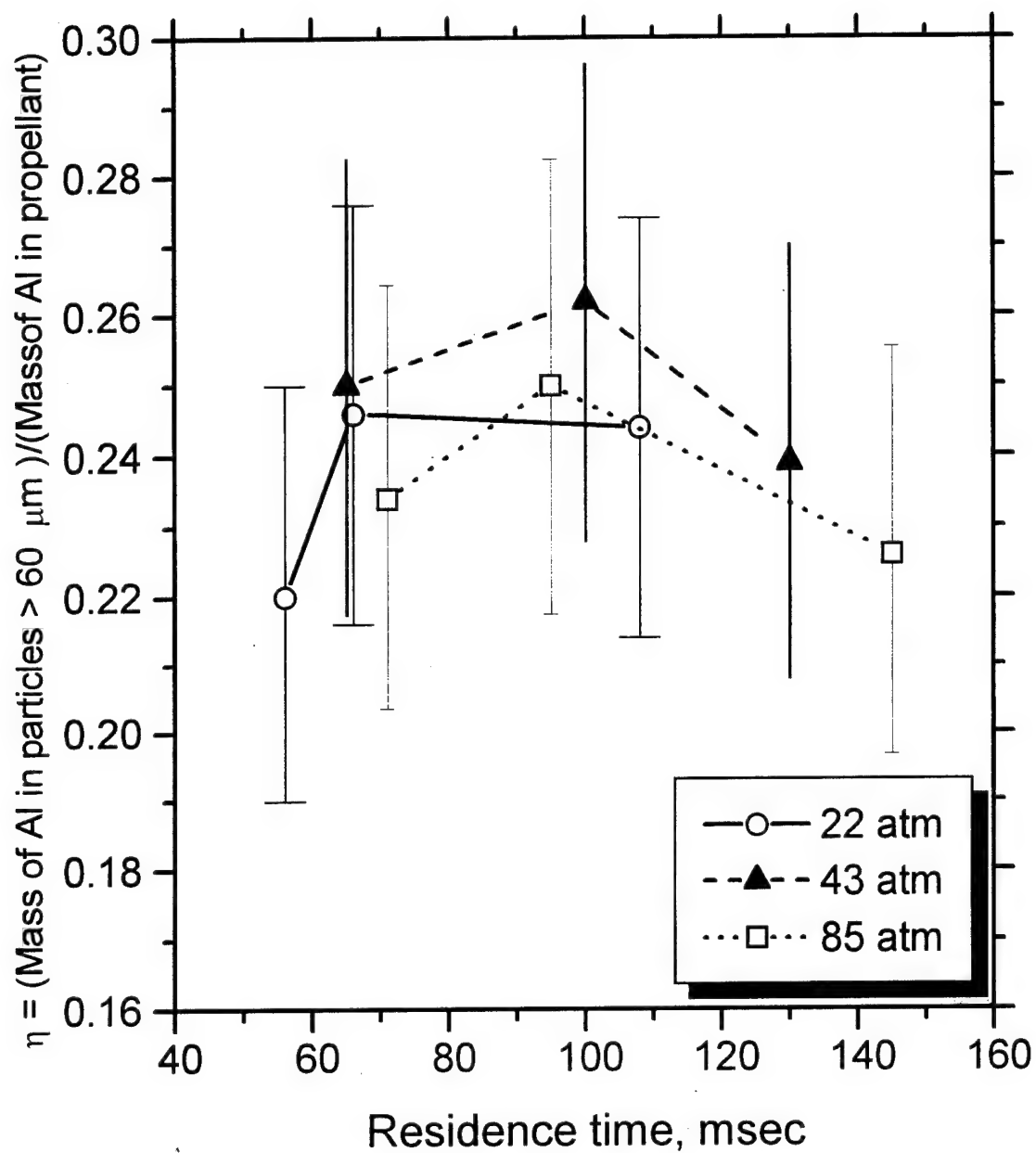
Fig. 4.3. Relative mass of non-consumed aluminum in agglomerates of IB propellant at varied combustion conditions.
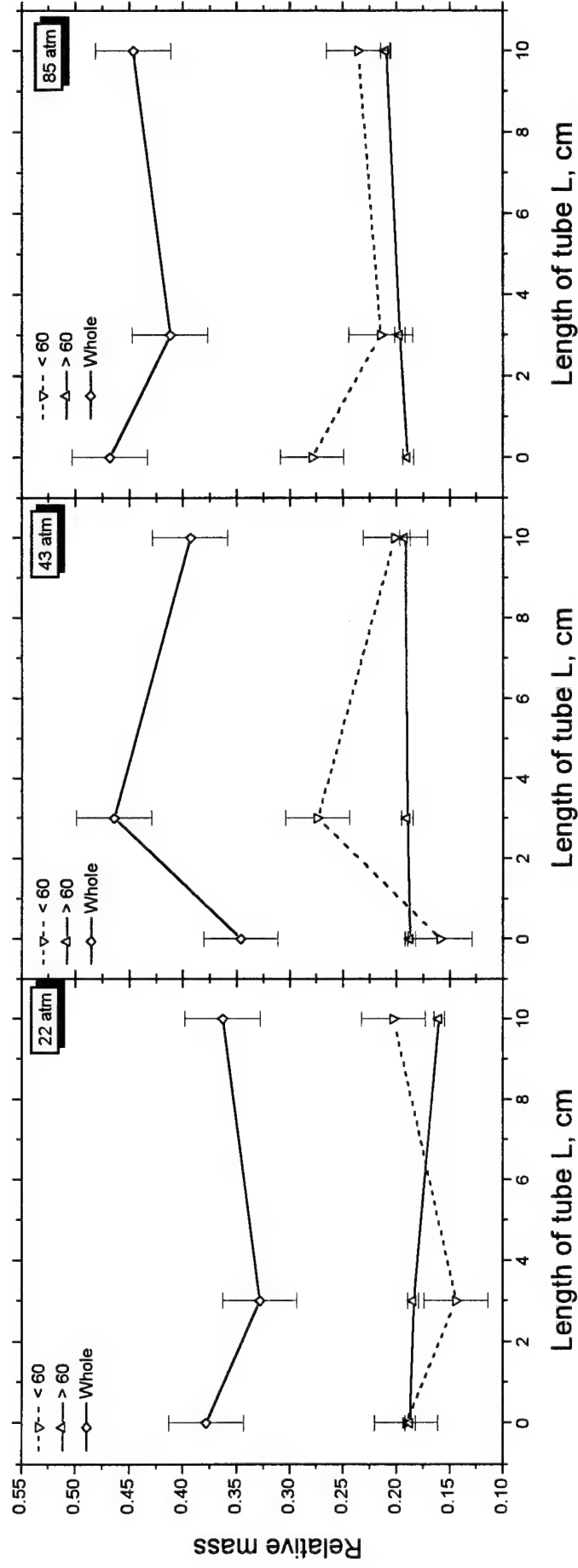
Fig. 4.4. Relative mass $R_>$, $R_<$, R_Σ of CCP of IB propellant collected at difference pressures versus length of protecting tube.

22

Table 4.2a Mean diameter of CCP particles D_{mn}, µm.
Propellant IB, particle > 60 µm.

Pressure	Tube length	Mean diameter D_{mn}, µm						
P, atm	L, cm	D_{10}	D_{20}	D_{30}	D_{21}	D_{32}	D_{43}	D_{53}
22	0	89	100	125	112	193	381	472
22	3	189	219	262	255	372	534	615
22	10	185	214	254	247	359	513	584
43	0	235	285	344	345	502	669	742
44	3	143	182	240	232	417	627	708
43	10	195	250	318	322	515	678	726
85	0	197	234	276	279	383	486	534
84	3	143	184	232	236	369	485	528
84	10	98	120	161	148	288	473	535

Table 4.2b "Mean diameter" of aluminum in CCP D_{mn}^{Al}, µm
Propellant IB, particle > 60 µm.

Pressure	Tube length	Mean diameter D_{mn}, µm						
P, atm	L, cm	D_{10}	D_{20}	D_{30}	D_{21}	D_{32}	D_{43}	D_{53}
22	0	155	194	240	244	367	489	544
22	3	246	288	335	336	453	588	656
22	10	192	222	262	257	366	510	576
43	0	289	345	404	412	553	693	757
44	3	200	258	322	333	502	658	726
43	10	221	281	350	359	542	689	734
85	0	231	273	315	322	420	507	546
84	3	220	266	310	322	421	500	532
84	10	195	246	297	310	435	535	576

Fig. 4.5. Mass size distribution of CCP and aluminum in CCP (shadowed) at different length of protecting tube.

Propellant IB, pressure 22 atm, particles > 60 μm.
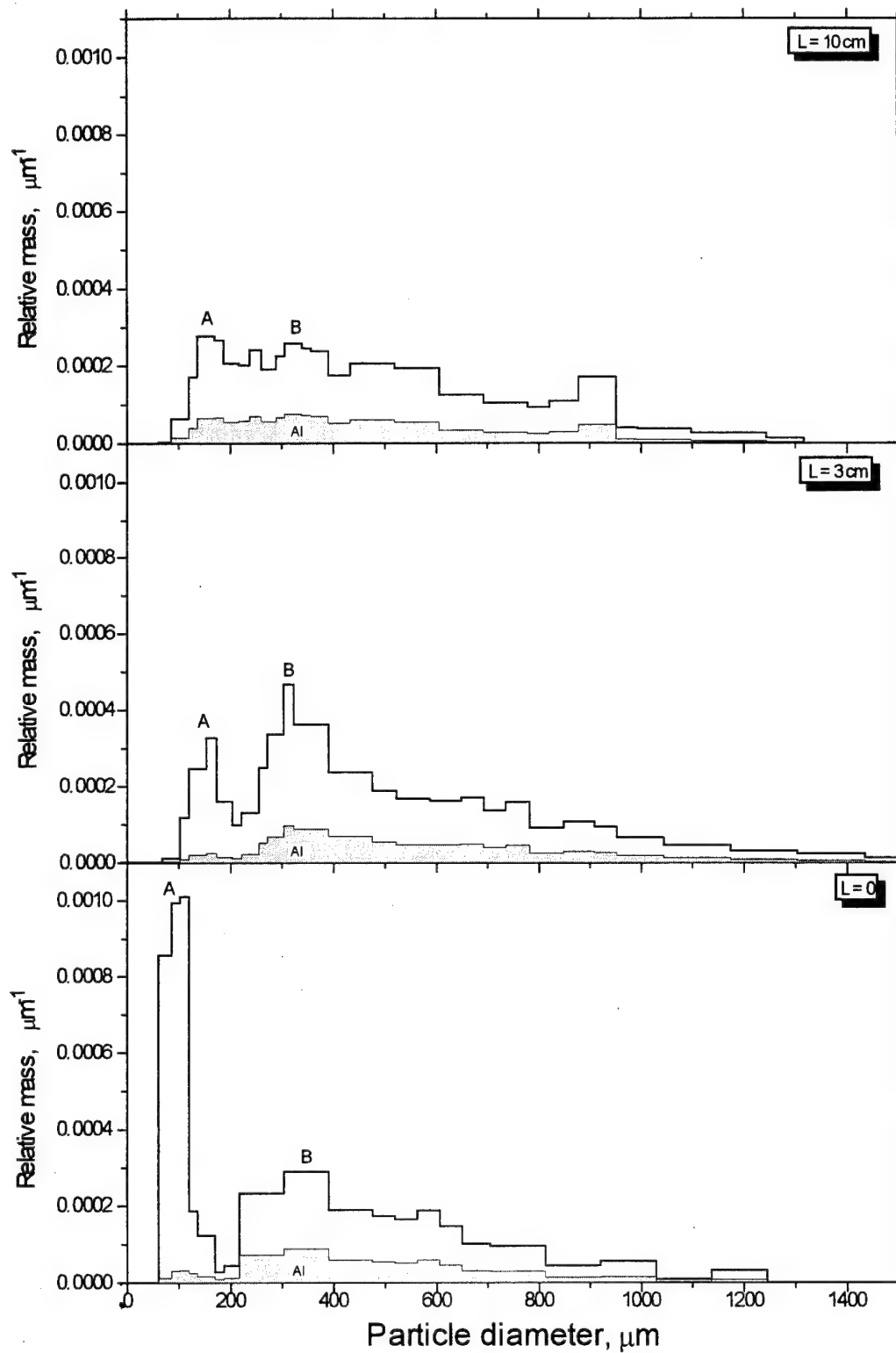
24

Fig. 4.6. Mass size distribution of CCP and aluminum in CCP (shadowed) at different length of protecting tube.
Propellant IB, pressure 43 atm, particles > 60 μm.
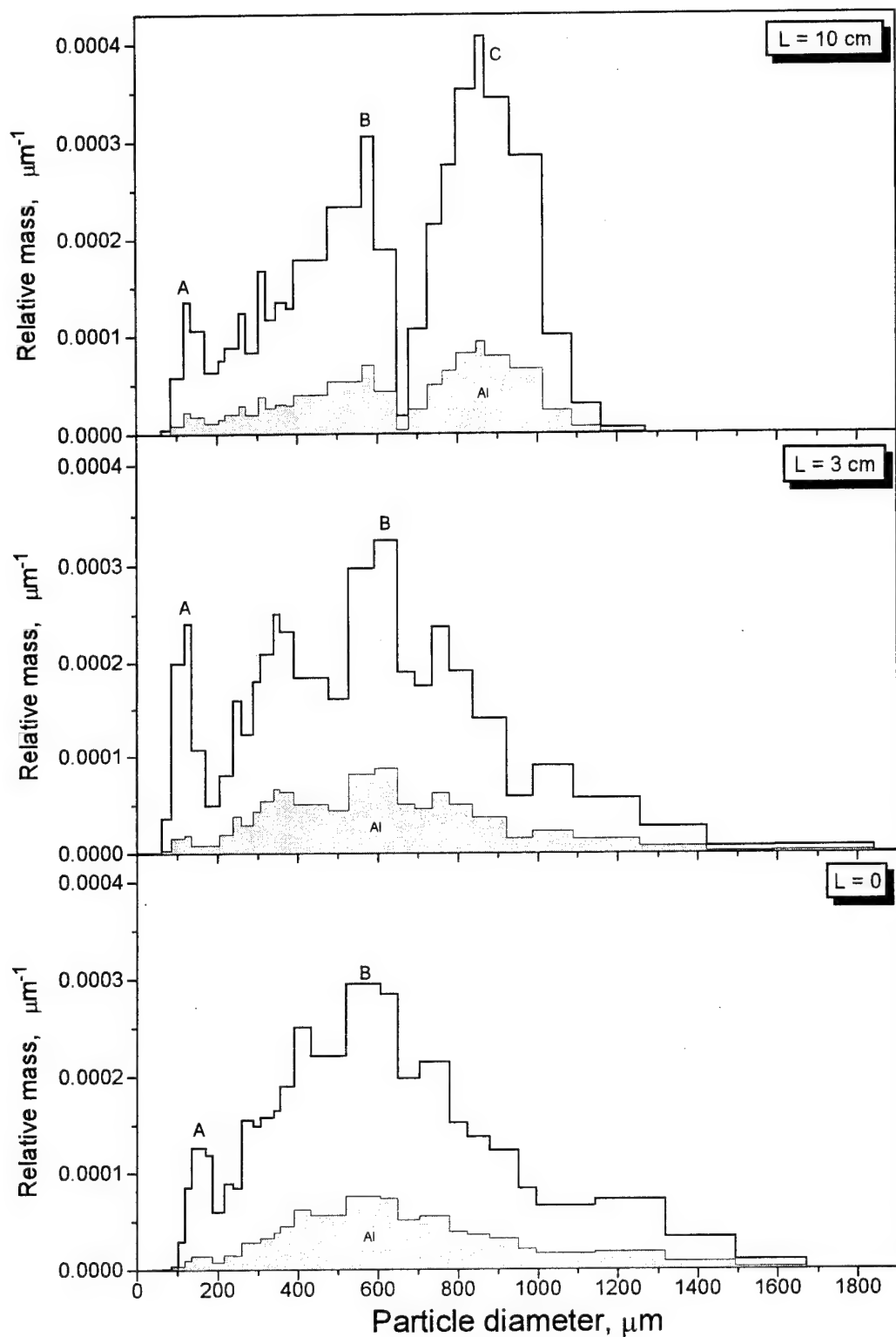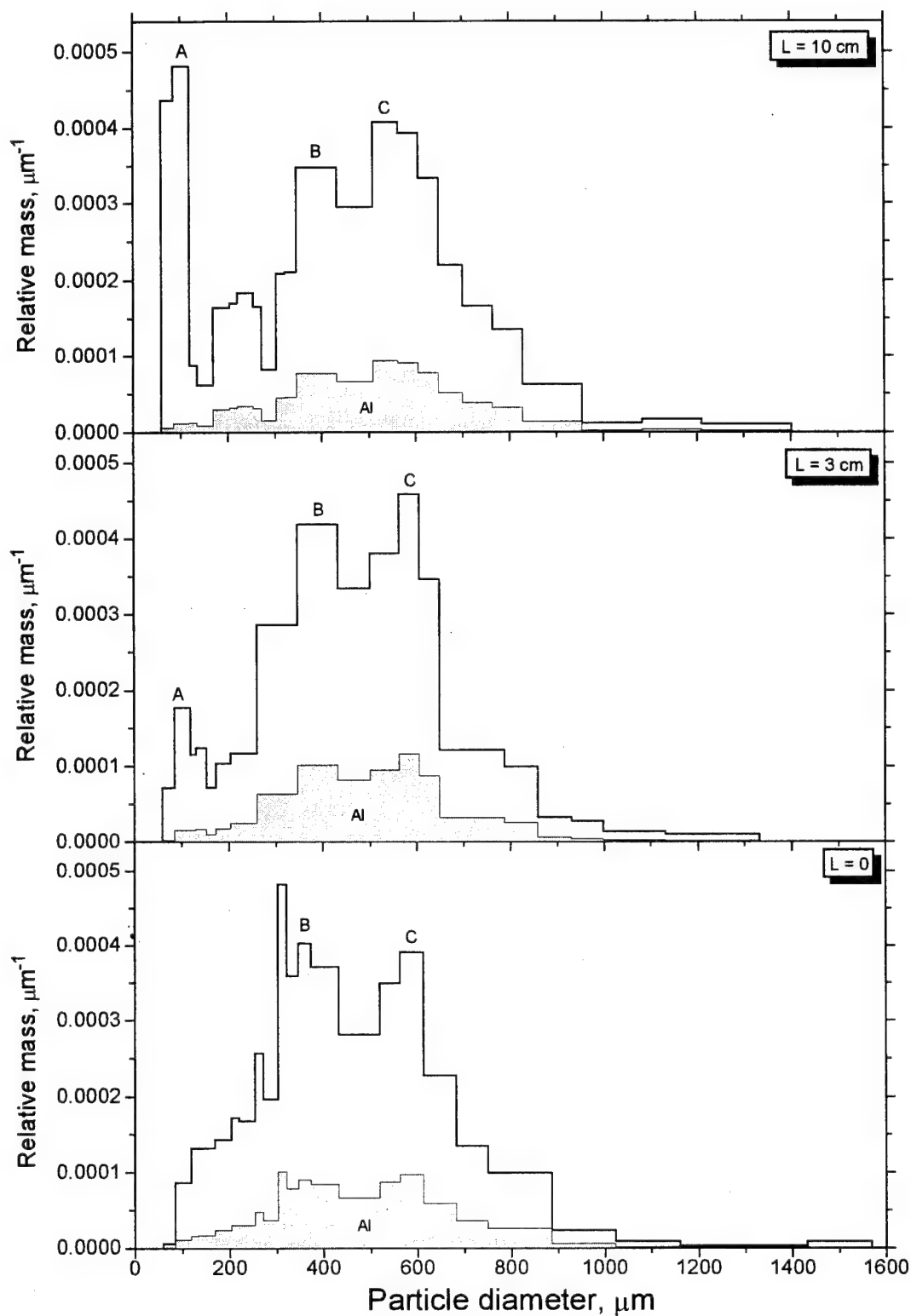
25

Fig. 4.7. Mass size distribution of CCP and aluminum in CCP (shadowed) at different length of protecting tube.

Propellant IB, pressure 85 atm,. particles > 60 μm.

4.5. Coarse size (> 60 μm) CCP of the propellant EB.

4.5.1. Overall characteristics.

Figure 4.8 presents the dependence of relative mass of non-consumed aluminum in agglomerates of propellant EB versus calculated residence time at different pressures.

Comparison with data presented in Fig. 4.3 for propellant IB reveals that:

• Propellant with energetic binder is characterized by much higher depletion degree of aluminum in CCP,

• For propellant EB the dependence of aluminum depletion degree on pressure exists, e.g. the value $(1-\eta)$ at $P = 22$ atm is equal ~0.88-0.94 while at $P = 84$ atm it is equal 0.985.

• There is dependence $\eta(L)$ for propellant EB at 22 atm which is nonmonotonous as in case of some other previously studied in our laboratory metalized propellants.

The cause for nonmonotonous behavior of $\eta(L)$ is still not clear and should be checked in future experiments with more detailed variation of tube length. One of the possible reasons could be uncertainty (incorrectness) in determination of η value at L=0.

Figure 4.9 shows the behavior of the relative mass of CCP particles > 60 μm ($R_>$), < 60 μm ($R_<$) and R_Σ (in whole range from 0.5 μm to $_{Dmax}$) collected at different pressures and with varied length of protecting tube. The distinctive feature of this Figure as compared with Fig. 4.4 (propellant IB) is relatively small contribution of coarse CCP particles into total mass of CCP. This effect is mostly pronounced at 84 atm that indicates more effective transportation of aluminum in combustion of propellant EB.

Below we analyze the behavior of CCP size distribution at different pressures under change of protecting tube length.

4.5.2. Pressures 22 atm - 84 atm.

Examination of plots in Fig. 4.10 and appropriate values in Table 4.3 shows that the mass size distributions both for CCP and aluminum in CCP are similar and practically don't depend on protecting tube length. Maximum of both distributions is in the size interval 120-160 μm.

Similar observations can be made from examination of the plots in Figs. 4.11 and 4.12 along with the data of Table 4.3.

Comparing the data corresponding to maximum value of η (P=22 atm, L=3 cm) and its minimum (P=84 atm, L=10 cm) it can be concluded that the depletion of aluminum (decrease of η) leads to decrease of the mass of coarse CCP particles (larger than 60 μm) and decrease of aluminum content in CCP without remarkable change in size of CCP particles (see Figs. 4.10-4.12 and Tables 4.1 and 4.3).

Special comments should be made concerning existence of extra large CCP particles (up to size of 1500 μm). The estimated density of these particles is 4.3 - 6.8 g/cm^3 and in fact they are the combustion products of electrically heated nichrome wire (initial density 8.4 g/cm^3) used for ignition of the propellant.

An X-ray photography of CCP shows that these particles can be also detected (Fig. 4.13) in CCP of the propellant with inert binder but their contribution in total CCP mass of this propellant is negligible. For propellant with energetic binder their contribution can be remarkable enough. Simple exclusion of these particles from consideration leads to the experimental error so as they are usually covered with finite thickness film of aluminum oxide, see Fig. 4.14. This makes extra large particles very similar in view to the ordinary CCP particles that prevents detecting these particles by microscope visualization technique. Note that nichrome does not react with sulfuric

acid used in chemical analysis for determination of aluminum content and does not affect the value of the detected non-consumed aluminum in CCP.

When drawing the plots in Fig. 4.8 the presence of nichrome particles was taken into account by enlargement of scatter limits. In addition , the characteristic sizes D_{mn} were calculated (Table 4.3c) on the basis of modified experimental data, i.e. without extra large CCP particles which size was defined as larger than one for which the size distribution function decreases up to zero with following rise to the finite value.

Calculated in this way values D_{43} are used for comparison of CCP particle sizes for propellants IB and EB, see Fig. 4.15. It is seen that when keeping in propellant formulation the same content of aluminum (18%) and coarse AP (37%, 200-315 μm) the substitution of inert binder with energetic one leads to essential decrease of mean volume size of CCP particles (from 700-380 μm to 230-150 μm). This is accompanied with increase of completeness of aluminum combustion from 0.73-0.77 to 0.88-0.98.
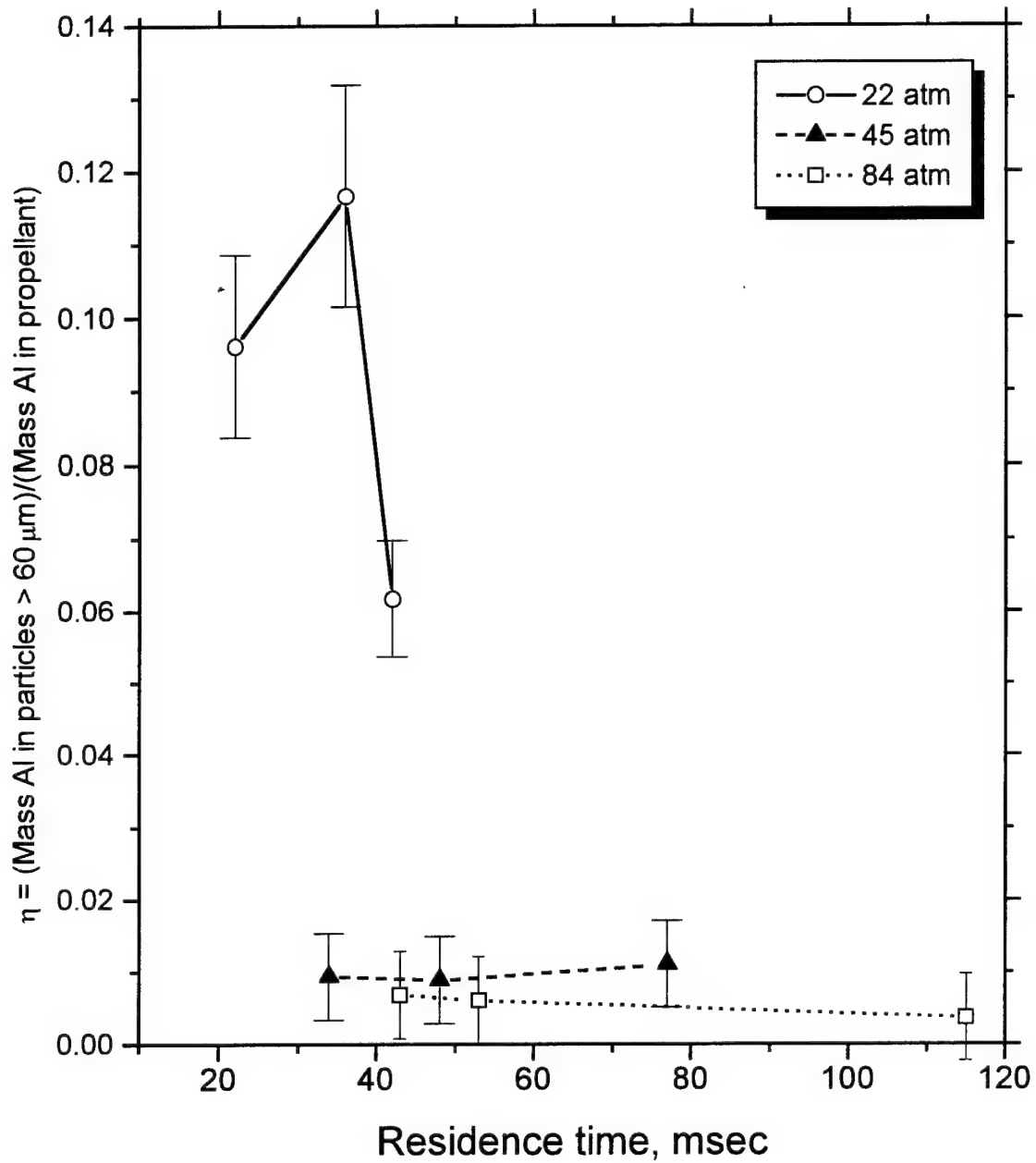
Fig. 4.8. Relative mass of non-consumed aluminum in agglomerates of EB propellant at varied combustion conditions.
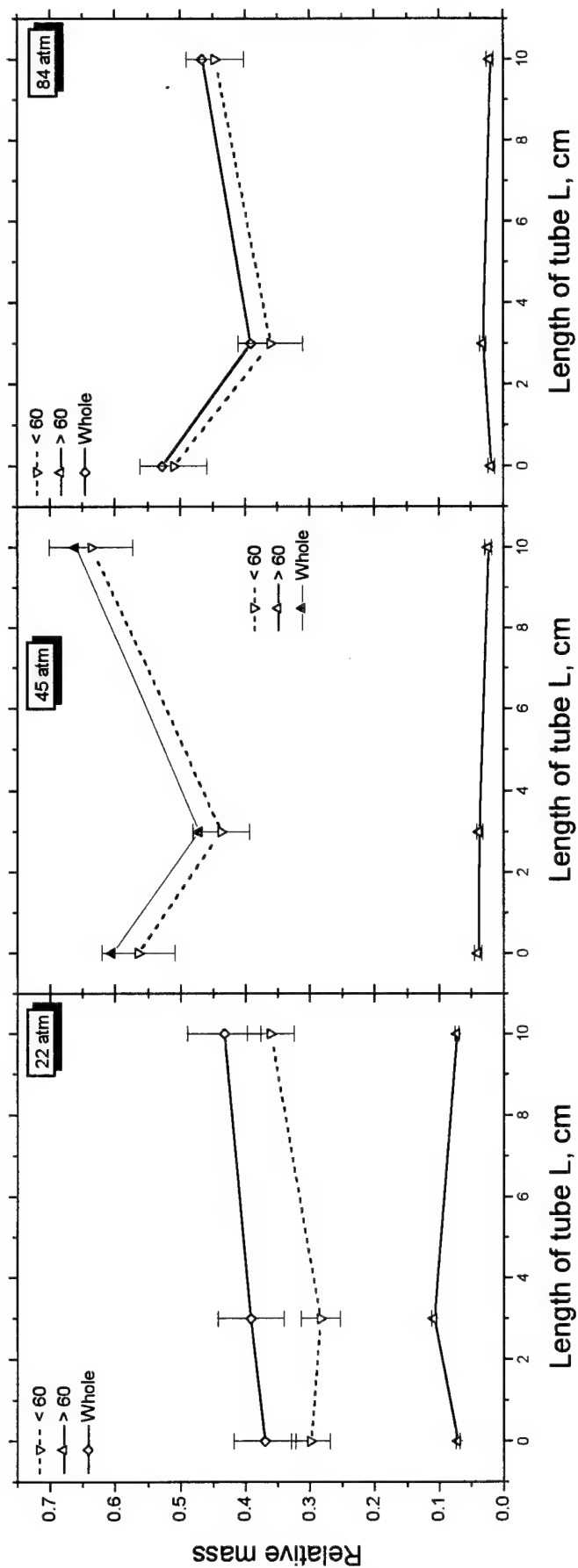
Fig. 4.9. Relative mass of $R_>$, $R_<$, R_Σ CCP of propellant EB collected at different pressures, length of protecting tube.

Table 4.3a. Propellant EB.
Mean diameter D_{mn} of CCP-particles in size range (60 µm - D_{max})

Pressure P, atm	Tube length L, cm	Mean diameter D_{mn}, µm						
		D_{10}	D_{20}	D_{30}	D_{21}	D_{32}	D_{43}	D_{53}
22	0	125	129	135	134	146	168	191
22	3	120	124	129	128	141	167	197
22	10	127	132	138	136	151	185	225
44	0	123	130	138	137	156	187	219
46	3	134	140	150	146	173	265	376
45	10	145	154	169	164	203	285	351
84	0	96	101	109	107	125	163	198
87	3	90	96	109	102	141	304	457
80	10	117	129	163	143	261	670	869

Table 4.3b. Propellant EB.
"Mean diameter" D_{mn}^{Al} of aluminum in CCP in size range (60 µm - D_{max})

Pressure P, atm	Tube length L, cm	"Mean diameter" D_{mn}^{Al}, µm						
		D_{10}	D_{20}	D_{30}	D_{21}	D_{32}	D_{43}	D_{53}
22	0	126	130	136	135	148	173	198
22	3	121	126	132	131	145	173	203
22	10	127	132	138	136	151	186	225
44	0	133	141	150	149	171	200	223
46	3	143	152	166	160	200	324	443
45	10	146	155	169	165	201	276	337
84	0	113	117	124	122	138	171	201
87	3	115	125	138	135	168	218	245
80	10	114	123	149	132	222	637	863

Table 4.3c. Propellant EB.
Mean diameter D_{mn} of CCP-particles in given size range

| Size range, µm	Pressure P, atm	Tube length L, cm	Mean diameter D_{mn}, µm						
			D_{10}	D_{20}	D_{30}	D_{21}	D_{32}	D_{43}	D_{53}
60-380	22	0	124	129	133	133	142	156	165
60-380	22	3	120	124	128	127	138	152	161
60-380	22	10	127	131	135	135	144	155	162
60-520	44	0	123	130	138	137	155	179	193
60-520	46	3	134	139	144	144	156	172	183
60-520	45	10	145	151	161	159	182	215	234
60-600	84	0	96	101	108	106	124	156	183
60-600	87	3	89	95	103	100	121	164	197
60-600	80	10	115	123	136	132	166	226	261
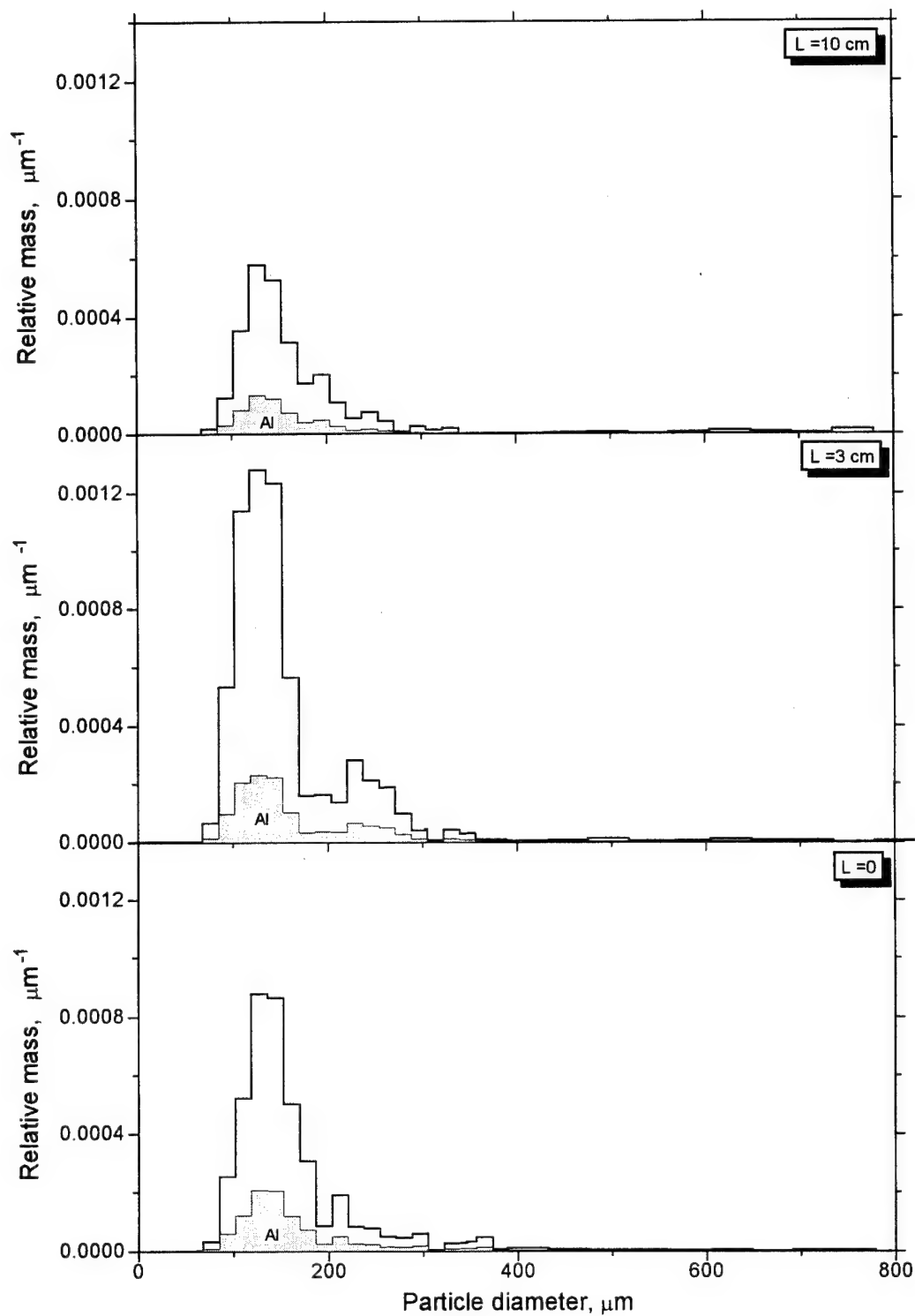
Fig. 4.10. Mass size distribution of CCP and aluminum in CCP (shadowed) at different length of protecting tube.

Propellant EB, pressure 22 atm, particle > 60 μm.

Fig. 4.11. Mass size distribution of CCP and aluminum in CCP (shadowed) at different length of protecting tube.

Propellant EB, pressure 44 atm, particle > 60 μm.
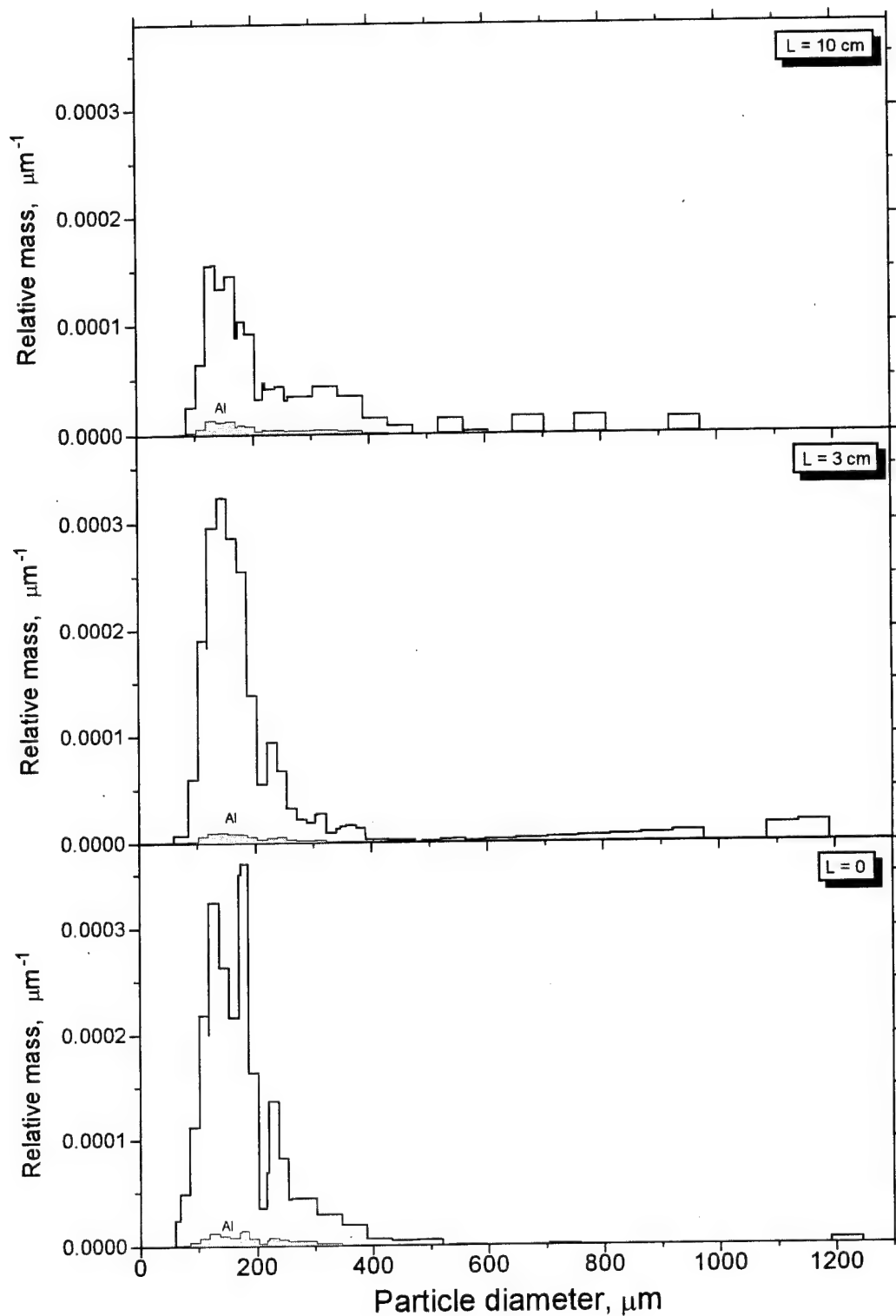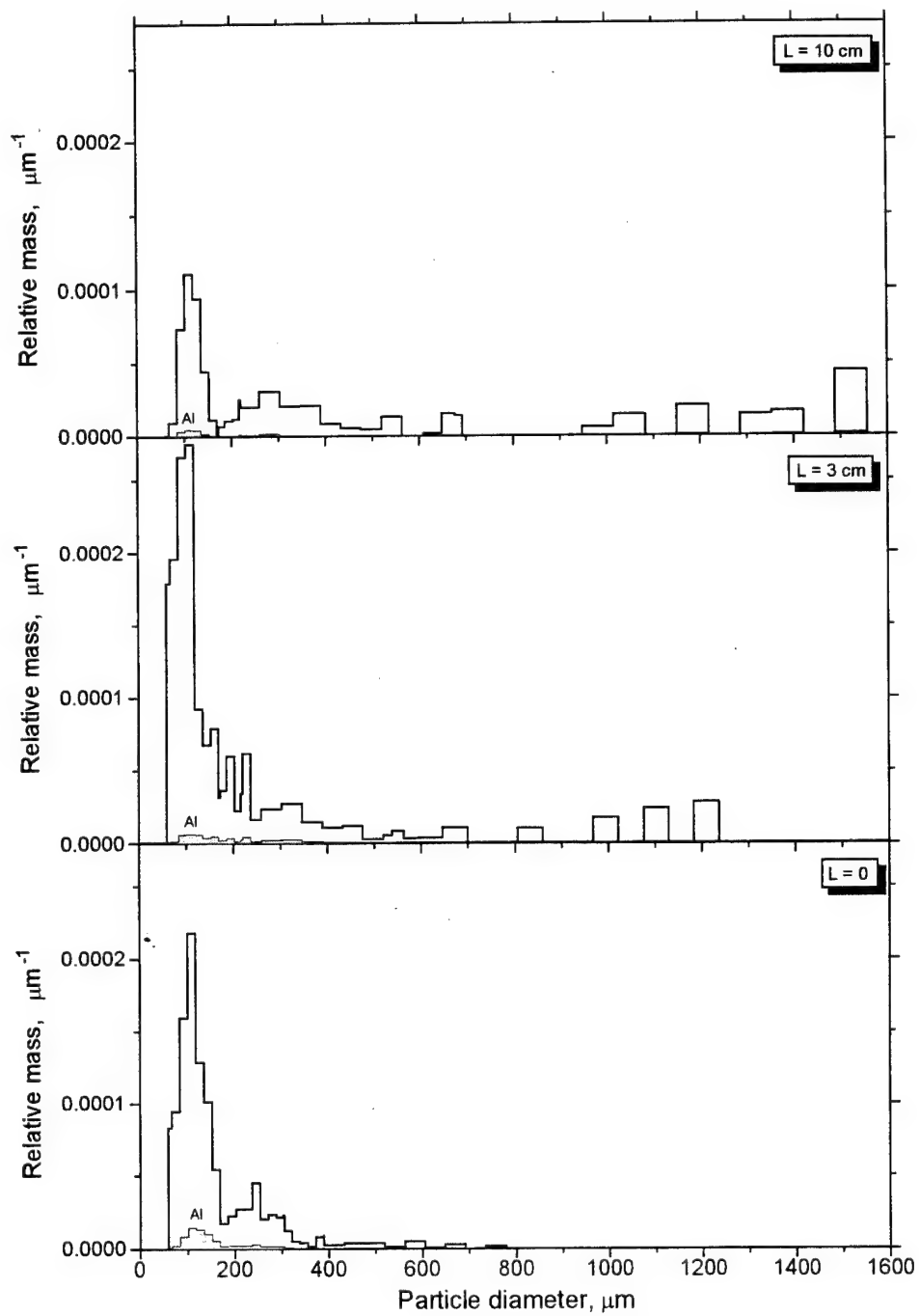
Fig. 4.12. Mass size distribution of CCP and aluminum in CCP (shadowed) at different length of protecting tube.

Propellant EB, pressure 84 atm, particle > 60 μm.

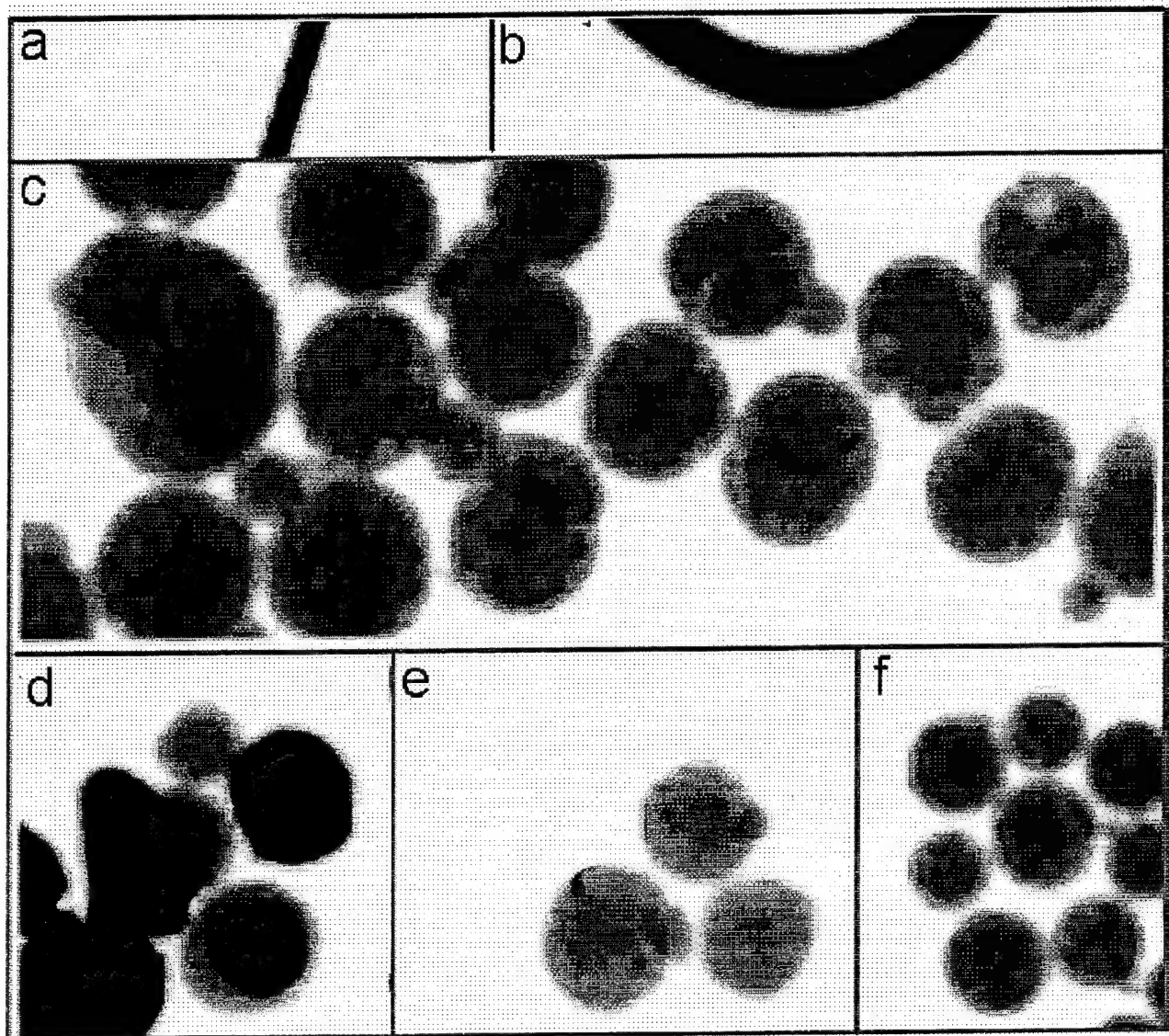Fig. 4.13. X-ray images of CCP particles and nichrome wire.

a - nichrome wire, d=300 μm.

b - nichrome wire, d=500 μm.

c - CCP particles, propellant IB, 44 atm, L = 3 cm, fraction > 1060 μm.

d - CCP particles, propellant EB, 81 atm, L = 10 cm, fraction 590-880 μm.
(The compact solid particle is covered with layer of less density).

d - CCP particles, propellant EB, 83 atm, L = 0, fraction 590-880 μm.

f - CCP particles, propellant IB, 85 atm, L = 0, fraction 480-590 μm.
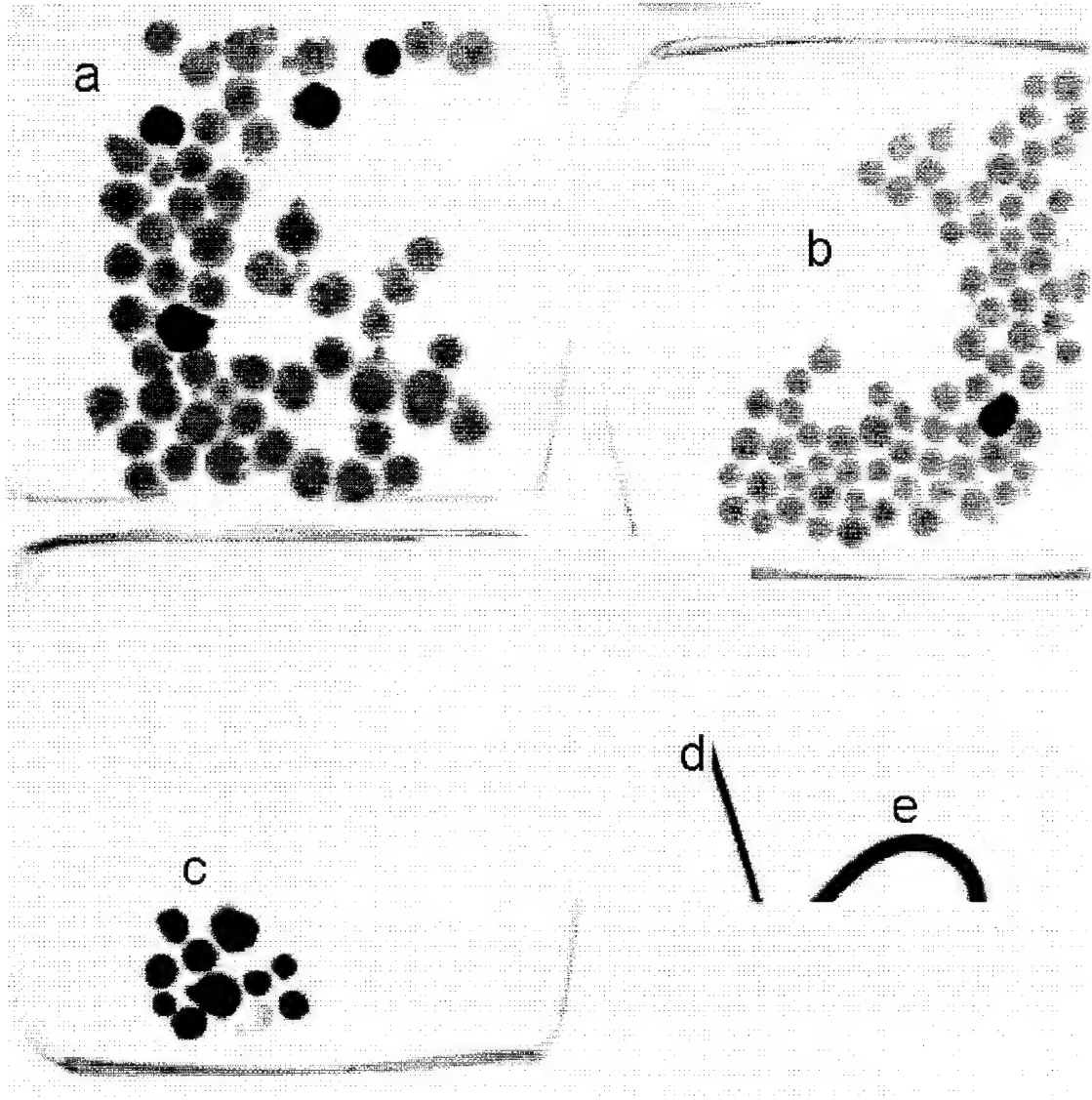
Fig. 4.14. X-ray images of CCP particles and nichrome wire.

a - CCP particles, propellant IB, 43 atm, L = 3 cm, fraction 880-1060 μm.
b - CCP particles, propellant IB, 85atm, L = 0, fraction 590-880 μm.
   (The fraction includes small portion of nichrome particles).
c- CCP particles, propellant EB, 45 atm, L = 3 cm, fraction 590-880 μm.
   (The fraction consists mainly of nichrome particles).
d - nichrome wire, d=200 μm.
e - nichrome wire, d=400 μm.

Fig. 4.15. Comparison of characteristic sizes D_{43} of CCP particles for propellants IB and EB at different pressures.

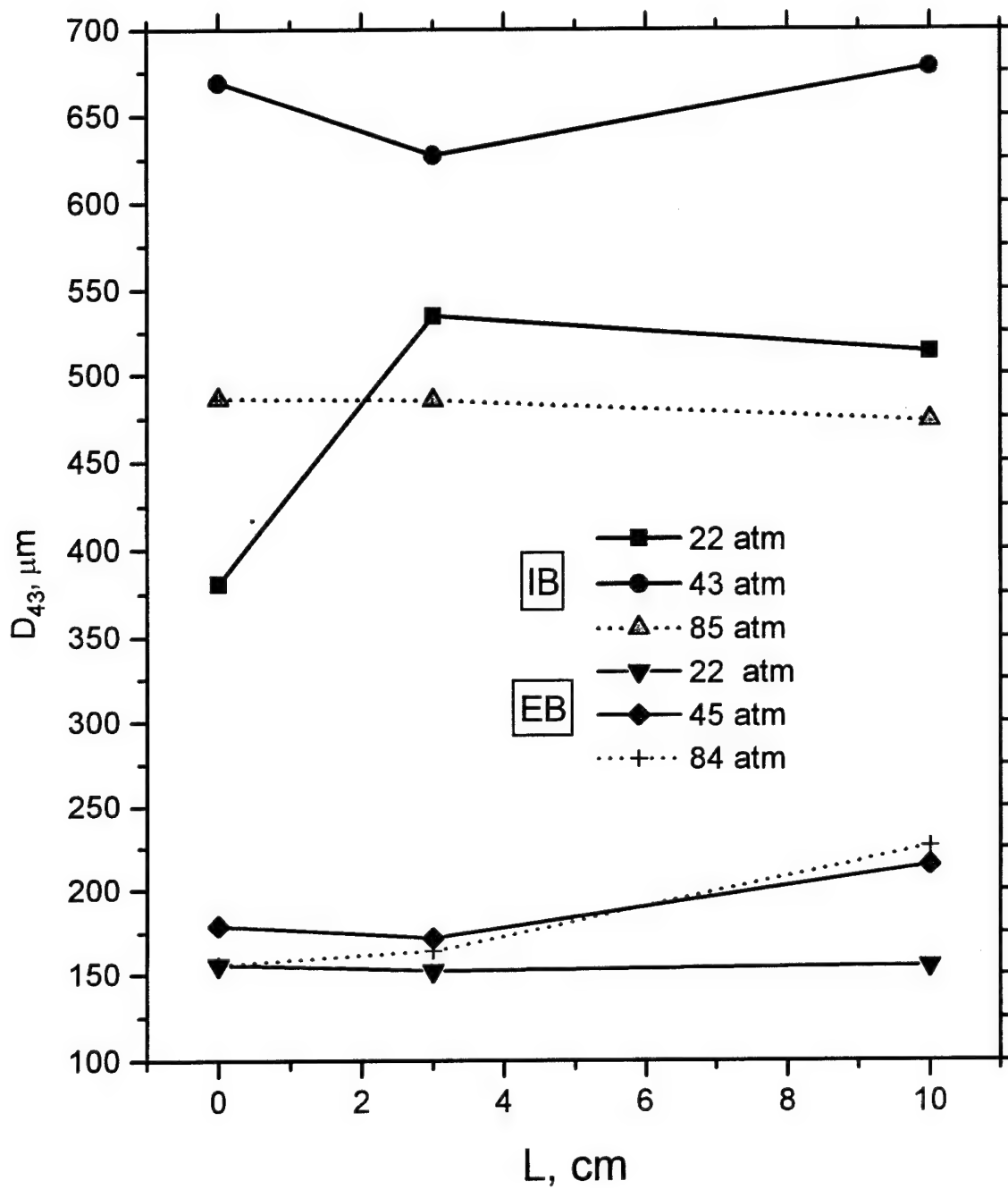## 4.6. Density of coarse CCP particles.

In the literature there is a very few data on agglomerate density [7, 23, 24, 27, 34, 35].

In present work the agglomerate density was determined for individual fractions of CCP with size exceeding 80 μm. To obtain density value a given CCP meshed fraction was placed on the inclined copper plate to eliminate electric charge and particles of round shape have been chosen. After that the particles were weighed and examined by microscope. The density was calculated by the formula

$$\rho = m \Big/ (N \frac{\pi}{6} D_{30}^3),$$

where m is the mass of the particles, N is their number, D_{30} is the average size.
The estimated error was calculated by

$$\Delta\rho = \rho \cdot \sqrt{\left(\frac{3\Delta D_{30}}{D_{30}}\right)^2 + \left(\frac{\Delta m}{m}\right)^2 + \left(\frac{\Delta N}{N}\right)^2}.$$

To calculate $\Delta\rho$ the instrumental errors of the method were taken as
- ΔD_{30} = 9, 22, 30-40 μm - in dependence of size,
- Δm = 0.00015 g (scale characteristic),
- ΔN = 0.

A reproducibility of the experimental data can be illustrated by the results obtained in identical conditions of firing.

Fig. 4.16 gives mean density of CCP particles collected in two separate experiments on combustion of propellant IB at pressure 85 atm (L=0). It can be easily recognized that within the relatively large scatter of the results the particle density is practically the same over the whole range of sizes. It can be also concluded that if the magnitude of coefficient of proportionality is about 0.00015 it really corresponds to zero dependence of particles density on their size.

Figures 4.17 and 4.18 present data for IB and EB propellants combusted at different pressures with tube length varied.

It is seen that with propellant IB the density of coarse CCP particles practically does not change with size while in case of propellant EB there is trend to the rise of mean density with particle size. At the same time it should be noted that a large amount of particles have density less than 2.7 g/cm³ (neat aluminum density). This indicates that the agglomerates are not compact solid particles.

Figures 4.19 and 4.20 present data for propellant EB on CCP particles density in dependence on pressure and aluminum content. It has been analyzed above that pressure rise from 22 to 84 atm increases aluminum depletion degree in case of propellant EB combustion. This causes increase of relative content of aluminum oxide in CCP particles and, as a result, increase of particles density. In case of propellant IB the depletion degree of aluminum is almost the same under varied conditions of firing and density of coarse CCP particles is not changed at different conditions, see Fig. 4.21. Finally, Fig. 4.22 presents summary data on coarse particles density for both propellants and all conditions of firing.
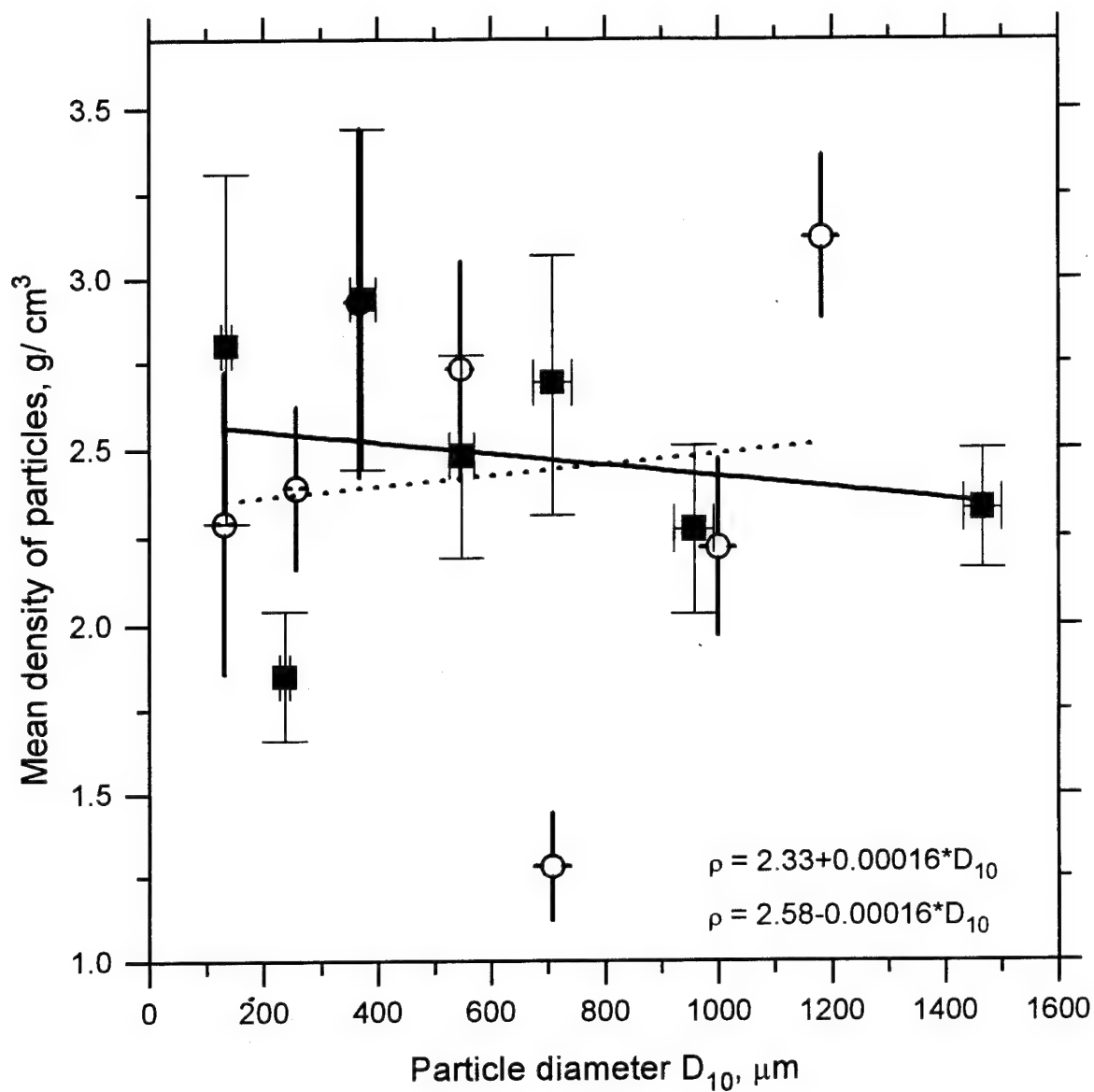
Fig. 4.16. Mean density of coarse CCP particles vs particle diameter. Propellant IB, P= 85 atm, L=0. Data for two individual firing tests.
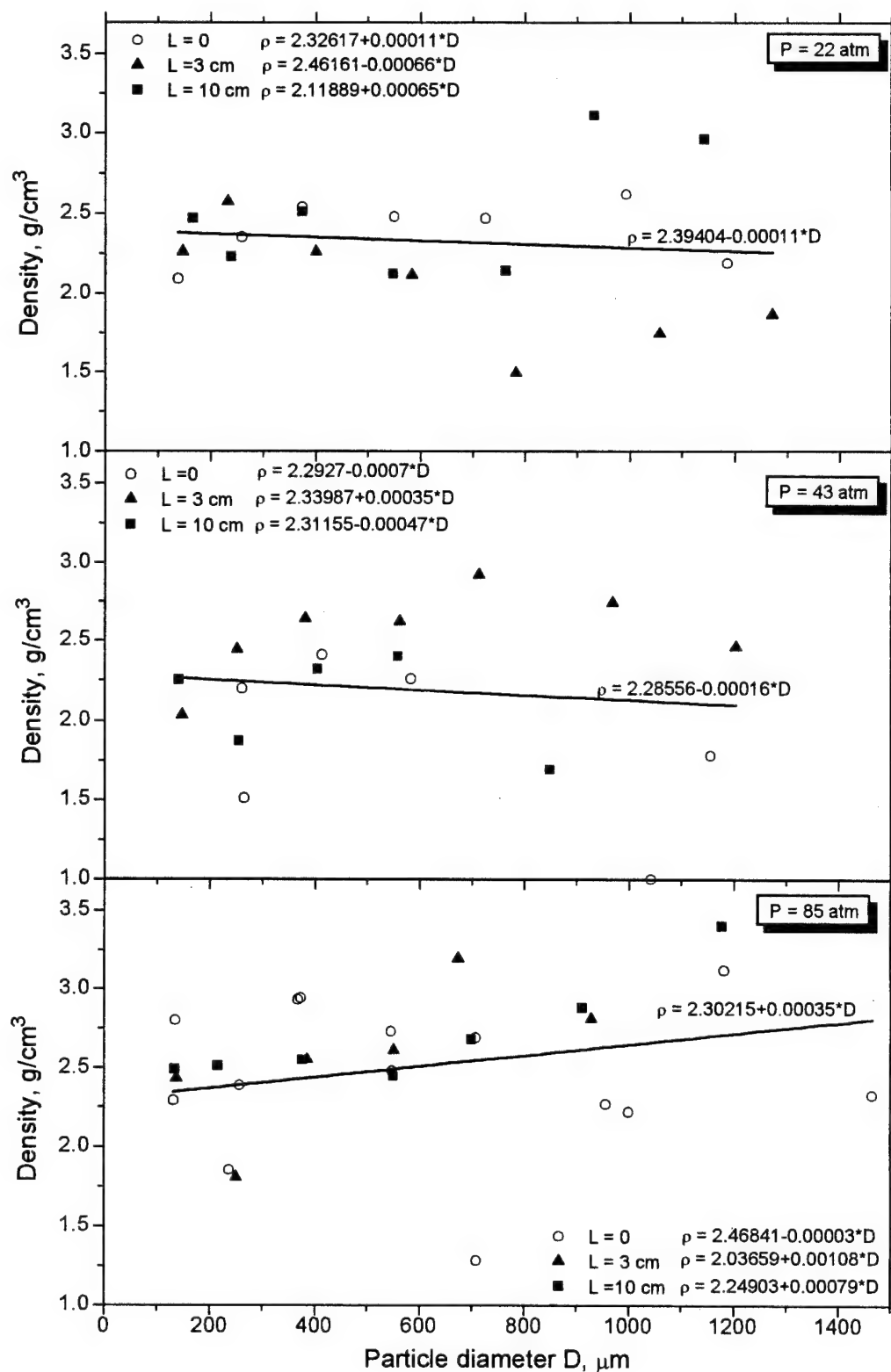
Fig. 4.17. Mean density of coarse CCP particles vs particle diameter. Propellant IB.
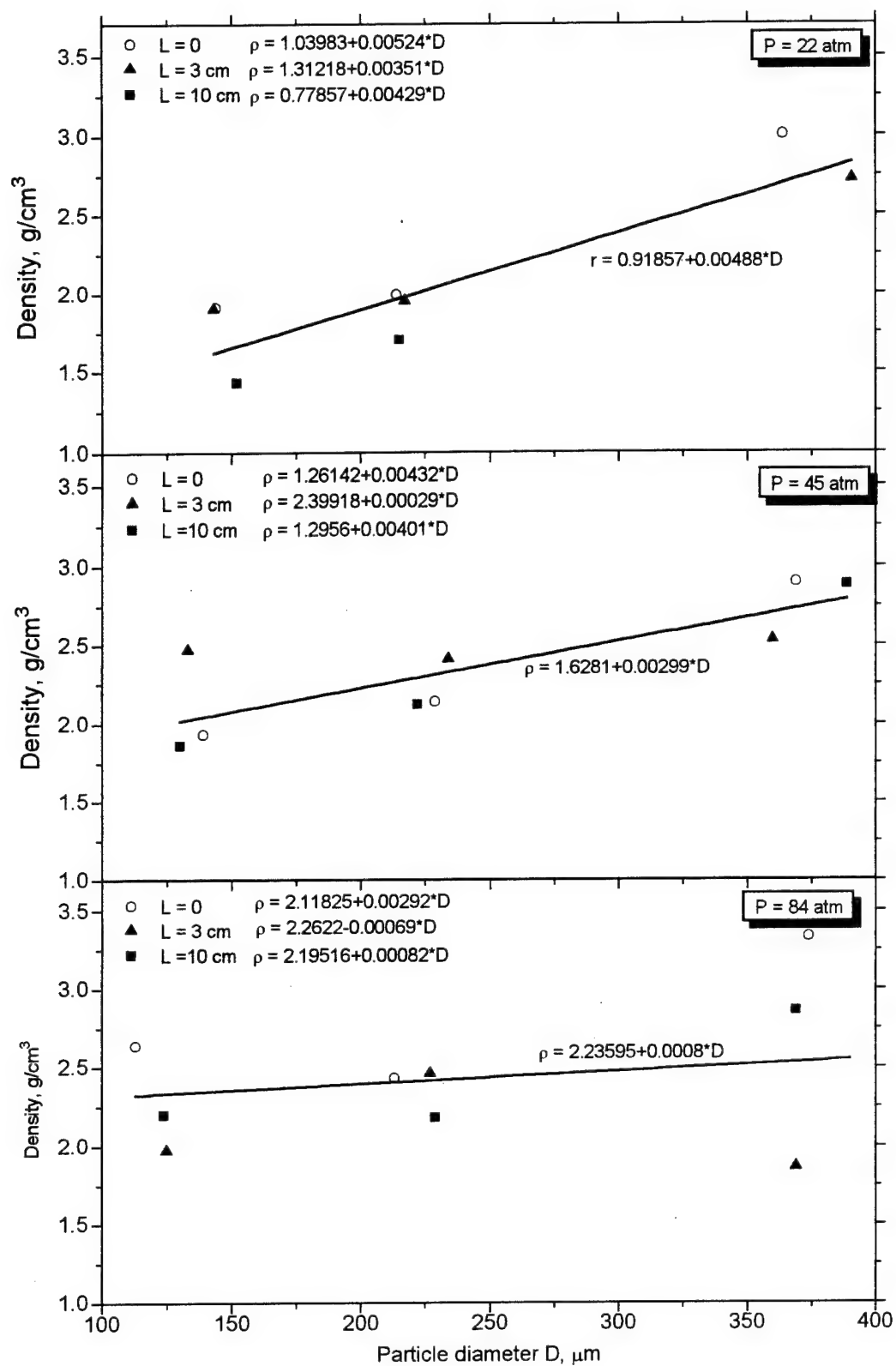
Fig. 4.18. Mean density of coarse CCP particles vs particle diameter. Propellant EB.
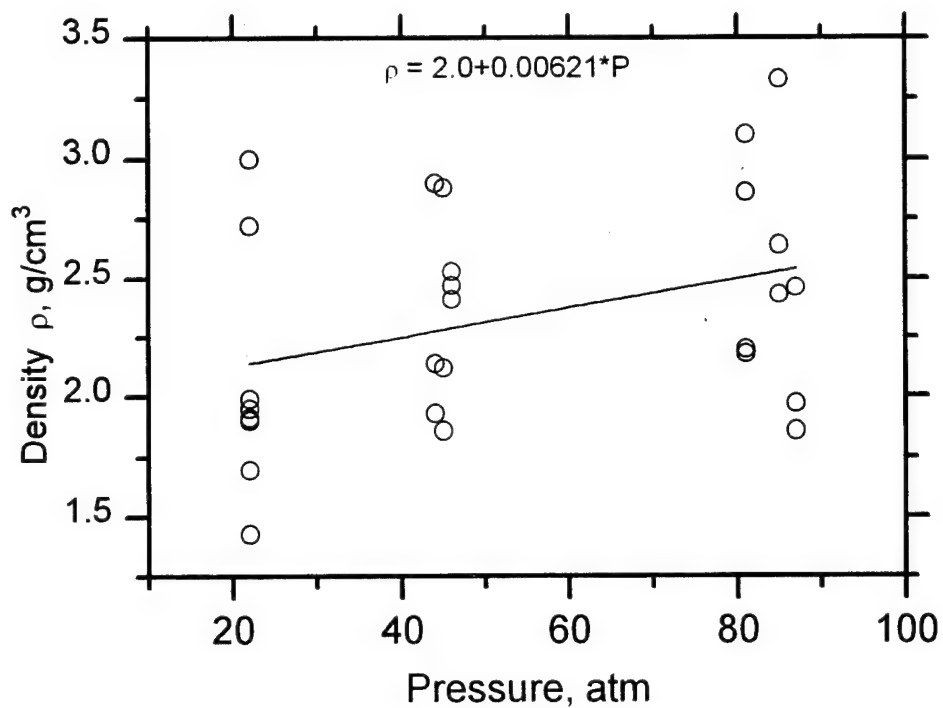
Fig. 4.19. Correlation between density of coarse particles and pressure. Propellant EB.

Fig. 4.20. Correlation between density and aluminum content in coarse particles.
Propellant EB.

Fig. 4.21. Absence of correlation between density and aluminum content in coarse particles. Propellant IB.

Fig. 4.22. Summary data on density of coarse CCP particles for propellants IB and EB correlated at different conditions of firing.

4.7. Morphological analysis of coarse CCP particles

4.7.1. The types of particles.

The CCP coarse particles (> 80 μm) were examined by optical stereoscopy microscope with magnification up to 56^X. The appearance of particle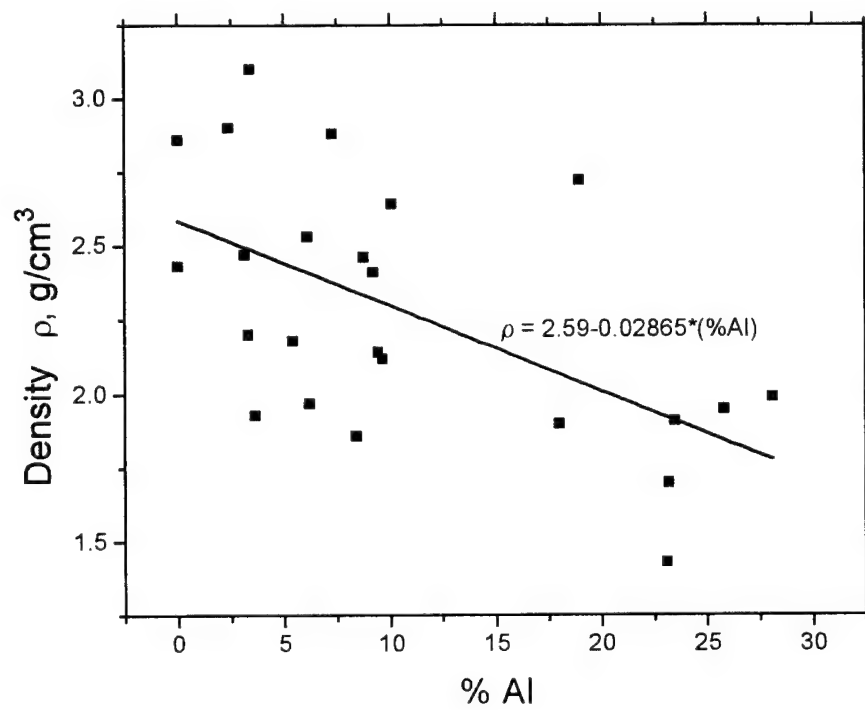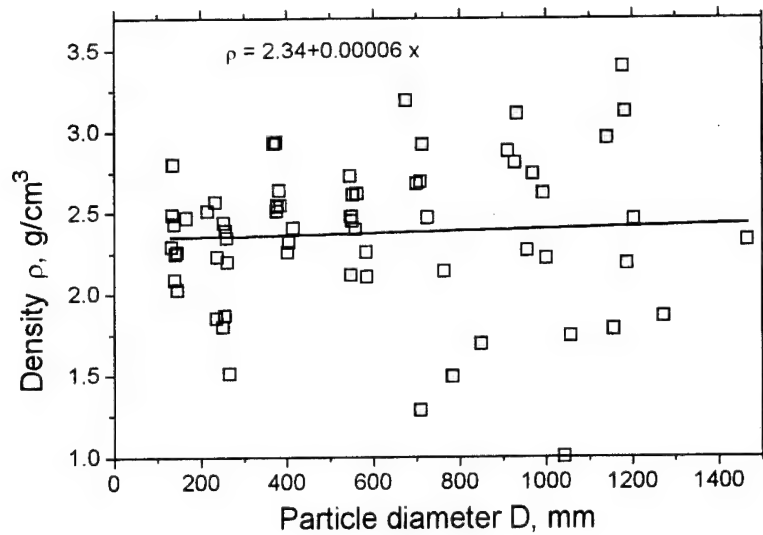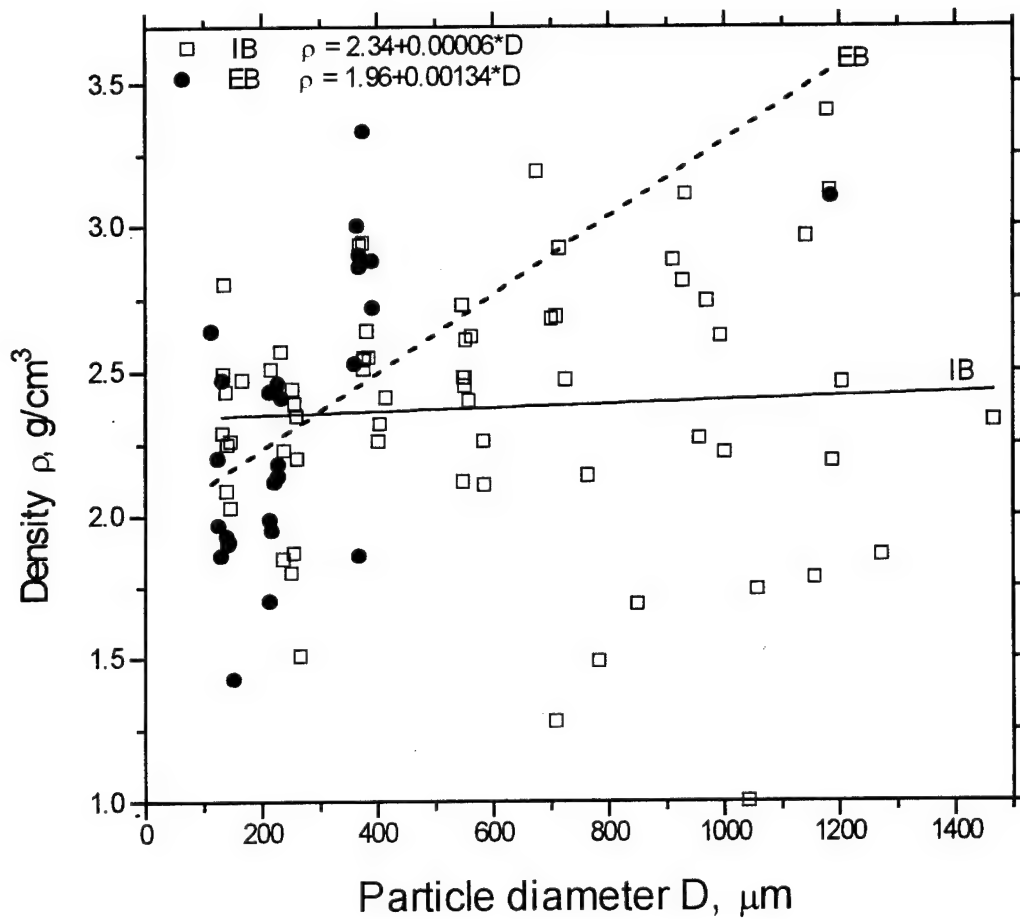s was different depending on the size and nature of material. Table 4.4 presents summary of the visualization data which is followed by description of typical view of collected particles.

Table 4.4. Content of certain type particles in coarse CCP fractions.
The sequence of listing corresponds to the frequency of observations.

Fraction size, μm	Propellant IB	Propellant EB
80 - 160	AggFl, Agg, OxC	AggFl, OxC, Agg
160-280	AggFl, OxC, Agg, OxH, AP	AggFl, OxC, Agg
280-480	Agg, OxC	Agg, OxC
480-590	Agg	Agg
590-880	Agg, AggIrr	Agg
880-1060	Agg	-
> 1060	Agg	-

Agg	-	agglomerate,	AP	- ammonium perchlorate,
AggFl	-	flake of agglomerates,	OxC	- compact oxide,
AggIrr	-	irregular agglomerate,	OxH	- hollow oxide.

Agg (agglomerate) - major condensed product of metallized propellant combustion with size in the range 80-2000 μm. The particles have spherical or acorn-type shape and are covered with hard surface layer of dark gray or black color. As a rule, there is a hole in a surface layer through which a non-compact material consisting partly of individual small spheres can be seen. Sometimes this material overflows the edge of hole.

A hard layer probably consists of aluminum oxide because it does not react with NaOH solution while non-compact material reacts actively that is easily detected by gas bubbles release, Fig. 4.23. When etching in NaOH, the agglomerate releases through the hole some unsolved condensed products (flake) that may indicate the presence of some amount of aluminum oxide inside agglomerate. The final residue after long time etching in NaOH is hollow spherical shell with hole. It can be seen through the hole a wrinkled interior surface of the shell.

A hard surface layer in the case of extra large agglomerates (> 590 μm) has some cracks that enables measuring the thickness of layer. The mean layer width appears to be about 30 μm.

The smaller agglomerates have thicker surface layer. In the extreme case the agglomerate consists of white or transparent sphere with small pit containing some quantity of aluminum. The visual examination of a large amount of agglomerate particles allows to describe the evolution of their exterior appearance as shown in Fig. 4.24. The main portion of particles examined with microscope corresponds to type Fig. 4.24, c. However, in case of combustion of propellant IB at 85 atm, L=0, an original agglomerate particle with two opposite side cap of aluminum oxide was observed in fraction 80-160 μm.
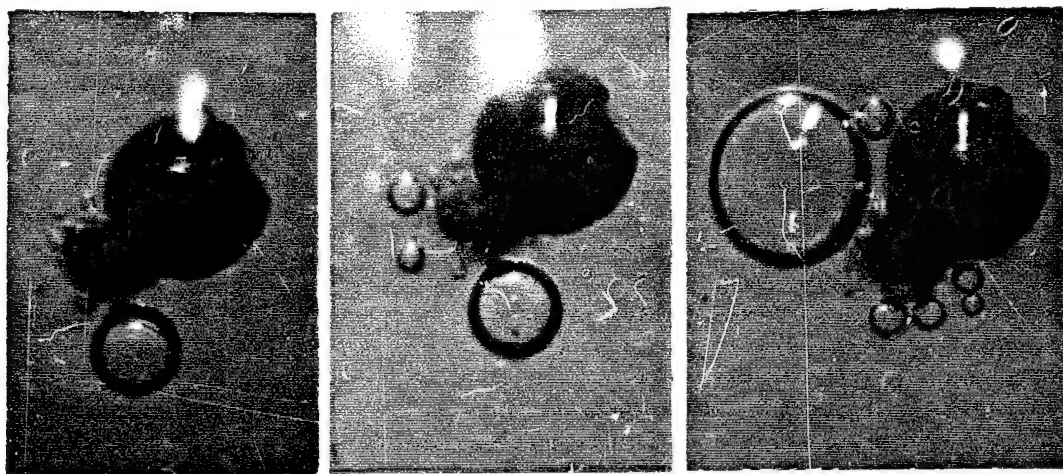
Fig. 4.23. Gas release at the etching of single Agg-type CCP particle by 1 % NaOH solution. Time interval between pictures is about 5 seconds.
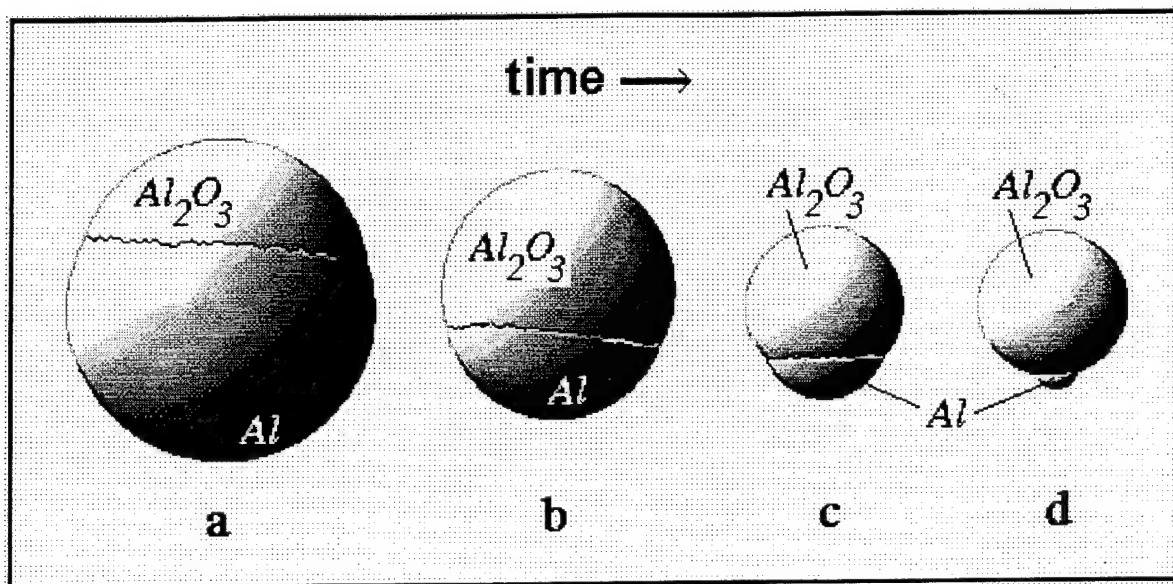

Fig. 4.24. Assumed scheme of the evolution of Agg-type CCP particle. While aluminum burns out, the oxide lobe becomes thicker and occupies more part of surface and volume of agglomerate.

AggFl (flake of agglomerates) - non-spherical shape aggregates of sintered small particles of partly oxidized aluminum or pure oxide. The possible way to form flake of agglomerates is to sinter CCP particles during their deposition on the metal screens installed above the collecting filter. The flakes of agglomerates particles do not destroy in course of wet sieving of CCP. They contribute up to 90 % of mass in fraction 80-160 μm.

AP (ammonium perchlorate) - grains of oxidizer with size up to 200 μm. Their contribution into total amount of CCP is negligibly small.

AggIrr (irregular agglomerate) - grapes shape irregular accumulate with characteristic size 250-500 μm consisting of spherical particles. There was observed relatively small number of AggIrr for both propellants at L=0 and L=3 cm. They correspond to detached from the burning surface the non-ignited aggregates of aluminum particles.

OxC (compact oxide) - solid oxide particles with maximum size about 200 μm. White color, sometimes transparent.

OxH (hollow oxide) - hollow oxide shell without metal inside. Color and size of these particles is similar to compact oxide particles, but quantity is smaller.

Two special chemical analysis were made with non-spherical (AggFl) and spherical (Agg+OxC) particles in order to compare aluminum content. The results are summarized below:

Propellant EB, P=84 atm, L=0,	Size range 160-480 μm:	AggFl	- 5 % Al,
		Agg+OxC	- 8 % Al
Propellant EB, P=81 atm, L=10 cm,	Size range 80-280 μm:	AggFl	- 3.3 % Al
		Agg+OxC	- 5.4 % Al

In subsequent treatment of the experimental data the aluminum content in CCP particles was averaged taking into account the relative contribution of AggFl and (Agg+OxC) particles in total mass of CCP fractions.

4.7.2. X-ray flash photography examination of CCP particles.

The coarse CCP particles were studied via X-ray photography in order to determine their spatial density distribution.

A commercial X-ray source IMA-5 was used with effective size of emission spot about 2.7 mm and radiation scattering angle about 40°. The voltage pulse was 100 kV in amplitude and 40 ns in duration. The distance between X-ray source and recording film was 0.6 to 1 m. The particle were placed directly on the visible light protected envelope with film so as the magnification was equal 1^X. The commercial film RT-1 with sensitivity $S_{0.85} \geq 25$ R^{-1} was used. The negative images of particles were examined using high resolution projection scanner UniScan (2048x2800 pixels). The spatial resolution of the film and scanner was about 40 μm.

It has already been mentioned that X-ray photography allowed to determine nichrome pollutants among CCP particles. Another finding can been illustrated by Fig. 4.25. It is seen that:

• There are particles mostly with non-uniform distribution of density, Fig. 4.25, a, c, e, f. In case of uniform density particles, Fig. 4.25, b, d, the attenuation of X-ray gradually increases when going to the center of particle and equidensity lines have regular round shape.

• The particles density does not simply correlate with size and combustion test conditions.

To get more detail information on particle density distribution it is necessary to improve spatial resolution of the technique.
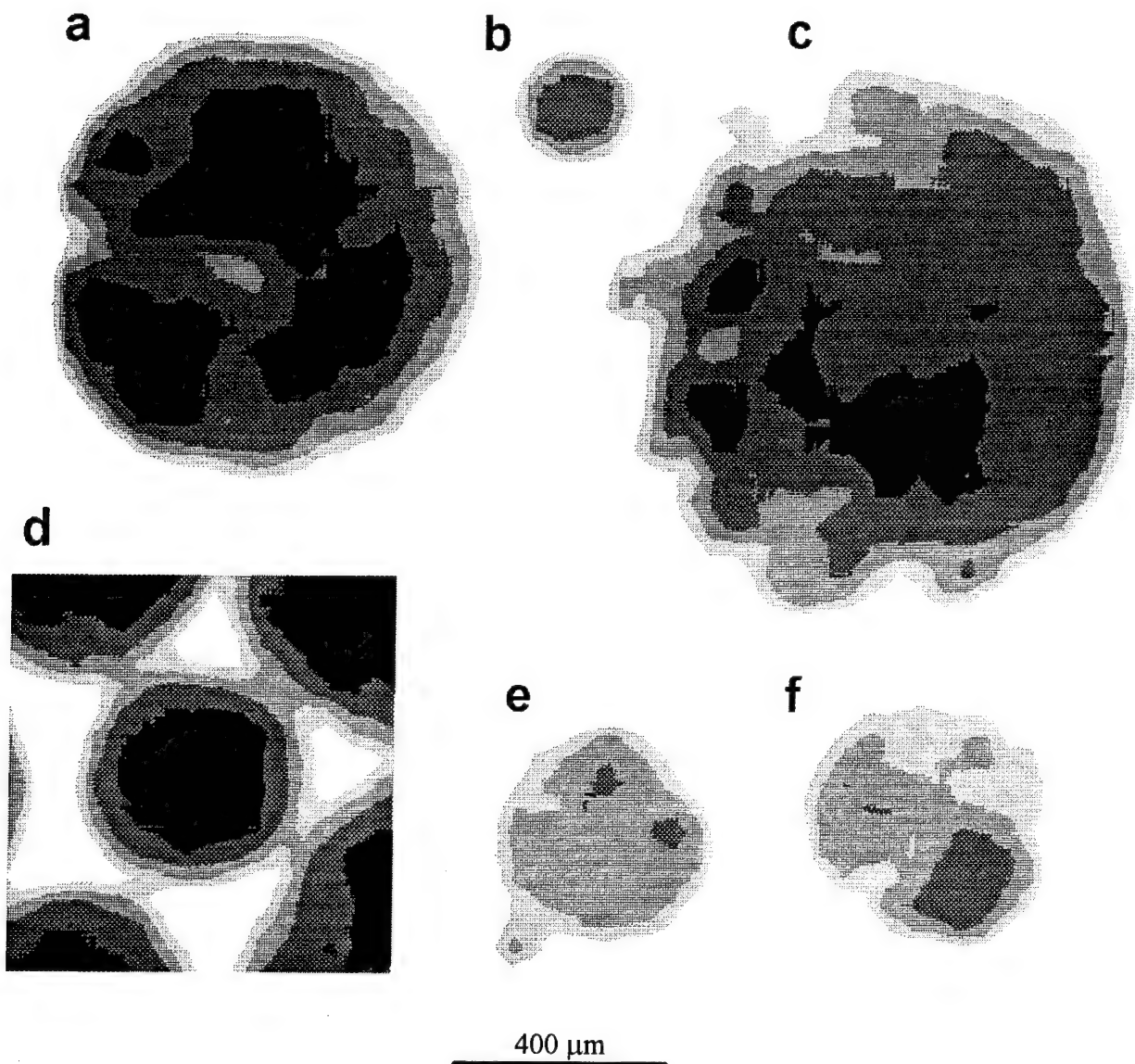
Fig. 4.25. X-ray images of CCP particles (a, b, c, e, f) and AP particles (d). The images are colored by five level of gray (including white).

a - Propellant IB,   pressure 85 atm,   L=0,   particle from fraction 590-880 μm;
b - Propellant IB,   pressure 85 atm,   L=0,   particle from fraction 280-480 μm;
c - Propellant IB,   pressure 44 atm,   L=10 cm,   particle from fraction >1060 μm;
d - AP particle among another AP particles, fraction 630-880 μm;
e - Propellant IB,   pressure 85 atm,   L=0,   particle from fraction 480-590 μm;
f - Propellant IB,   pressure 85 atm,   L=0,   particle from fraction 880-1060 μm.

4.8. CCP particles smaller than 60 μm.

4.8.1. Preliminary notes (particle's origin, analysis and collection peculiarities).

The results of chemical analysis have shown that CCP fraction < 80 μm in both propellants contains less than 0.7 % mass of neat aluminum. Hence, the particles of < 80 μm in size are mostly alumina containing. At the same time, according to the results of experiments with non-metalized propellants IBN and EBN, there is remarkable amount of carbon-based small CCP particles with size less than 60 μm. One may assume that similar particles could form upon combustion of metalized propellants as well. The size distribution of small particles was determined by Malvern 3600E particle sizer based on light scattering principle. For clarity, we will use below the figures of corresponding size sub-range (SSR) in order to identify the size of certain particle. The correspondence between SSR figure and dimension size range is shown in Table 4.5.

Table 4.5. Correspondence between No. of SSR and dimensional size sub-range (SSR) for histogram of particle sizer Malvern 3600E in mode with lens F=63 mm.

No. of SSR	Left bound, μm	Right bound, μm
1	0.5	1.2
2	1.2	1.5
3	1.5	1.9
4	1.9	2.4
5	2.4	3.0
6	3.0	3.9
7	3.9	5.0
8	5.0	6.4
9	6.4	8.2
10	8.2	10.5
11	10.5	13.6
12	13.6	17.7
13	7.7	23.7
14	23.7	33.7
15	33.7	54.9
16	54.9	118.4

The left bound of the first SSR (0.5 μm) has conventional meaning. More correctly, the 1-st SSR contains particles with size less than 1.2 μm. However, the time of particle sedimentation during filter matter removing was specially chosen in the way to precipitate particles > 0.5 μm size. One may expect that the most portion of < 0.5 μm in size particles was left in the carrier liquid. In present work the technique of collection of small CCP particles on the filter had some unpleasant peculiarities. Due to the nature of combustion products and to the relatively low room temperature (it amounted +14°C), the liquid condensate formed on internal walls of cylinder (Fig. 3.1, *3*) as well as on the metallic screens

(Fig. 3.1, *5*) mounted above the filter. If the condensate drop occasionally left down on the filter, the 1-4 holes with size of 1-2 mm formed that resulted in uncontrolled loss of particles with size less than 80 μm (the mesh size in the closest to filter metallic grid). The information about damage of the filter is indicated in Table 4.6. Note that the higher the pressure the more the probability of filter damage.

Table 4.6. Full list of experimental series conditions and main parameters

Propellant	Pressure P, atm	Tube length L, cm	Filter state: D-damaged, ND - safe	Burning rate r, mm/s	Residence time calculated for gas, ms	R_Σ	$R_<$
IB	22	0	ND	8.9	6	0.38	0.19
IB	22	3	ND	11.0	9	0.33	0.14
IB	21	10	ND	10.2	22	0.36	0.20
IB	43	0	ND	10.8	9	0.35	0.16
IB	44	3	D	10.3	19	0.46	0.27
IB	43	10	ND	14.4	29	0.39	0.20
IB	85	0	D	12.7	16	0.47	0.28
IB	84	3	ND	14.3	27	0.41	0.22
IB	84	10	D	12.8	66	0.45	0.24
EB	22	0	ND	12.4	4	0.37	0.30
EB	22	3	ND	10.6	10	0.39	0.28
EB	22	10	ND	13.5	17	0.43	0.36
EB	44	0	ND	15.6	7	0.60	0.57
EB	46	3	D	16.6	13	0.47	0.44
EB	45	10	ND	14.2	32	0.66	0.64
EB	85	0	ND	no data	12	0.53	0.51
EB	87	3	D	19.1	22	0.39	0.36
EB	80	10	D	14.7	68	0.47	0.45
IBN	22	0	D	10.0	$8^{*)}$	0.17	≈0.17
IBN	85	10	ND	14.8	$7^{*)}$	0.12	≈0.12
EBN	23	0	D	13.3	$6^{*)}$	0.09	≈0.09
EBN	86	10	D	18.9	$21^{*)}$	0.35	≈0.35

*) - calculated at T_f = 2500 K.

4.8.2. The reproducibility test.

Figure 4.26 presents the plots with mass size distribution of CCP particles less than 60 μm in size and calculated particle mean sizes obtained after treatment of experimental results for propellant IB in two series of runs: one with damaged and another one with non-damaged filter. The most pronounced difference in size distributions is observed in the range of small sizes (1 and 2 SSR) that can be attributes to the loss of tiny particles through the holes in the filter. In these experiments the ratio $R_<$ = (mass of CCP particles < 60 μm)/(mass of propellant

sample) was equal 0.31 and 0.28 for the run with non-damaged and damaged filter, correspondingly. The fact of the filter damage is reflected in Fig. 4.4 as enhanced experimental data scatter.
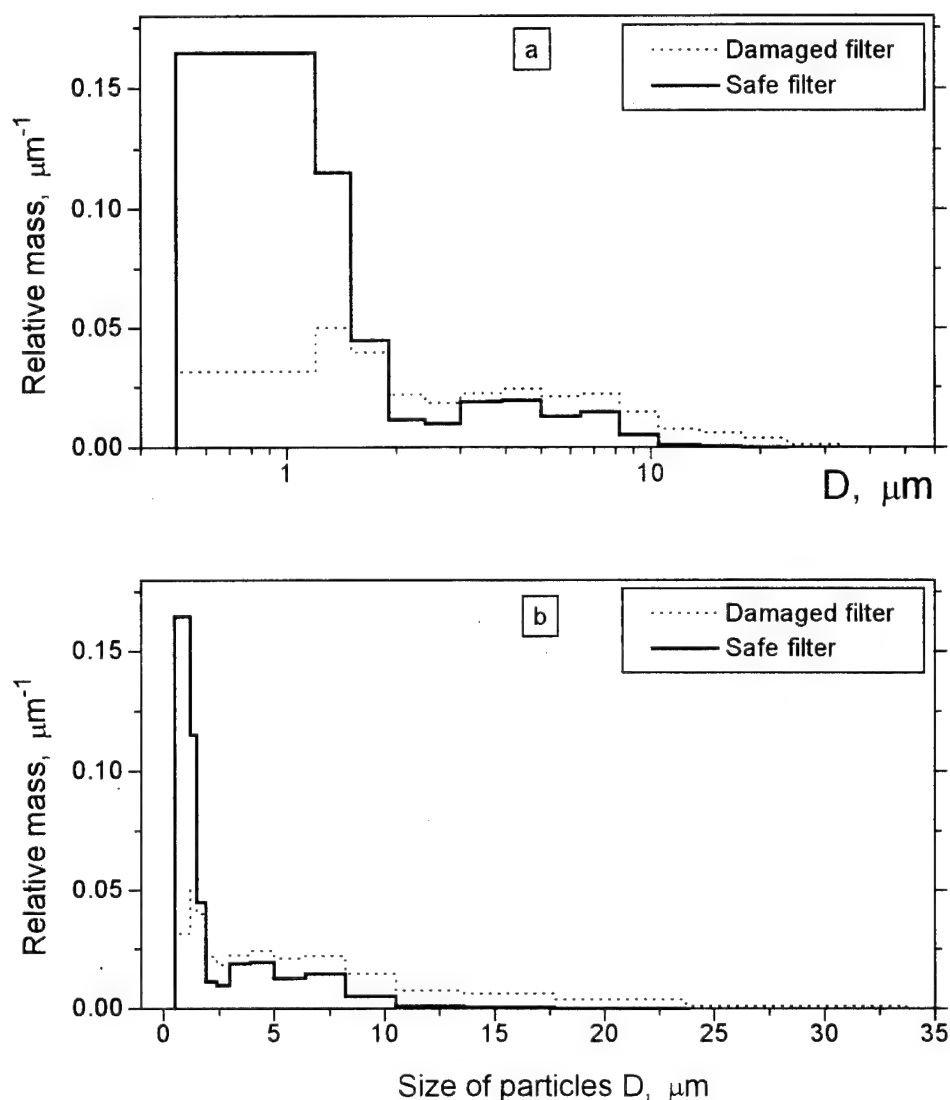
Fig. 4.26. Mass size distribution of CCP particles less than 60 μm in logarithmic (a) and linear (b) coordinates. The results of two parallel series at the same conditions are shown. In one of them the filter was damaged and some fraction of particles was lost through the holes.
Propellant IB, pressure 85 atm, L=0.

Mean diameter D_{mn} calculated in size range 0.5-60 μm

	Mean diameter D_{mn}, μm						
	D_{10}	D_{20}	D_{30}	D_{21}	D_{32}	D_{43}	D_{53}
Without loss	0.9	1.0	1.1	1.0	1.4	3.0	4.3
With loss	1.1	1.3	1.9	1.6	3.6	8.7	11.6

4.8.3. CCP particles of less than 60 μm size, propellant IB.

Figures 4.27-4.29 present the experimental data on size distribution of fine CCP particles of propellant IB. Characteristic mean sizes are presented in Table 4.7a.

Let analyze in detail Fig. 4.27 because all experiments at pressure 22 atm were conducted with non-damaged filters. The bottom plot presents also mass size distribution of CCP for non-metalized propellant IBN (dotted curve). It was drawn using scaling coefficient 0.82 (to take into account the aluminum content in propellant IB). This curve can be treated as potential contribution of CCP from non-metalized portion of propellant IB into total mass of CCP for this propellant. It is easy to recognize that CCP of non-metalized propellant have sizes less than 18 μm with maximum of distribution being in 6-th SSR. When comparing mass size distributions for IB and IBN propellants, it is seen that they are not similar. This may result from the fact that the temperature of combustion of metalized propellant is higher and the contribution of non-metalized part of propellant in total amount of CCP is not significant. At L = 3 cm, P = 22 atm one may recognize 3 characteristic peaks on mass size distribution. These are D, E and F which correspond 2-3, 6-7 and 9th SSR. Similar peaks can be recognized at pressures 43 atm and 84 atm. The existence of these peaks should be checked by independent experimental data. However, there are literature data reporting on multi-modal size distribution of CCP for aluminized propellants [21, 22, 35]. In particular, in combustion of propellant with 15% aluminum at 40 atm there were found the peaks corresponding to submicron and 3-4 μm sizes [21]. When residence time for particles increased from 6 to 19 and to 31 ms the peaks changed appropriately from 0.4 to 0.5 and to 0.7 μm in submicron size range and from 3.6 to 3.9 and to 4.3 μm in micron size range. The mean mass diameter of particles D_m calculated in the range 0-20 μm changed according the relationship [21] $D_m = 3.3 \cdot exp(0.01 \cdot t)$, where t is residence time.

The plots with time dependence of characteristic particle sizes for propellant IB (pressure 84 atm) are shown in Fig. 4.30 in comparison with data [21].

4.8.4. CCP particles of less than 60 μm size, propellant EB.

Figures 4.31-4.33 present mass size distribution of CCP particles for propellant with energetic binder. Characteristic mean sizes are presented in Table 4.7b.

Let analyze plots in Fig. 4.31 (pressure 22 atm, propellant EB). The bottom plot shows mass size distribution of CCP particles for non-metalized propellant EBN which is drawn using scaling coefficient 0.82 (to take into account the aluminum content in propellant EB). The exterior appearance of CCP for propellant EBN is similar to that for propellant IBN but their potential contribution to total amount of CCP for propellant EB is rather small. As in the case with propellant IB, the peaks D, E, F corresponding to 1-3, 6-7 and 9th SSR can be recognized in Fig. 4.31. The amplitude of the D-peak increases when L increases. Because of remarkable depletion of neat aluminum with L (see Fig. 4.8, $\eta(t)$) it can be assumed that enhancement of mass in submicron SSR (D-peak) occurs due to formation of submicron oxide particles resulted from aluminum combustion in vapor regime. With L = 10 cm E and F peaks merge and the relative mass of particles of size more than 10 μm increases. It can be supposed that these particles form due to complete burn out of agglomerates. Indeed, according to theoretical and experimental findings [9, 10] about 17% of theoretical available oxide is deposited on the burning drop of aluminum. Therefore, the residual oxide mass can be calculated by $m_{ox} = m_{Al} \cdot 0.17 \cdot 1.889 \cong 0.32 \cdot m_{Al}$, where 1.889 is the stoichiometry coefficient in conversion aluminum into Al_2O_3. In terms of diameters one obtains

$$D_{ox} = D_{Al} \cdot \sqrt[3]{0.32 \cdot \frac{\rho_{Al}}{\rho_{ox}}} \cong 0.61 \cdot D_{Al} \cdot$$

Taking D_{43} as D_{Al} which is equal 29 μm for aluminum powder under study, one obtains D_{ox}=18 μm. The presence in CCP of oxide particles of this size may indicate that some part of virgin aluminum particles burns individually in propellant EB flame and gives oxide particles in the range 10-40 μm. It is interesting to note that the sum of ignition delay and burn out times for 30 μm aluminum particles is about 10 ms [2, 34] that agrees well with calculated residence time for aluminum particles in flame of propellant EB at L = 3 cm (12 ms) and L = 10 cm (19 ms). It should be noted that complex transformation of size distribution of CCP particles under discussion leads to non-monotonous change in D_{mn} values with tube length (Table 4.7b). As addition, in Tables 4.7c and 4.7d there are presented characteristic mean sizes D_{mn} for CCP particles of propellants IBN and EBN.

4.8.5. Unified features of small oxide particles formation and evolution.

Let examine evolution of the mass size distribution for small particles (< 60 μm) in dependence only on residence time in flame environment. To this end, we will treat the results of experiments with non-damaged filter. The sequences of distributions for propellants IB and EB are shown in Figs. 4.34, 4.35. For both propellant 3 peaks on distributions can be recognized: D (1-3 SSR, 0.5-1.9 μm), E (6-7 SSR, 3-5 μm), and F (9 SSR, 6.4-8.2 μm). The D-peak is higher than others by 1.3-2 times. Due to relatively large experimental data scatter it is difficult to discuss variation of the characteristic particle size and/or amplitude of the peak with time. However, the amplitude peak value correlates with completeness of aluminum combustion in propellants IB and EB. Note, that according to chemical analysis data the consumption of aluminum stops and the discussed size distributions correspond to the evolution of oxide particles after quenching of aluminum combustion (agglomerate combustion). It is seen from Figs. 4.34, 4.35 that the shape of size distribution function for small particles is conservative in spite of the change of the binder type and variation of large agglomerate size (D_{43} = 160 μm for propellant EB at P=84 atm, L =0 and D_{43} =680 μm for propellant IB at P=43 atm, L = 10 cm). Such conclusion could not be made in case of "coarse" oxide particles formed in course of alumina deposition on the burning agglomerate (metal drop). For those particles size distribution function should correlate with that for agglomerates.
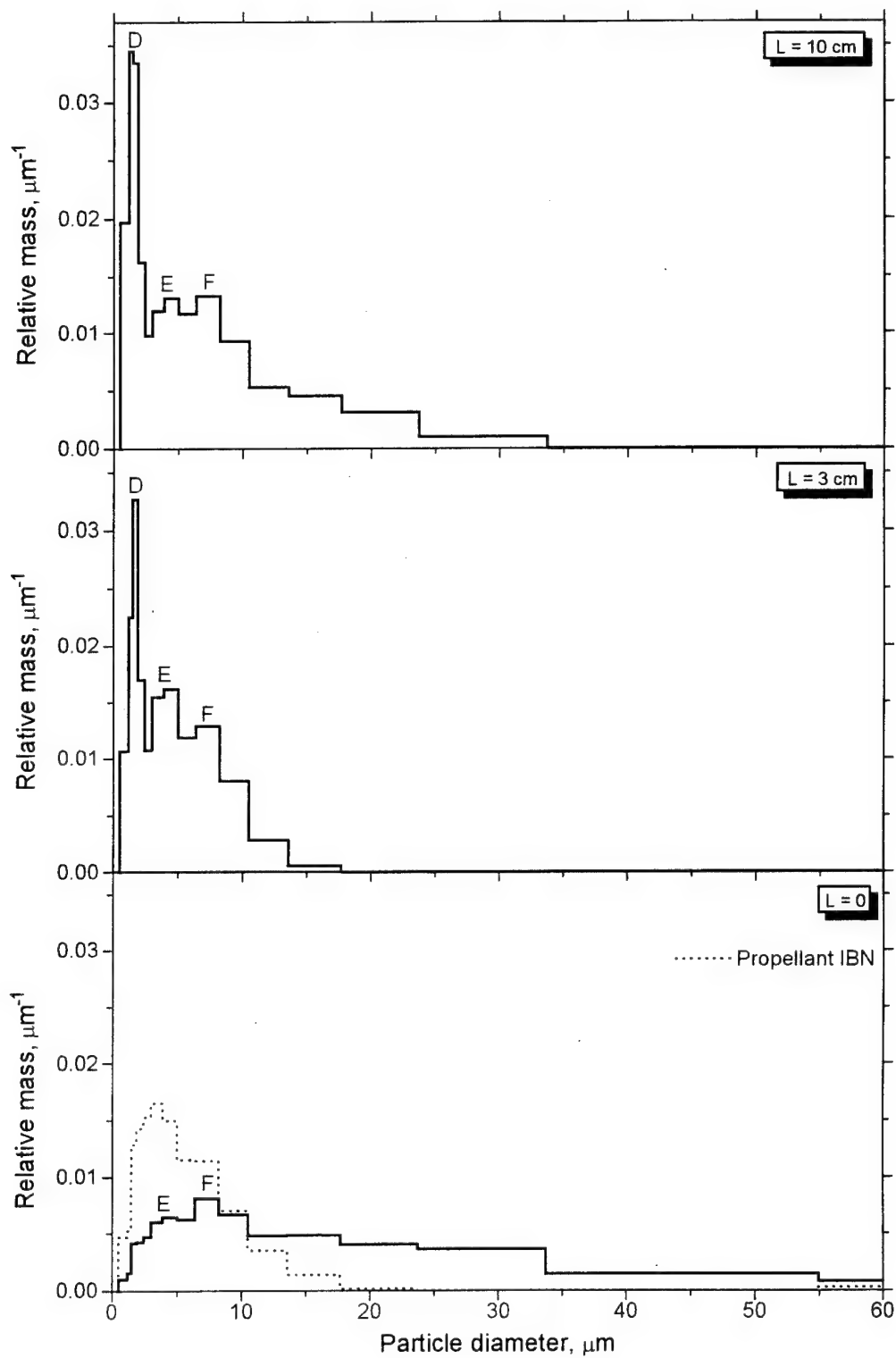
Fig. 4.27. Mass size distribution of CCP particles less than 60 μm at different protecting tube length.

Propellant IB, pressure 22 atm.
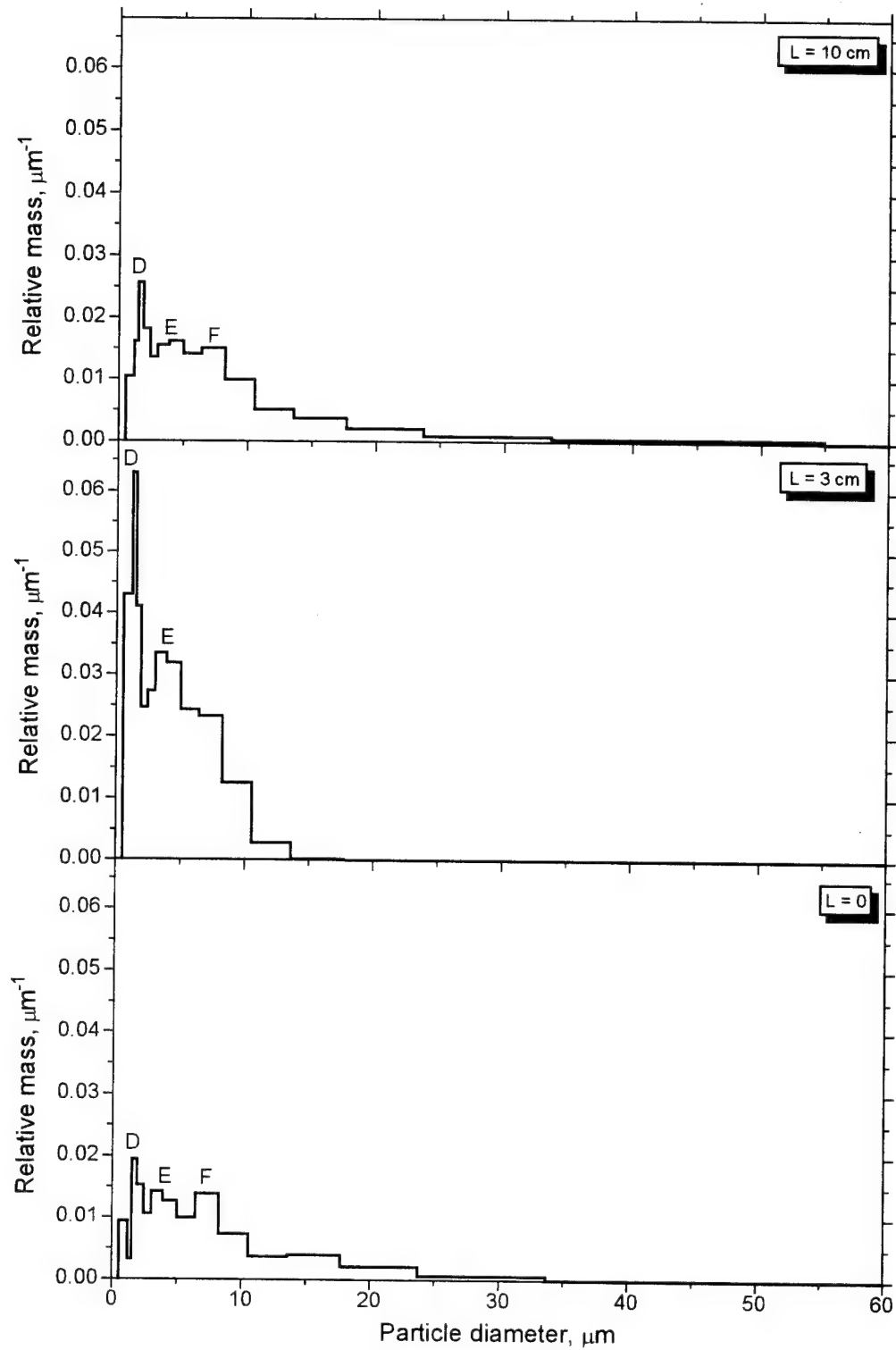
Fig. 4.28. Mass size distribution of CCP particles less than 60 μm at different protecting tube length.
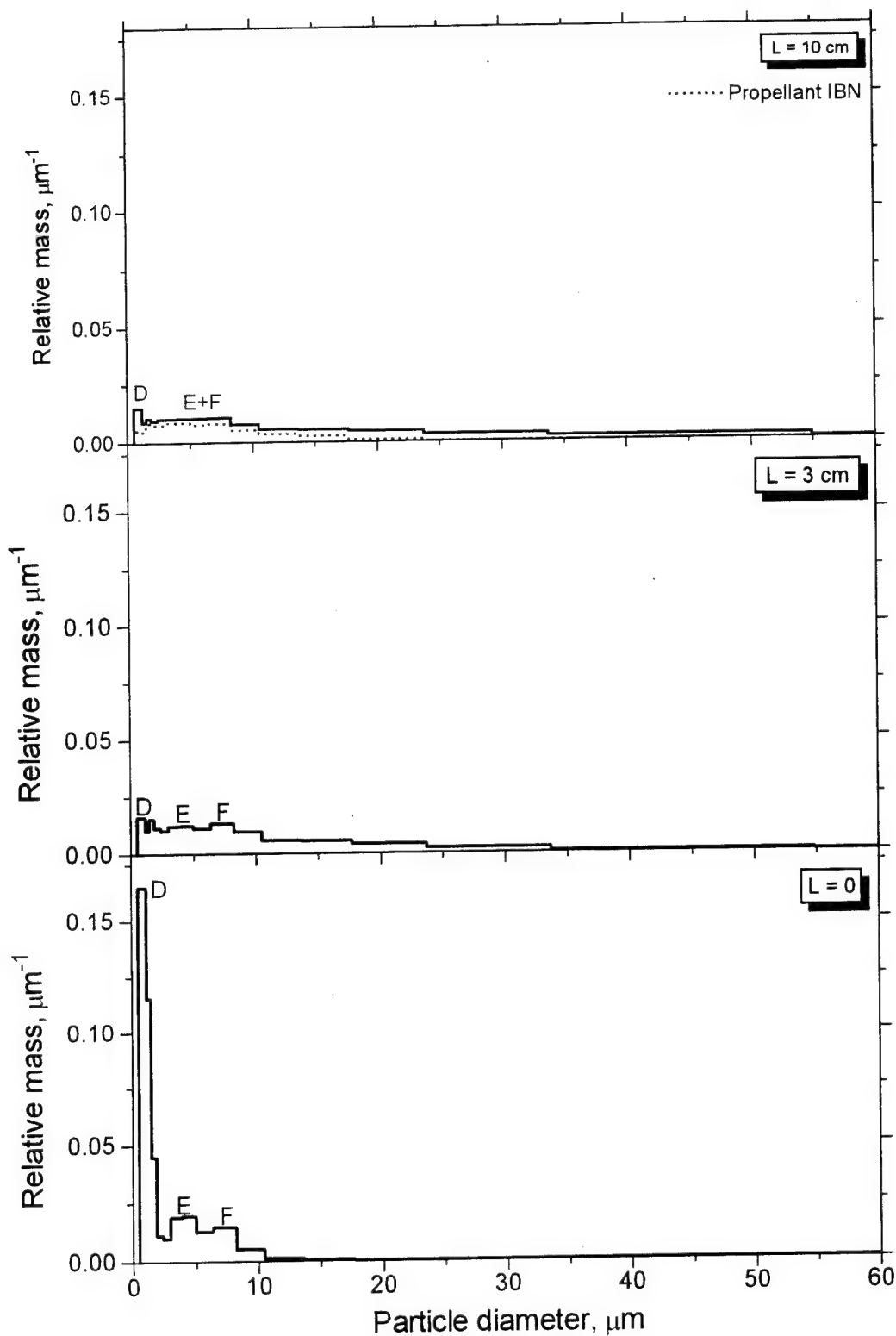Propellant IB, pressure 43 atm.

Fig. 4.29. Mass size distribution of CCP particles less than 60 μm at different protecting tube length.

Propellant IB, pressure 84 atm.

Table 4.7a. Propellant IB. Mean diameter D_{mn} of CCP-particles in size range 0.5-60 μm

Pressure P, atm	Tube length L, cm	Mean diameter D_{mn}, μm						
		D_{10}	D_{20}	D_{30}	D_{21}	D_{32}	D_{43}	D_{53}
22	0	1.9	2.8	4.3	4.1	10.4	21.3	25.8
22	3	1.3	1.5	1.9	1.8	3.2	5.4	6.4
22	10	1.1	1.3	1.9	1.6	3.6	9.1	11.9
43	0	1.2	1.6	2.2	2.0	4.4	9.0	11.5
44	3	1.1	1.3	1.6	1.5	2.7	4.8	5.8
43	10	1.3	1.6	2.2	2.0	4.3	10.2	14.4
85	0	0.9	1.0	1.1	1.0	1.4	3.0	4.3
84	3	1.1	1.4	2.1	1.8	4.9	12.9	16.9
84	10	1.1	1.4	2.3	1.8	6.0	18.2	23.5

Table 4.7b. Propellant EB. Mean diameter D_{mn} of CCP-particles in size range 0.5-60 μm

Pressure P, atm	Tube length L, cm	Mean diameter D_{mn}, μm						
		D_{10}	D_{20}	D_{30}	D_{21}	D_{32}	D_{43}	D_{53}
22	0	1.2	1.5	1.9	1.7	3.0	5.2	6.2
22	3	1.0	1.2	1.4	1.3	2.2	4.8	6.0
22	10	1.0	1.1	1.4	1.2	2.2	5.3	7.3
44	0	1.1	1.3	1.8	1.5	3.2	7.8	10.8
46	3	1.4	1.8	2.6	2.3	5.5	13.1	17.0
45	10	1.0	1.2	1.6	1.4	2.7	6.6	8.7
84	0	1.1	1.4	2.0	1.7	4.5	12.3	16.7
86	3	1.1	1.4	2.0	1.7	4.6	14.0	18.9
80	10	0.9	1.0	1.1	1.0	1.3	1.8	2.3

Table 4.7c. Propellant IBN. Mean diameter D_{mn} of CCP-particles

Pressure P, atm	Tube length L, cm	Mean diameter D_{mn}, μm						
		D_{10}	D_{20}	D_{30}	D_{21}	D_{32}	D_{43}	D_{53}
22	0	1.5	1.9	2.5	2.4	4.5	14.8	28.9
84	10	1.3	1.6	2.3	2.1	4.3	7.9	9.5

Table 4.7d. Propellant EBN. Mean diameter D_{mn} of CCP-particles

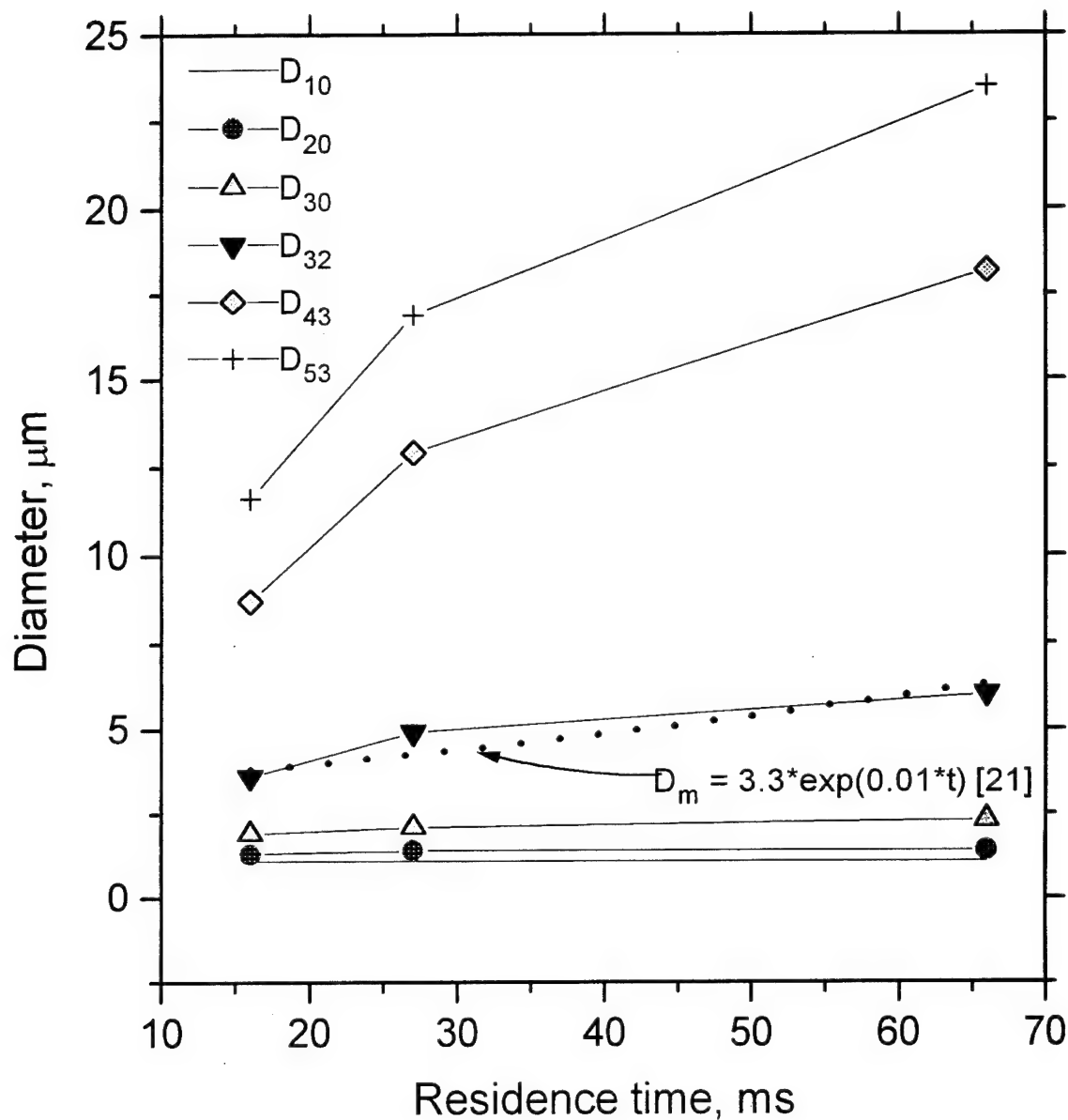| Pressure P, atm	Tube length L, cm	Mean diameter D_{mn}, μm						
		D_{10}	D_{20}	D_{30}	D_{21}	D_{32}	D_{43}	D_{53}
23	0	1.4	1.9	2.8	2.5	6.1	18.9	30.0
86	10	1.5	2.1	3.3	2.9	8.2	28.1	41.5

Fig. 4.30. Mean diameters D_{mn} for CCP particles of size less than 60 μm in dependence of residence time calculated for gaseous products.

Propellant IB, pressure 84 atm.

Dotted line is the empirical temporal dependence for mean mass size $D_m(t)$ [21] for the propellant containing 15 % aluminum tested at the pressure 40 atm.
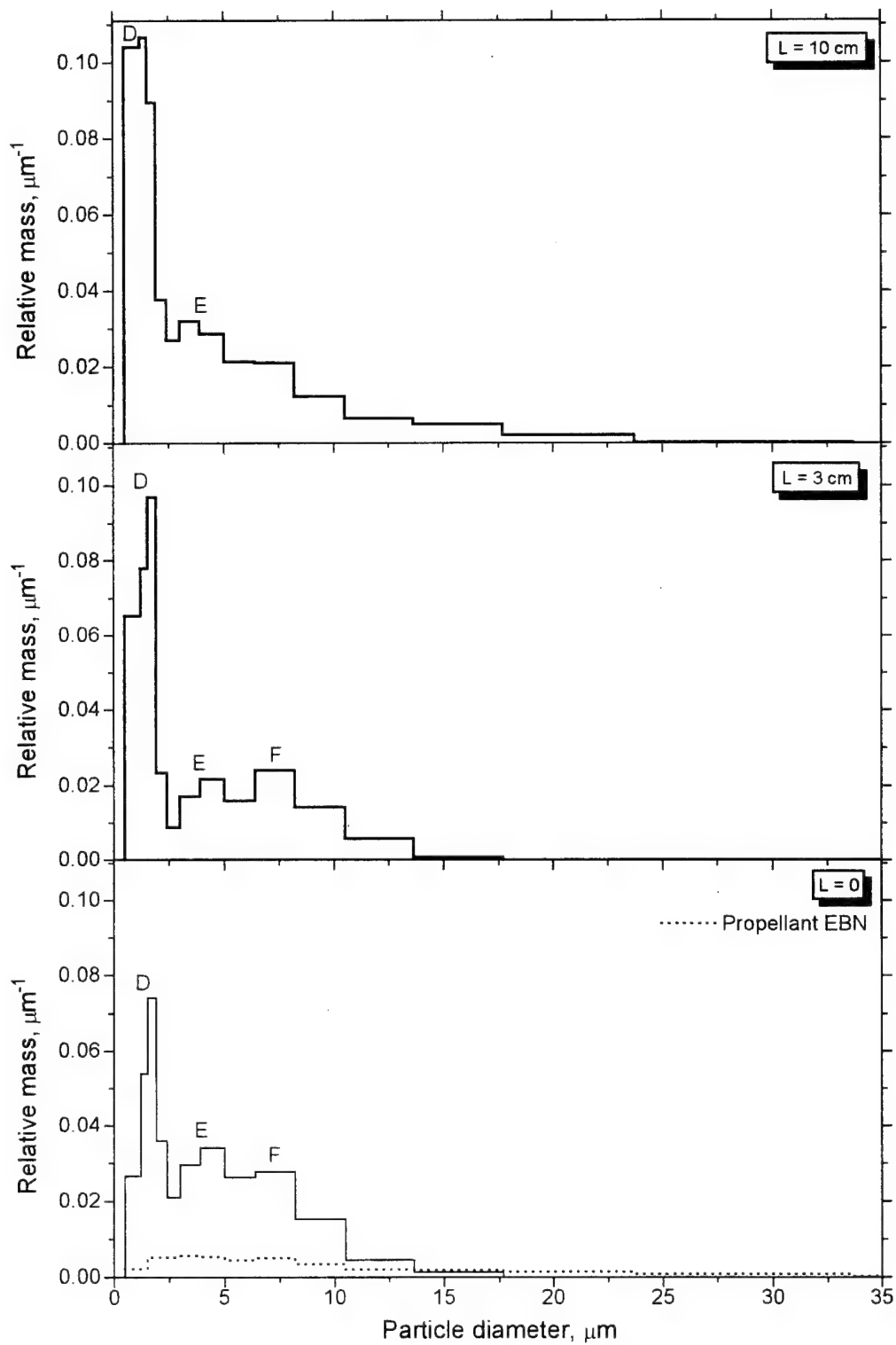
Fig. 4.31. Mass size distribution of CCP particles less than 60 µm at different protecting tube length.
Propellant EB, pressure 22 atm.

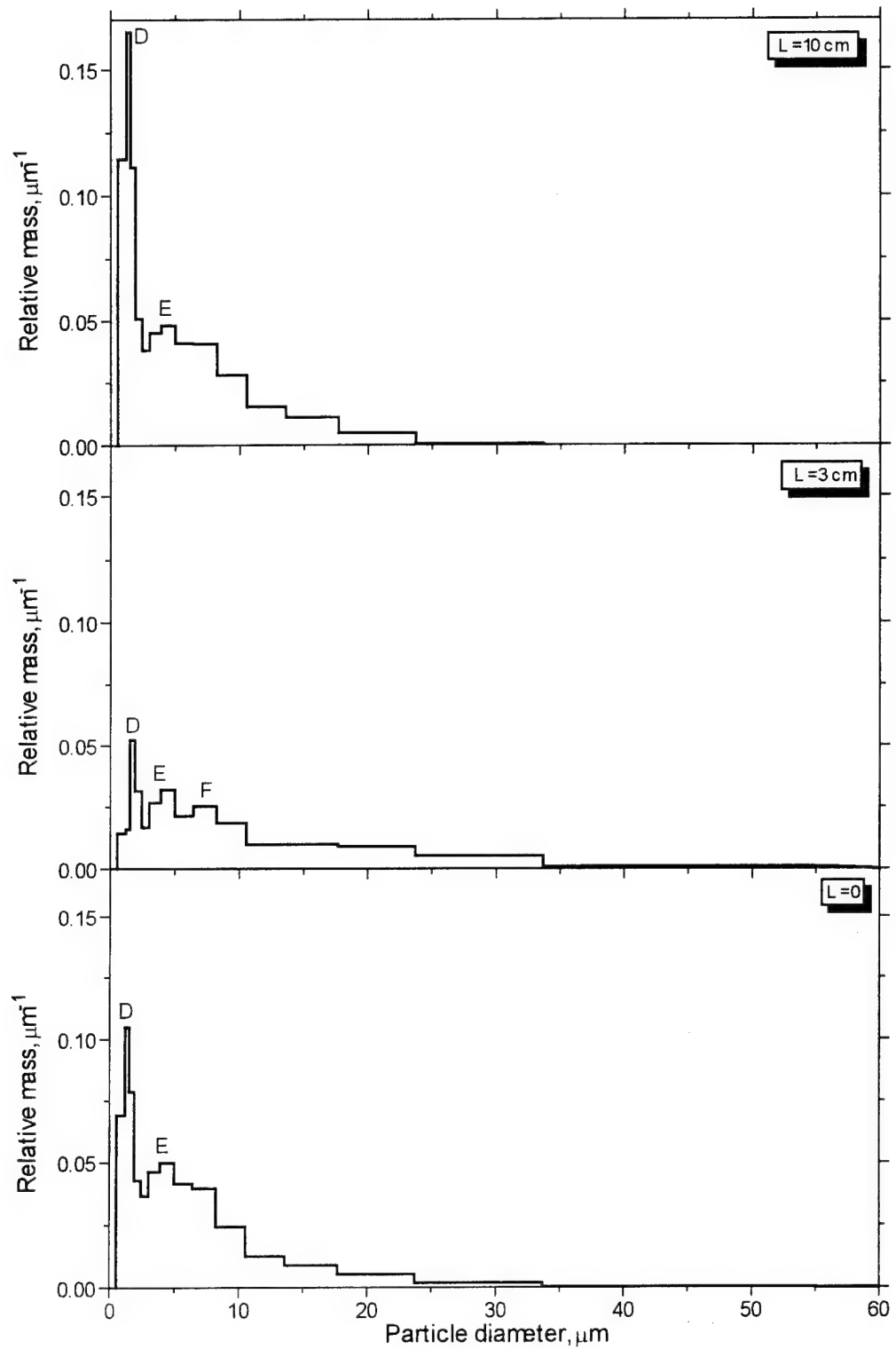Fig. 4.32. Mass size distribution of CCP particles less than 60 μm at different protecting tube length.

Propellant EB, pressure 45 atm.
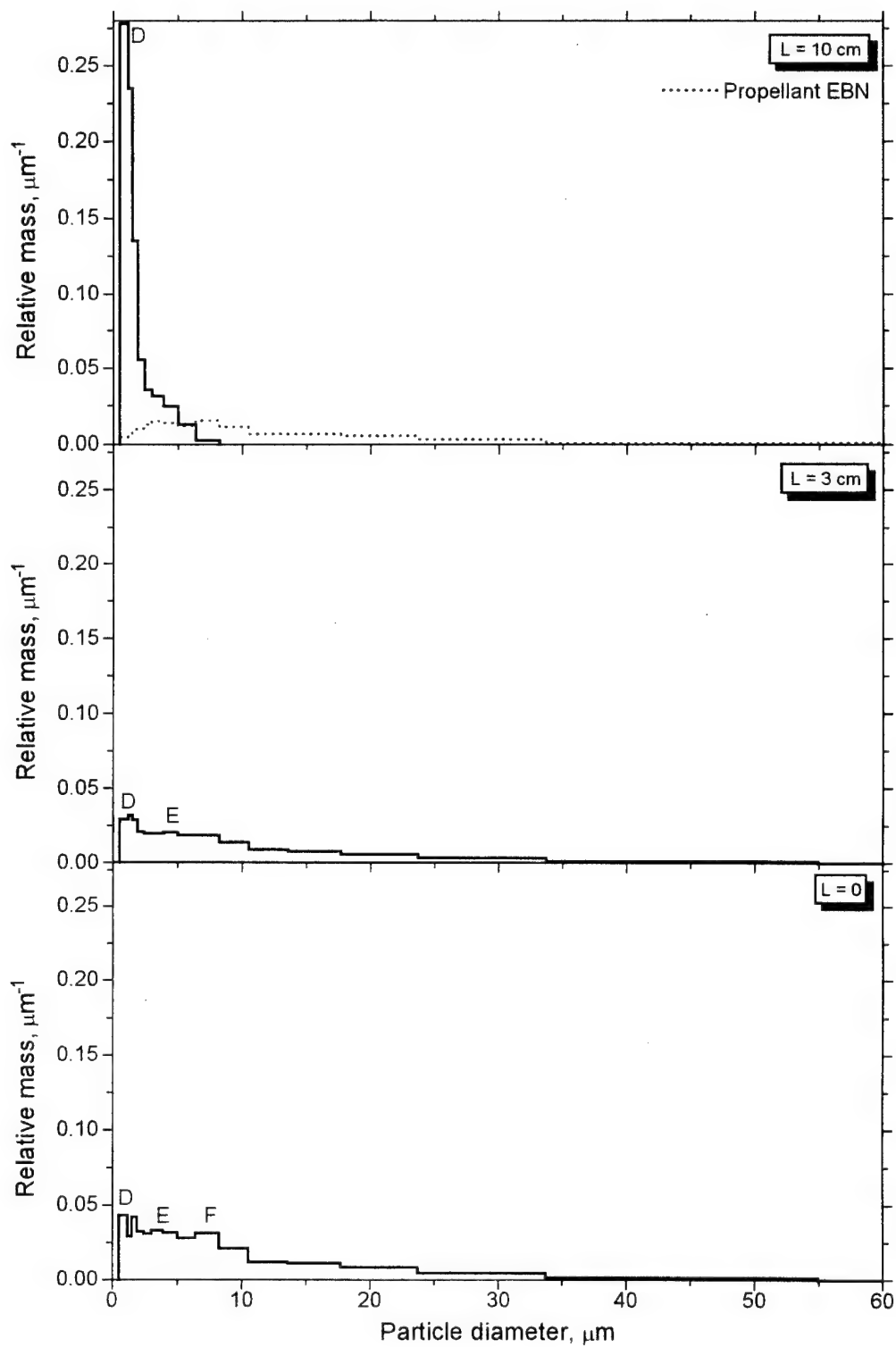
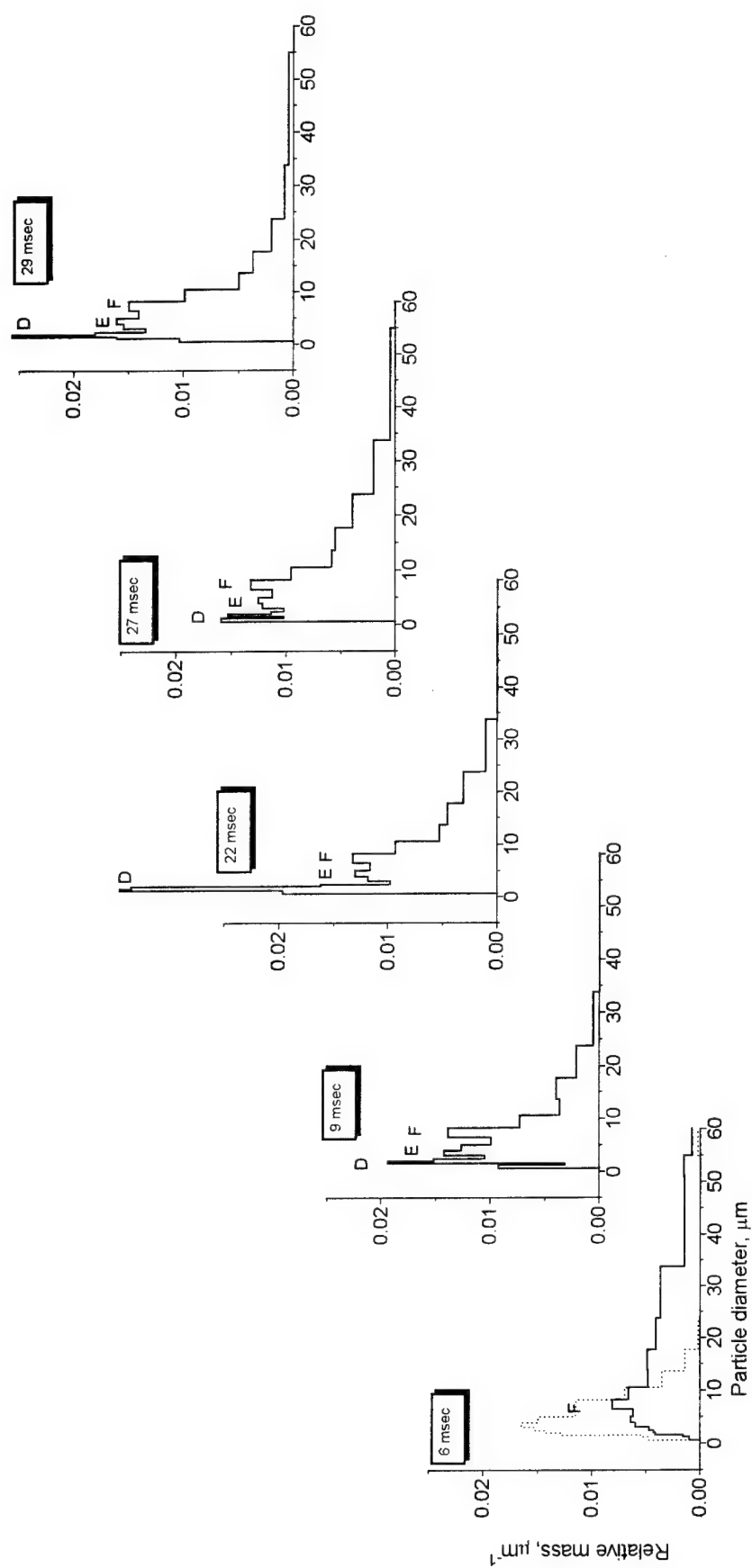Fig. 4.33. Mass size distribution of CCP particles less than 60 μm at different protecting tube length.

Propellant EB, pressure 84 atm.

Fig. 4.34. Evolution of mass size distribution of CCP particles less than 60 μm in dependence of residence time for propellant IB.
6 msec - pressure 22 atm, L=0. Dotted line - propellant IBN at the same conditions of testing.
9 msec - pressure 43 atm, L=0.
22 msec - pressure 22 atm, L=10 cm.
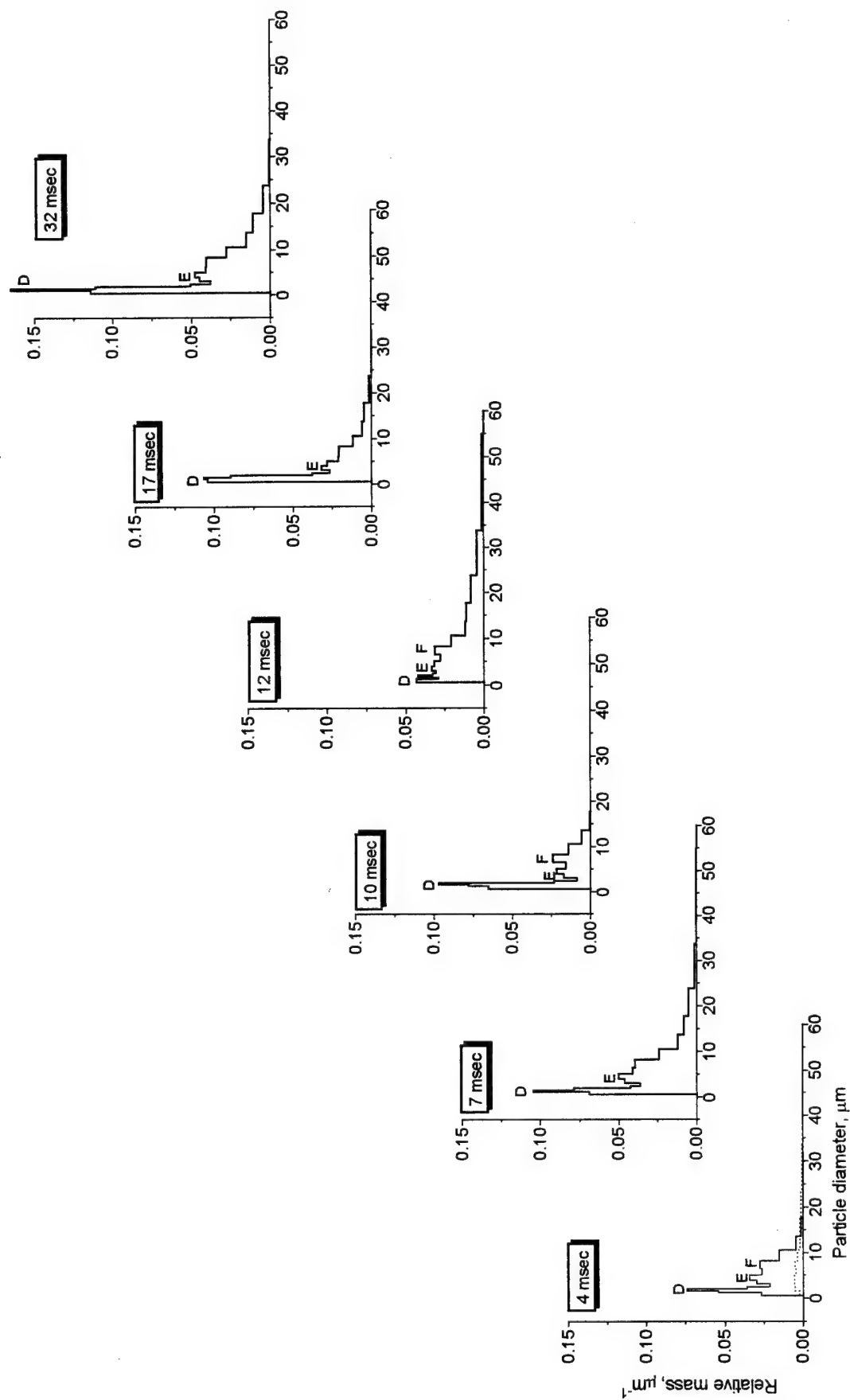27 msec - pressure 84 atm, L=3 cm.
29 msec - pressure 43 atm, L=10 cm.

61

Fig. 4.35. Evolution of the mass size distribution of CCP particles < 60 μm in dependence of residence time for propellant EB. Dotted line - propellant EBN at the same conditions of testing.

4 msec - pressure 22 atm, L=0.

7 msec - pressure 44 atm, L=0.

17 msec - pressure 22 atm, L=10 cm.

10 msec - pressure 22 atm, L=3 cm.

32 msec - pressure 45 atm, L=10 cm.

12 msec - pressure 85 atm, L=0.

62

5. HIGH SPEED PHOTOGRAPHY DATA

5.1. Experimental technique.

Experiments on subsurface zone visualization during burning of propellants EB and IB have been carried out under pressure of 1 and 7.5 atm. The visualization has been accomplished by high speed photography under pulse periodic illumination (1.5 microsecond pulse duration) using xenon lamp ISH-400 as a light source (Fig. 5.1).

Samples under study had a shape of rectangular slabs with following dimensions: 8 mm in height, 6 mm in width, 3 mm in thickness (in direction of the optical axis of the set up). The samples have been made by cutting from the bulk of propellant. The lateral surface of the samples was not inhibited. Flame torch was directed upwards in all experiments. The samples were ignited by nichrome wire heated by electric current. Experiments at P=1 atm were carried out in air, ones at P=7.5 atm were accomplished in bomb in nitrogen environment. To prevent window contamination a low velocity blowing of the windows and sample was performed during combustion run. Pressure rise in the vessel during combustion did not exceed 0.7 atm at full pressure of 7 atm. The set of blue light filters was placed behind drawing lens to suppress self illumination of burning agglomerates. High speed 16 mm camera SKS-1M used in the experiments has been modified as follows: rotating prism, that compensates the image displacement on a film, was removed, the dimensions of the field stop placed in front of the film were enhanced providing the total area of image 16x15 mm^2 (i.e. image frame involves film perforation). Records of each experiment were carried out on the film with length of 30 m. In this case approximately a thousand frames contain useful information. Space resolution in all tests was about 15 micron, focal depth in the object space at P=7.5 atm was about 1 mm. Image magnification on a film in tests at P = 1 atm was 4^x ; at p = 7.5 atm it was 3^x ; frame repetition frequency at P=1 atm was equal 2.5 kHz (propellant EB) and 3.0 kHz (propellant IB); at P = 7.5 atm it was equal 2.0 kHz for both propellants.

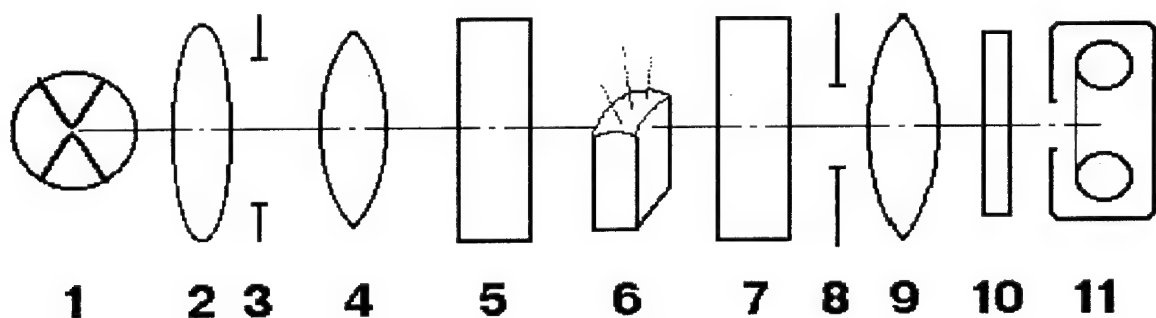Fig. 5.1. Optics arrangement for high speed shadow photography of burning propellants under pulse illumination:

1 - xenon flash lamp ISH-400;	7 -	bomb window;
2 - lens-collector;	8 -	aperture stop;
3 - aperture stop;	9 -	drawing lens;
4 - lens-condensor;	10 -	color filter;
5 - bomb window;	11 -	high-speed movie camera SKS-1M.
6 - propellant specimen;		

5.2. Peculiarities of experimental results processing.

Movies obtained in the tests were statistically treated in a standard manner. Discrete distributions of particle sizes (histograms) were obtained for different type of particles ejected from the burning surface. On the basis of histograms the averaged diameters D_{mn} were determined (without additional treatment of size distributions). For all histograms obtained the following condition was fulfilled:

$$\frac{\sigma_N^2}{N} \leq \left(\frac{\Delta D}{2}\right)^2$$

where N - total number of particles in statistics; σ_N^2 - sample dispersion (variance) of distribution, $\sigma_N^2 = D_{20}^2 - D_{10}^2$; ΔD - size interval used in constructing the histograms.

Note that histograms obtained by treatment of high speed photography data corresponding atmospheric pressure have relatively crude size interval. The reason is that the major portion of condensed phase in CCP of both propellants are particles-aggregates for which error in size estimation is relatively large due to irregular shape. The existence of great number of such particles indicates poor combustion of propellant. Histograms can be used for qualitative description of propellant burning at atmospheric pressure and, in general, there was no special goal to obtain more reliable quantitative data on size distribution of CCP particles. When deriving parameters of agglomerates motion the distance was measured between particle center and burning surface in direction of flow line. Flow lines were visualized by lengthy smoke tail of burning agglomerates (Fig. 5.2, 5.3). Particle velocity values were calculated on the basis of data on distances passed by the particles. The unique size interval has been chosen for statistical treatment of size distribution: at P=1 atm it was equal 50 μm while at P=7.5 atm - 22 μm.

5.3. Experimental Results.

5.3.1. Characteristics of CCP particles in the flame of tested propellant.

When examing the film records of burning tested propellants at atmospheric pressure the particles near the surface have been classified into 3 types (Fig. 5.4):

a). Round shape particles heaving typical halo of smoke. It is generally recognized that they are burning metal agglomerates, Fig. 5.4a.

b). Particle with irregular shape (non-compact, coral type, scarred boundary particles with recognizable porosity), Fig. 5.4b. When constructing histograms a diameter of such particles was determined by comparing particle image with a circle with the same area as area of particle image. The diameter of the circle was considered to be conventional diameter of the particle (so called mean projected diameter). It is necessary to note that the irregular particles rotate in random manner during motion in gas flow. This leads to occasional angular position and shape of particle when it is exposed. Due to this effect shadow image of the same particle may have different shape and dimensions (equivalent diameter) in neighboring frames. In this case arithmetical mean equivalent diameter derived from the images on the neighboring frames considered to be the equivalent diameter of the particle.

c). Compact particles having smoothed boundaries and typical light spot inside due to lens effect caused by the light propagation through the grain of AP crystal, Fig. 5.4c. From

high speed photography test results it follows that at P=7.5 atm almost all particles in flame of propellants EB are the burning metal agglomerates. At the same about 25% of number of relatively large-scale particle-aggregates leaves the burning surface of IB propellant. These particles are finally melted and form drops at the distance of 0-3 mm from the burning surface.

5.3.2. Burning surface profile and burning rate.

Series of subsequent burning surface profiles of IB and EB propellants burning at P=7.5 atm are presented on Fig. 5.5. The values of linear burning rates obtained by treatment of these profiles are as follow: $r = 5.0\pm0.2$ mm/s in the case of propellant IB, $r = 5.5\pm0.2$ mm/s in the case of propellant EB. Figures 5.5a, 5.5b shows uniformity (layer by layer character) of samples burning down and typical dimensions (scales) of heterogeneities on the burning surface of propellant IB (a) and EB (b). The typical profile heterogeneities for propellant IB are several times as much in comparison with propellant EB.

5.5.3. Size distribution and velocities of particles leaving burning surface.

Figures 5.6-5.8 present histograms of size distribution by number for particles in the flame of propellants IB and EB at P=1 atm and P=7.5 atm.

The results of measurements of particle velocities and sizes are displayed in Fig. 5.9, 5.10 in the form of velocities vs distance from the burning surface plots. The marks connected by segments correspond to the same particle. Only particles with images within the focal depth of the object space on two or more neighboring frames have been selected for these measurements. The value $(1/t_{rlx})$, where t_{rlx} is the inertia relaxation time of particle-agglomerate in the gas flow has been used as a parameter for experimental points in Fig. 5.9, 5.10. It was calculated as follows:

$$\frac{1}{t_{rlx}} = \frac{18\mu}{D_{halo}^2 \cdot \rho_{Al} \cdot \left(\dfrac{D_{part}}{D_{halo}}\right)^3}$$

The numerical values of this parameter (dimension 1/s) are shown in legend on Fig. 5.9, 5.10. It is necessary to note that diameter of halo was determined as its maximum dimension in the normal direction to the gas flow. As a rule, agglomerate sizes and halo dimensions do not vary during the whole sequence of frames containing their image. As it follows from the plots on Fig. 5.9, 5.10 even at constant values of $(1/t_{rlx})$ there is a significant scatter of data. This effect may occur due to local velocity fluctuations of gas flow in different points of the flame.

In Fig. 5.11 ratio between halo diameter and particle diameter is plotted versus particle diameter for both propellants and two values of pressure. In spite of significant scattering the experimental data it should be noted that the values of this ratio at P=7.5 atm are within the range of 1.4 -2 and 1.8 - 2.4 at P=1 atm Data presented on Fig. 5.12 show that the value $(1/t_{rlx})$ much better correlates with a diameter of particles than with a halo's diameter..

5.5.4. Mass balance and representativity of high speed photography.

To estimate representativity of size distribution of CCP particles obtained by high speed photography the calculations on aluminum mass (volume) balance in initial sample and in agglomerates leaving the burning surface have been carried out. The estimations have been made for IB and EB propellants at P =7.5 atm. The calculated volume ΔV_{calc} of metal leaving the burning surface during time period $\Delta\tau$ is as follows:

$$\Delta V_{calc} = \Delta z \cdot a \cdot r \cdot \Delta \tau \cdot \beta_{Al} \cdot k$$

where Δz - focal depth in the image space, a - frame width in the plane of object, r - linear burning rate of the sample, β_{Al} - volume fraction of aluminum in bulk of initial sample, k - coefficient to account for conversion degree of aluminum of agglomerate into oxide and thermal expansion of aluminum and oxide. It is obviously that $\beta_{Al} = \alpha_{Al} \cdot \rho_p / \rho_{Al}$, where α_{Al} - mass fraction of aluminum in propellant, ρ_p - average density of a sample, ρ_{Al} - density of aluminum. Condensed phase volume measured in the test equals:

$$\Delta V_{test} = \frac{\pi}{6} D_{30}^3 \cdot \Delta N,$$

where D_{30} - mean volume diameter calculated on the basis of size distribution, ΔN - number of particle-agglomerates, leaving the burning surface during period $\Delta \tau$. Thus:

$$\frac{\Delta V_{test}}{\Delta V_{calc}} = \frac{1}{k \cdot \Delta z} \cdot \frac{\pi D_{30}^3}{6} \cdot \frac{\Delta N}{\Delta \tau} \cdot \frac{\rho_{Al}}{a \cdot r \cdot \alpha_{Al} \cdot \rho_p}$$

Each value in this formula has limited accuracy. From the general point of view, the following values may have considerable errors: k, Δz, α_{Al}, D_{30}. Specifically, error of Δz depends upon subjective error of researcher when selecting particle images on a film. Errors of α_{Al} may occur because of local fluctuation of aluminum content when a small volume sample (tenth parts of mm^3) is burnt. Errors of D_{30} can be estimated as $\pm \Delta D/2$, where $\Delta D \cong$ 22 μm is the value size sub-range (during accumulation of histogram). Let's estimate the above expression with following values of parameters: $k \cong 1.2$, $\Delta z \cong 1$ mm, $\Delta \tau \cong 0.25$ s, $\rho_{Al} =$ 2.7 g/cm^3, $a \cong 5$ mm, $\alpha_{Al} = 0.18$, and ($D_{30} \cong 220$ μm, $\Delta N \cong 139$ particles, r $\cong 5.0$ mm/s, ρ_p =1.62 g/cm^3) for propellant IB or ($D_{30} \cong 124$ μm, $\Delta N \cong 495$ particles, r $\cong 5.5$ mm/s, $\rho_p =1.73$ g/cm^3) for propellant EB. Substituting these values and taking into consideration errors of D_{30} we obtain:

$$\frac{\Delta V_{test}}{\Delta V_{calc}} \approx 1.11 \div 0.83 \text{ for propellant IB,}$$

$$\frac{\Delta V_{test}}{\Delta V_{calc}} \approx 0.67 \div 0.40 \text{ for propellant EB.}$$

Taking into account the errors of parameters used in calculations the closeness of the values $\frac{\Delta V_{test}}{\Delta V_{calc}}$ to 1 can be considered as satisfactory. The fact that the major part of mass (in case of propellant EB) is in the form of high-disperse particles with sizes less than 10 μm (which is below space resolution for this method) may explain the lack of mass of CCP recorded in experiments with propellant EB. Experiments show that for propellant EB at 22 atm near the burning surface approximately 40% of condensed phase mass is in the form of particles with sizes less than 5 μm.
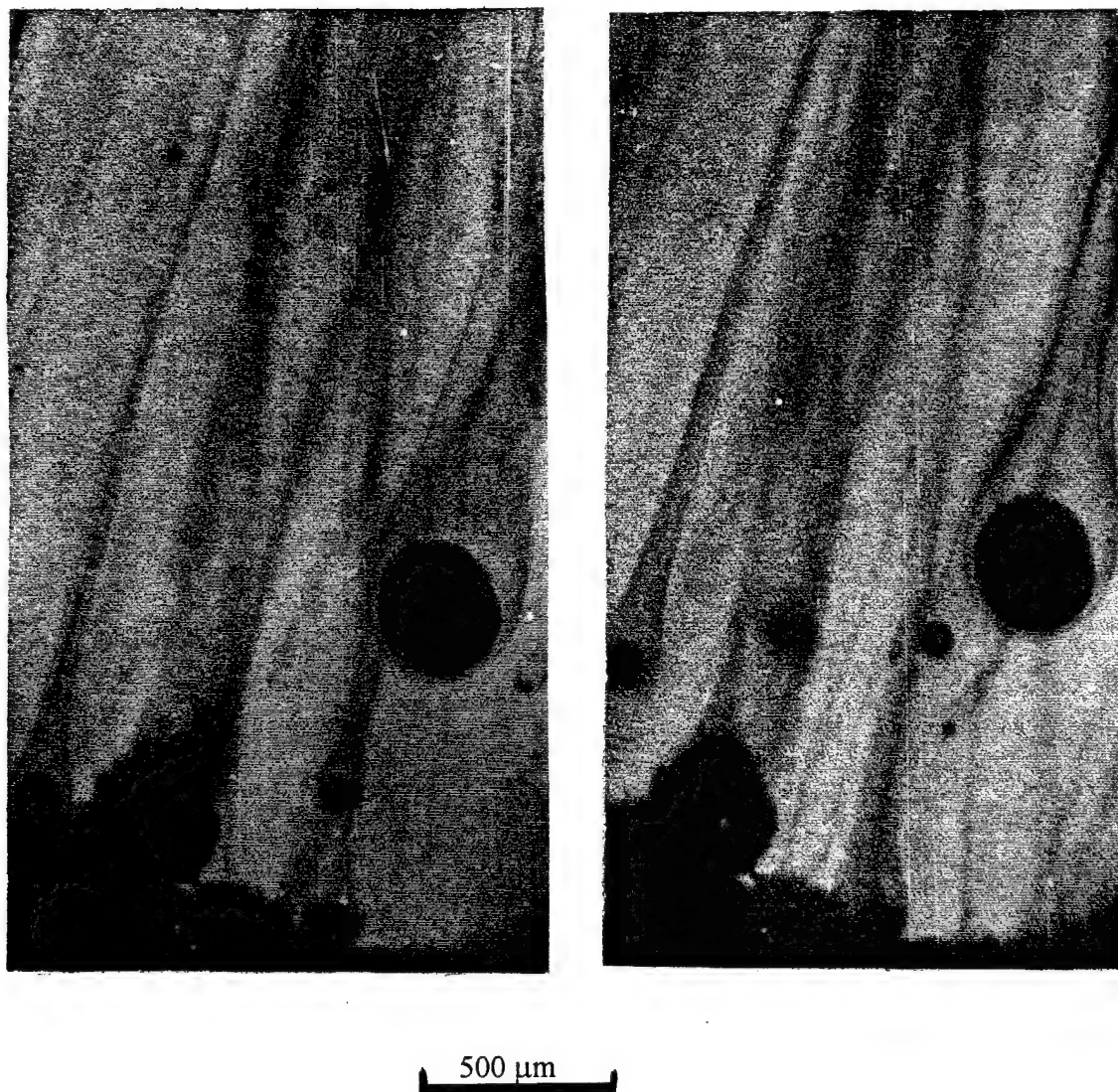
500 μm

Fig. 5.2.
The neighboring frames in high speed shadow photography of combustion of propellant IB, pressure 7.3 atm, frame repetition frequency 2 kHz.
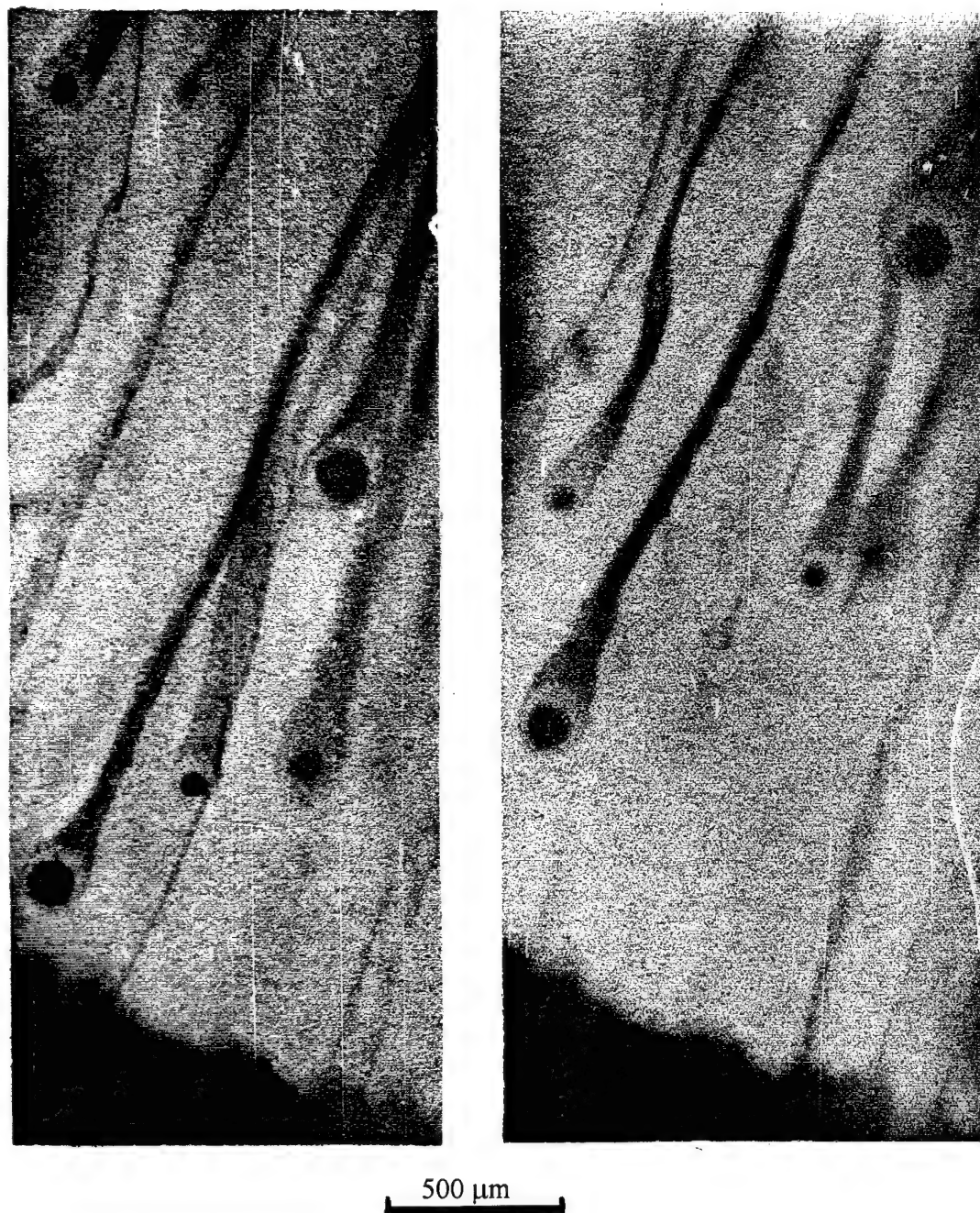
500 μm

Fig. 5.3.
Individual frames of high speed photography records. Propellant EB, pressure 7.5 atm, frame repetition frequency 2 kHz.
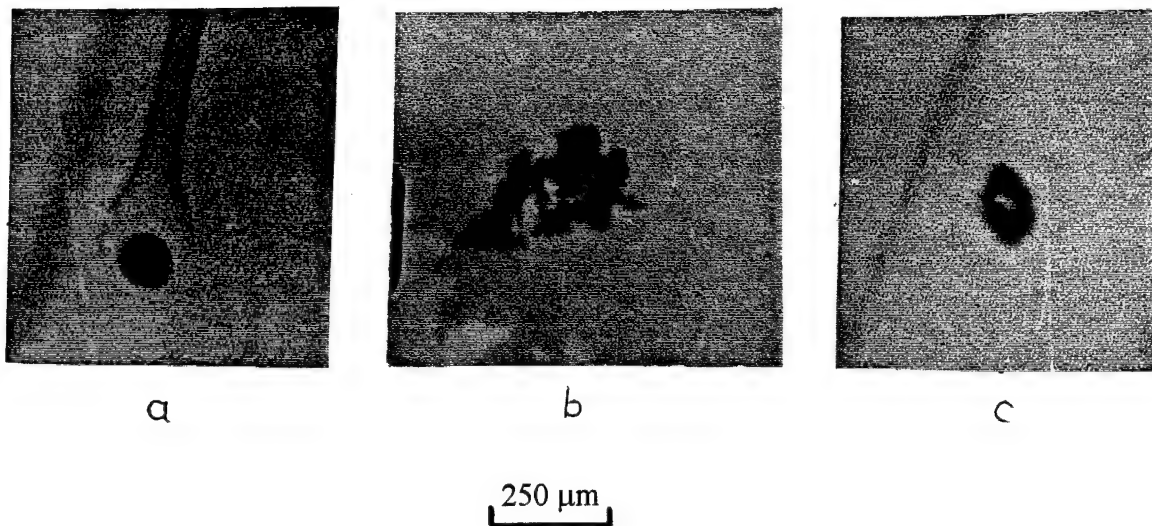
68

250 μm

Fig. 5.4.
Different particle types in flame zone adjusting the burning surface (propellant IB and EB, atmospheric pressure):
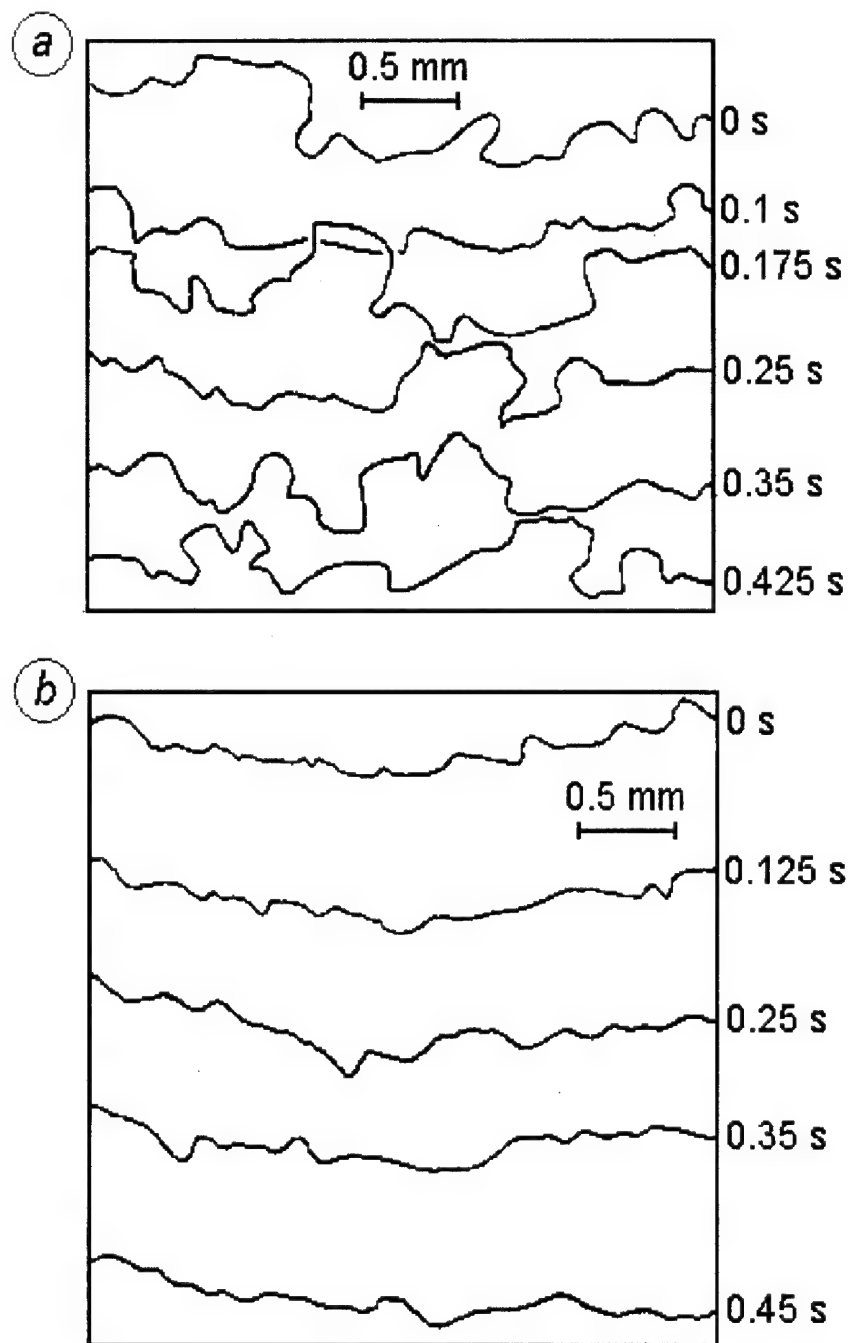
a - burning agglomerate;
b - aggregate;
c - AP crystal.

Fig. 5.5. Series of successive burning surface profiles of IB (a) and EB (b) propellants burning at P=7.5 atm. The profiles were plotted on the basis of images obtained by high speed shadow photography under pulse periodic illumination. Numbers on the right from the curves are corresponding points of time. Sample thickness in both cases was approximately equal to 3 mm.
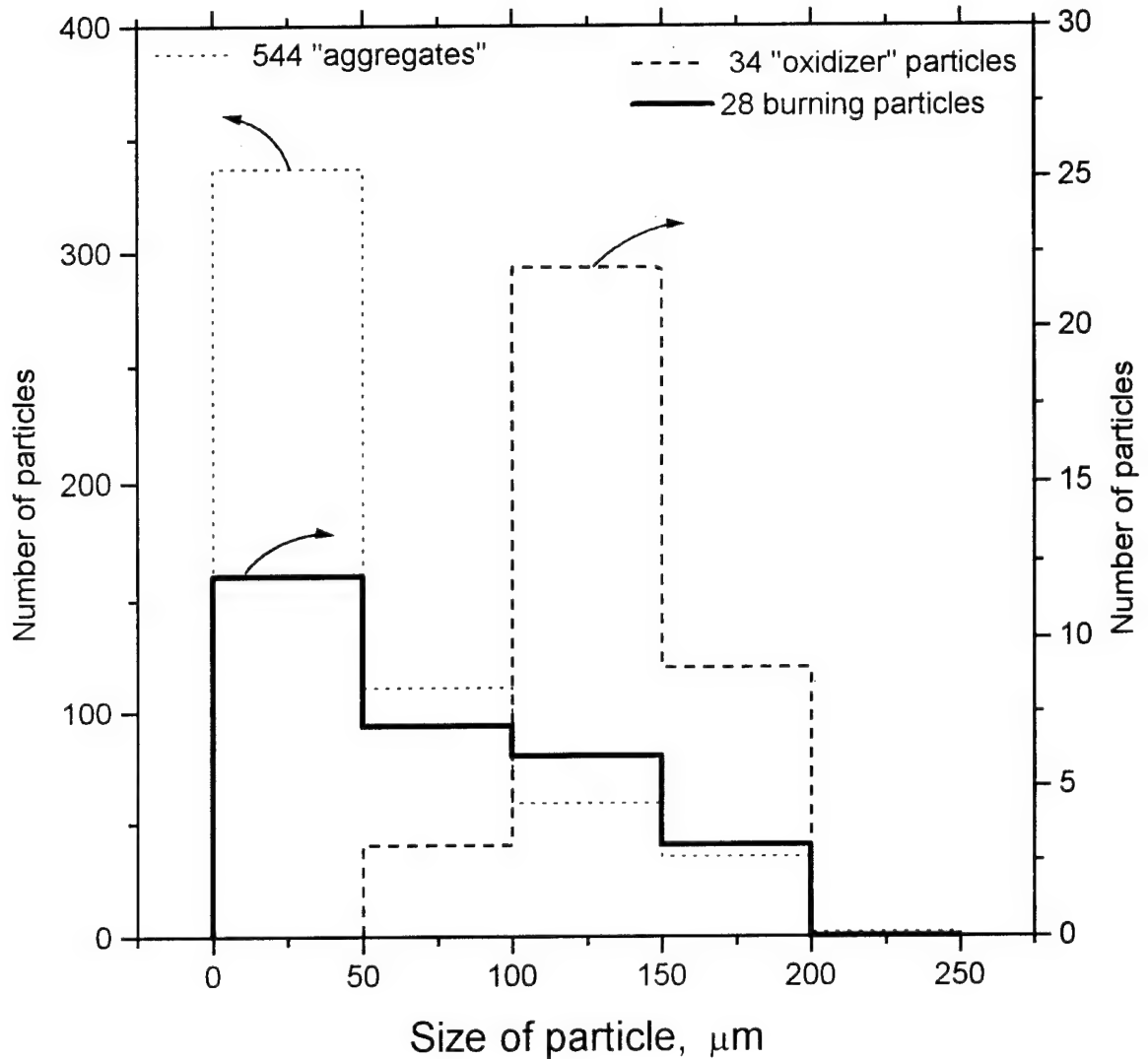
Fig. 5.6. Histograms of number size distribution of particles in flame of propellant IB (height above surface 0-3 mm), P=1 atm, air. High speed shadow photography under pulse illumination by Xe-lamp, pulse frequency 3 kHz.

.... "aggregates" of irregular shape, N = 544.

D_{mn}, µm: D_{10}=56, D_{20}=73, D_{30}=89, D_{21}=95, D_{32}=129.

—————————————————— burning Al agglomerates, N = 28.

D_{mn}, µm:, D_{10}=75, D_{20}=91, D_{30}=103, D_{21}=111, D_{32}=133 µm

— — — — — — — — — — — — compact particles with speck inside image, N = 34.

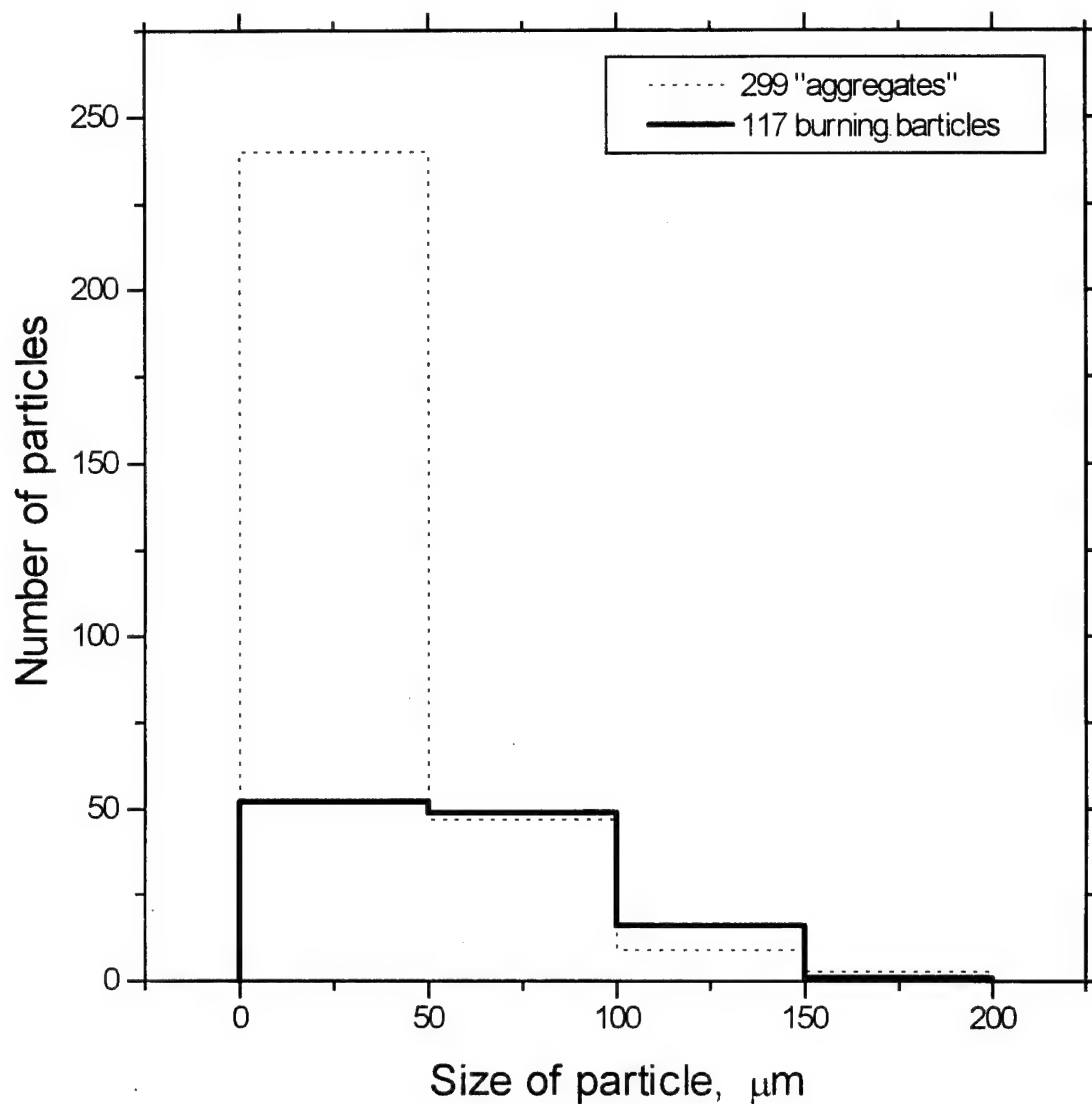D_{mn}, µm: D_{10}=134, D_{20}=137, D_{30}=140, D_{21}=140, D_{32}=145 µm

Fig. 5.7. Histograms of number size distribution of particles in flame of propellant EB (height above surface 0-3 mm), P=1 atm, air. High speed shadow photography under pulse illumination by Xe-lamp, pulse frequency 2.5 kHz.

.... "aggregates" of irregular shape, N = 299.
D_{mn}, μm: D_{10}=37, D_{20}=47, D_{30}=58, D_{21}=58, D_{32}=89.

———————————————— burning aluminum agglomerates, N = 117.
D_{mn}, μm:, D_{10}=61, D_{20}=71, D_{30}=79, D_{21}=82, D_{32}=99.
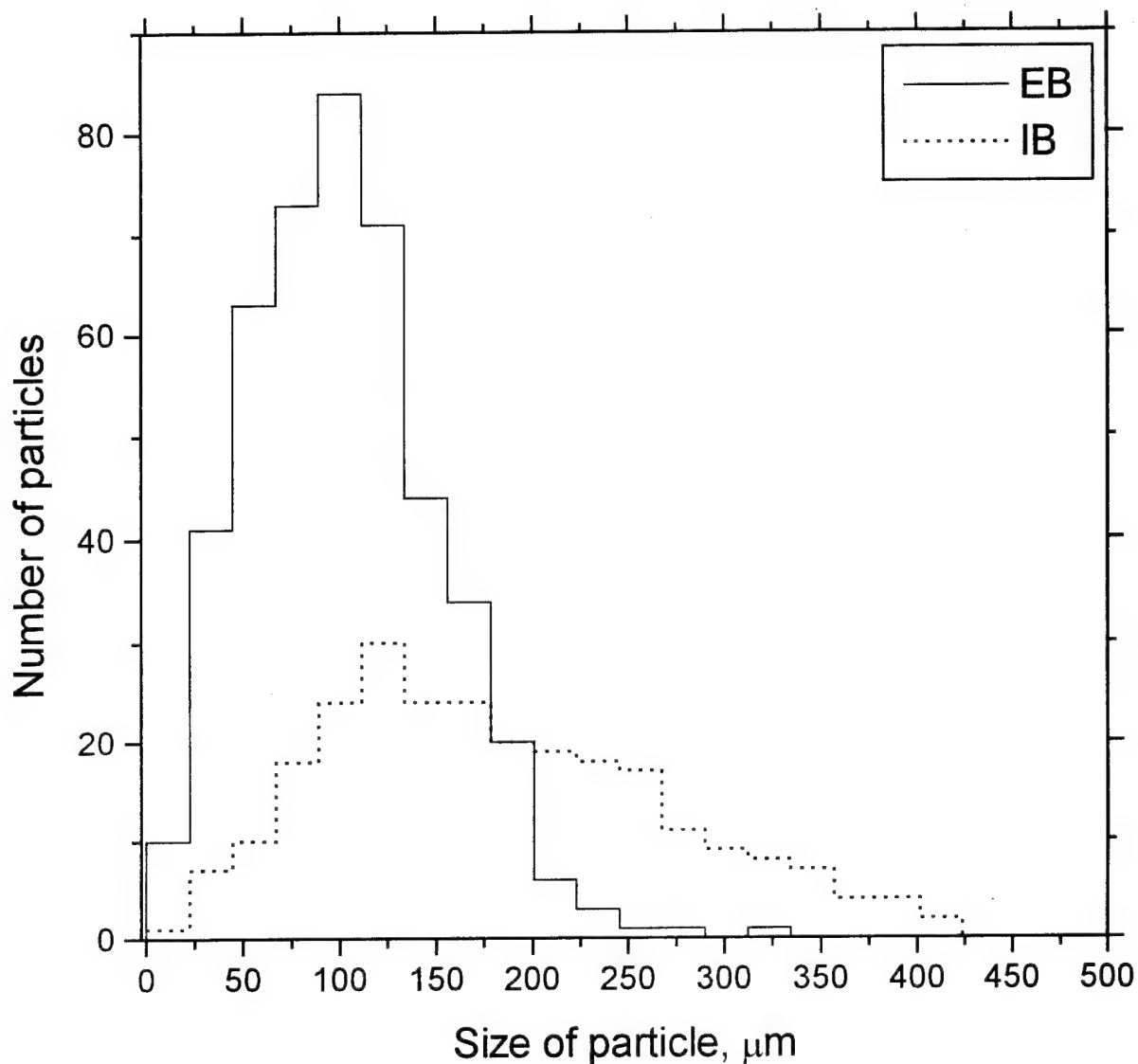
Fig. 5.8. Size distribution of burning aluminum agglomerates by number. Propellants IB (257 particles) and EB (449 particles), pressure 7.5 atm, nitrogen. Height above burning surface 0-3 mm. High speed shadow photography under pulse illumination by Xe-lamp, pulse frequency 2 kHz.

Propellant	Mean diameter D_{mn}, μm:				
	D_{10}	D_{20}	D_{30}	D_{21}	D_{32}
IB	182	203	220	225	260
EB	103	114	124	127	147

Fig. 5.9. Plots of particle-agglomerates velocities in the flame versus distance from the burning surface for propellant IB at P=7.5 atm. The marks connected by segments correspond to the same particle. The values $(1/t_{rlx})$ in s^{-1} are presented in frame on the plot.
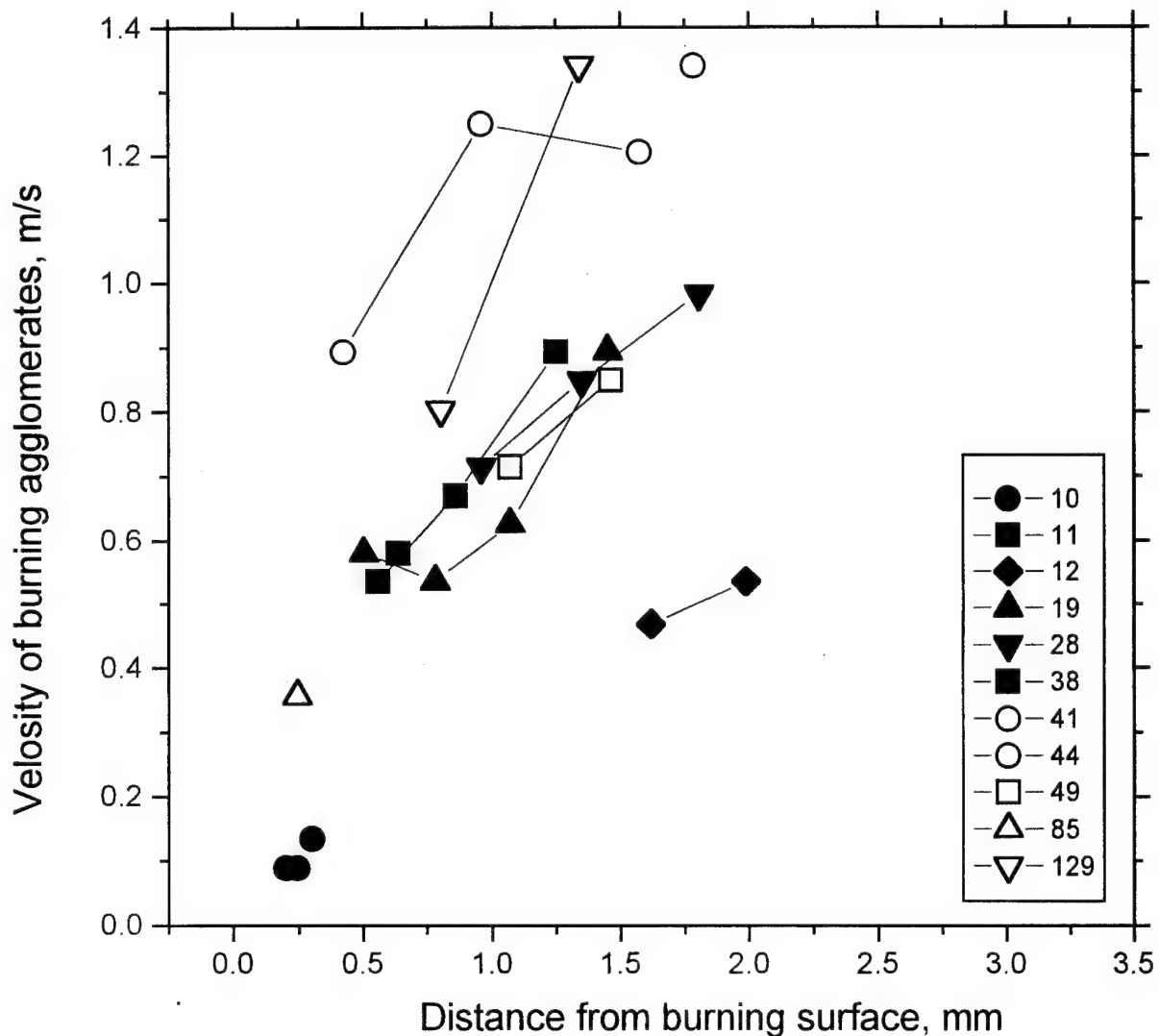
Fig. 5.10. Plots of particle-agglomerates velocities in the flame versus distance from the burning surface for propellant EB at P=7.5 atm. The marks connected by segments correspond to the same particle. The values ($1/t_{rlx}$) in s^{-1} are presented in the right out the plot.

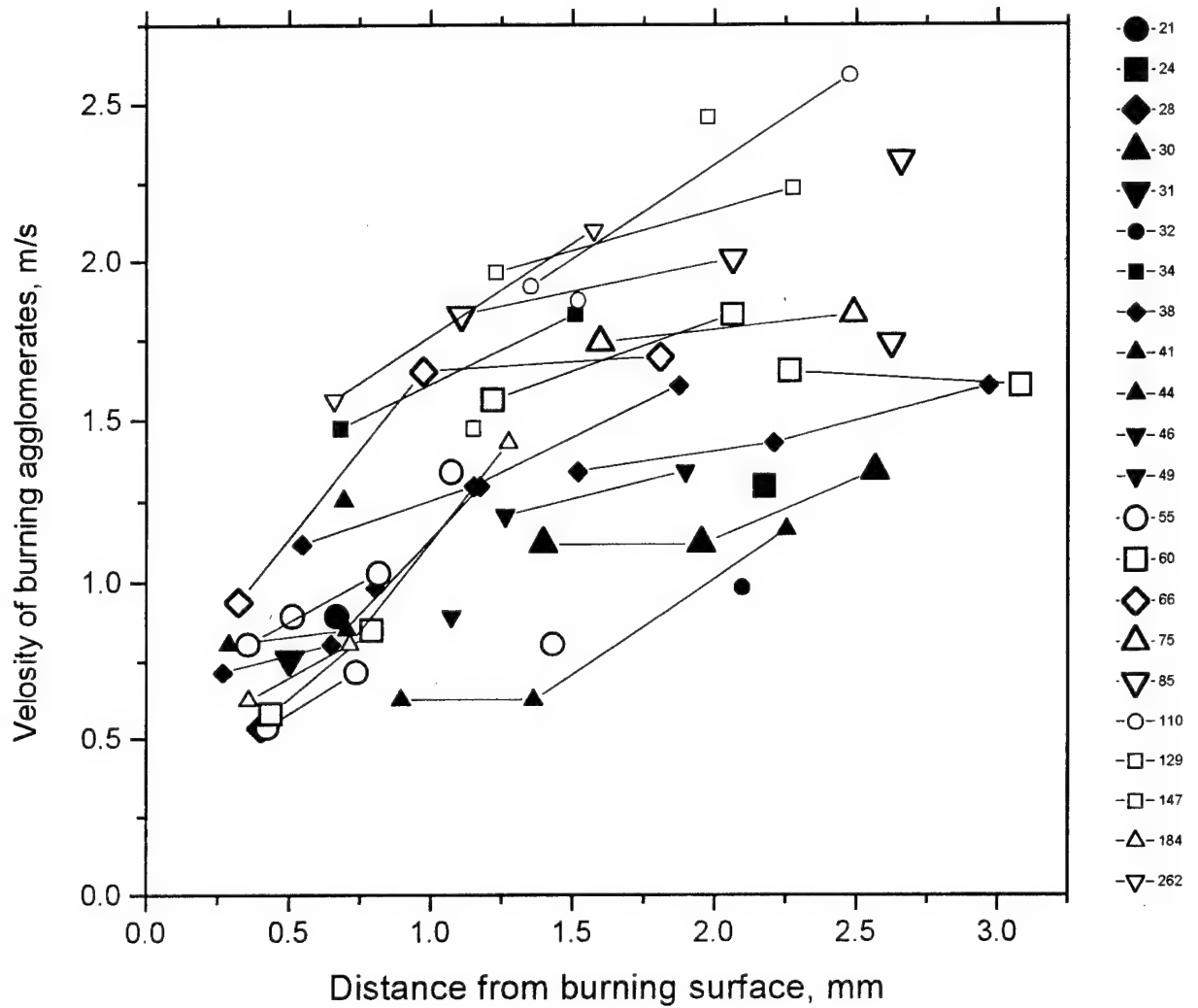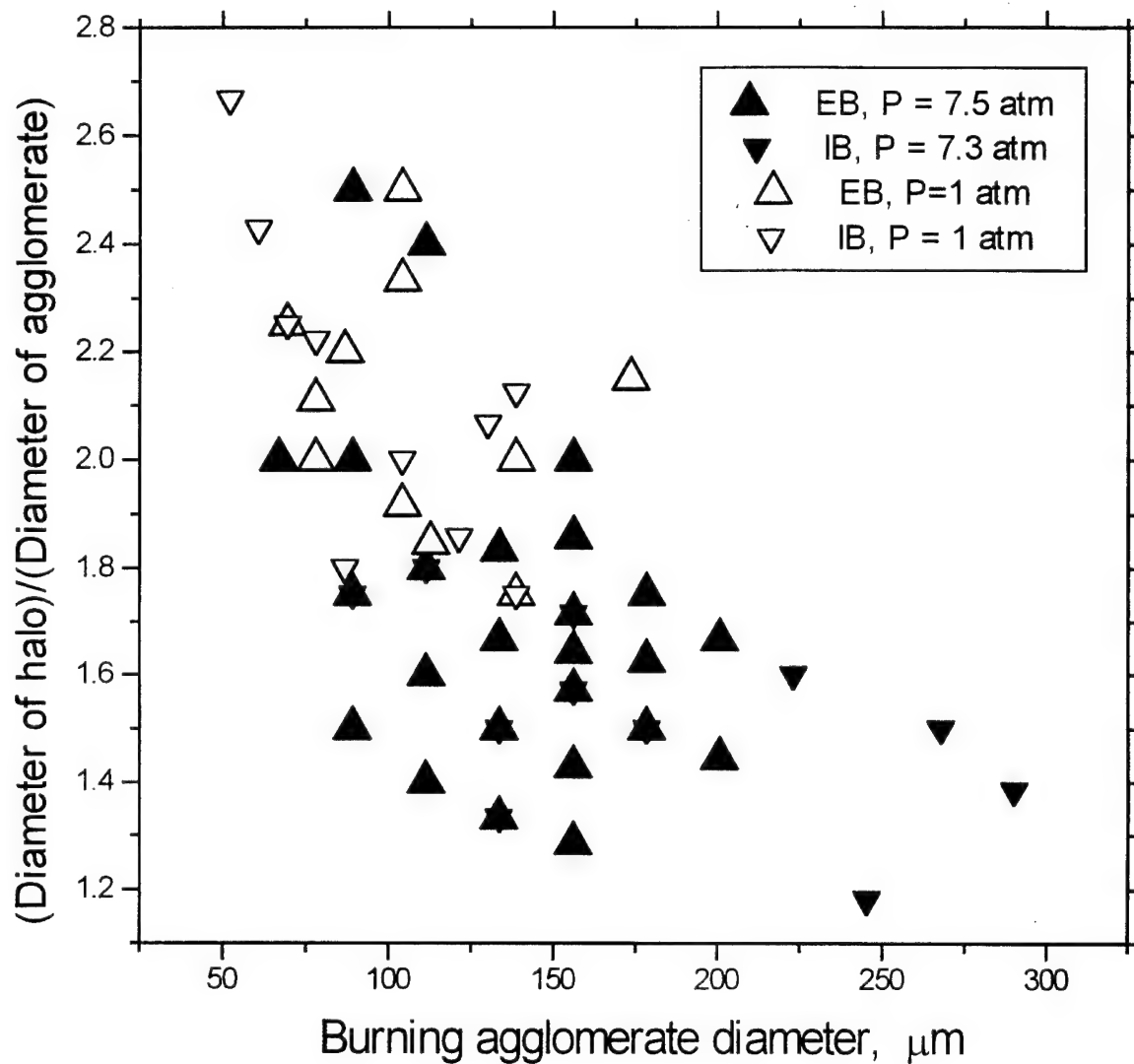Fig. 5.11. Plots of ratio $D_{halo}/D_{particle}$ versus particle diameter for propellants EB and IB at atmospheric and elevated pressure.
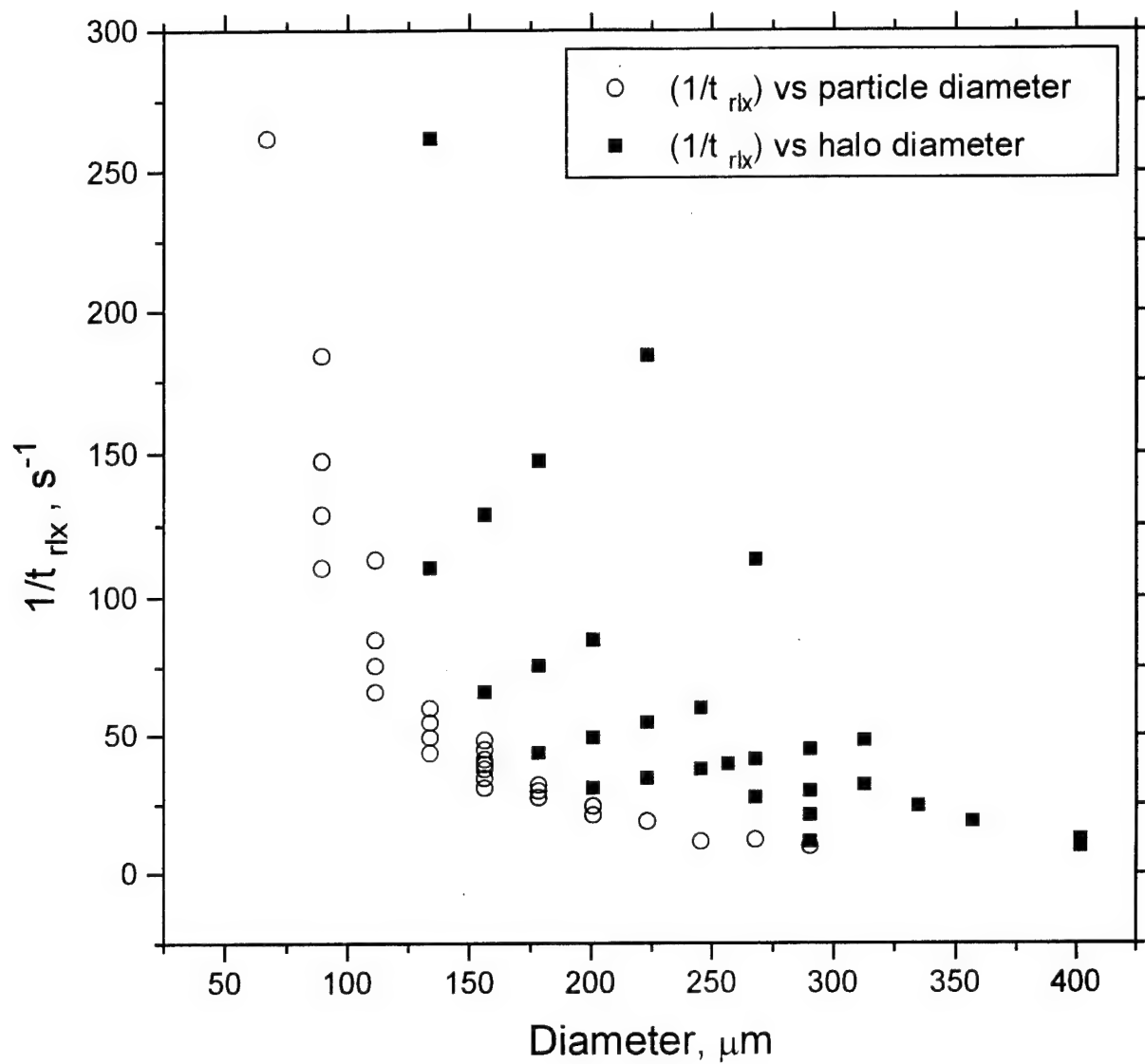
Fig. 5.12.
The value ($1/t_{rlx}$) as a function of particle diameter and halo diameter. Propellant EB, P=7.5 atm.

CONCLUSIONS

The methods of condensed combustion products collection and high speed photography were used in order to reveal difference in combustion behavior of aluminized propellants with inert and energetic binder. The propellants contained the same mass fractions of aluminum and coarse AP that provided very similar geometrical structure. The expected residence time for aluminum particles in subsurface layer and in the flame was also similar due to small difference in burning rates (12 mm/s for propellant IB and 16 mm/s for propellant EB at pressure 43 atm). Nevertheless, according to experimental data the combustion efficiency of aluminum higher and characteristic sizes of agglomerates significantly smaller in case of propellant with energetic binder. For example, at pressure 43 atm we found for propellant EB D_{43} = 190 μm, η = 0.01 and for propellant IB D_{43} = 670 μm, η = 0.25 (η corresponds to fraction of non-consumed aluminum in agglomerates). The difference in combustion behavior manifests itself also in the shape of burning surface. According high speed photography data the roughness of burning surface at 7.5 atm is about 300 μm for propellant EB and about 800 μm for propellant IB. Consequently, characteristic sizes of agglomerates near (above) the burning surface differ: D_{30} = 124 μm (propellant EB) and D_{30} = 220 μm (propellant IB).

Chemical analysis of aluminum content in agglomerates showed that variation of agglomerate size distribution is caused by evolution of oxide particles population in the flame rather than the burn out of aluminum. It can be concluded that for propellants under study the combustion of aluminum ceased at a relatively short distance above the burning surface. Supposedly, high completeness of aluminum combustion for propellant with energetic binder is caused by the deep conversion of aluminum in subsurface layer.

It is interesting to note that, in case of propellant EB, the higher oxide portion in individual agglomerate the higher agglomerate density is. Such correlation does not exist in case of propellant IB. The data of X-ray photography and visual observations show that the agglomerates of the same size may differ significantly in structure and aluminum content. It is a result of different initial structure of agglomerates formed at the burning surface.

Size distribution of fine oxide particles does not depend on pressure and nature of propellant binder (as well as on the size of agglomerates). Mass size distribution of these particles presumably has 3 peaks in the ranges 0.5-1.9 μm, 3-5 μm, and 6.4-8.2 μm. The existence of the listed peaks should be checked further with independent experimental methods. For both propellants mass fraction of fine oxide particles corresponds directly to the amount of aluminum burnt.

Thus, a combination of sampling and high speed photography techniques allows to obtain valuable information on aluminum agglomeration and condensed combustion products behavior in combustion of aluminized propellants. It should be noted that the observed in movies behavior of burning agglomerates correlates well with shadow diameter of particle in flame and does not correlate with "halo" diameter. However, there is no enough experimental data to describe the beginning stage of agglomeration ejection from the surface as well as on metal conversion in subsurface and adjusting to surface zone. Therefore, in the future study it is reasonable to manufacture special model propellants which may generate as uniform as possible agglomerates at the burning surface with well characterized geometry structure and proper ballistic parameters of the propellant.

REFERENCES

1. Price, E. W. (1984), "Combustion of Metalized Propellants", In: *Fundamentals of Solid Propellant Combustion,* Progress in Astronautics and Aeronautics, Vol. 90, pp. 479-514.

2. Frolov, Yu. V., Pokhil, P. F., and Logachev, V. S. (1972), "Ignition and Combustion of Powdered Aluminum in High-Temperature Gaseous Media and in a Composition of Heterogeneous Condensed Systems", *Combustion, Explosion and Shock Waves,* Vol. 8, No. 2.

3. Pokhil, P. F., Logachev, V. S., and Mal'tsev, V. M. (1970), "Coalescence of Metal Particles During the Combustion of Metallized Ballistite Compositions and Fuel-Oxidized Mixtures", *Combustion, Explosion and Shock Waves,* Vol. 6, No. 1.

4. Babuk, V. A., Vasiliev, V. A., Romanov, O. Ya., Maryash, V. I., Tolmachev, G. A. (1993), "Phisico-Chemical Transformation of Al-Al$_2$O$_3$ drops in Active Gas Flux", *Combustion, Explosion and Shock Waves,* Vol. 29, No. 3.

5. Babuk, V. A., Belov, V. P., Khodosov, V. V., and Shelukhin, G. G. (1988), "Study of the Structure of Agglomerates With Combustion of Aluminized Mixed Condensed Systems", *Combustion, Explosion and Shock Waves,* Vol. 24, No. 5.

6. Glotov, O. G., Zyryanov, V. Ya. (1991), "The Effect of Pressure on Characteristics of Condensed Combustion Products of Aluminized Solid Propellant", *Archivum Combustionis,* Vol. 11, No. 3-4, pp. 251-262.

7. Babuk, V. A., Belov, V. P., and Shelukhin, G. G. (1981), "Combustion of Aluminum Particles in Composite Condensed Systems Under Low and High Pressures", *Combustion, Explosion and Shock Waves,* Vol. 17, No. 3.

8. Grigor'ev, V. G., Zarko, V. E., and Kutsenogii, K. P. (1981), "Experimental Investigation of the Agglomeration of Aluminum Particles in Burning Condensed Systems", *Combustion, Explosion and Shock Waves,* Vol. 17, No. 3.

9. Gremyachkin, V. M., Istratov, A. G., Leipunskii, O. I. (1980), "Theory of Metal Particle Combustion". In: *Physical Processes in Combustion and Explosion,* pp. 4-67. Atomizdat Publ., Moscow, USSR (in Russian).

10. Gremyachkin, V. M., Istratov, A. G., Kolesnikov-Svinarev, and al. (1977), In: *Chemical Physics of Combustion and Explosion processes.* The Condensed Systems Combustion. AN SSSR Publ., Chernogolovka. (in Russian).

11. Eisel, J. L., Brown, B. G., and Price, E. W. (1975), "Pressure, Velocity, and Geometry Effect on Al$_2$O$_3$ Produced During Aluminized Propellant Combustion", *AIAA Journal,* Vol. 13, No. 7, pp. 913-917.

12. Caveny, L. H., Gany, A. (1979), "Breakup of Al/Al$_2$O$_3$ Agglomerates in Accelerating Flowfields", *AIAA Journal,* Vol. 17, No. 12, pp. 1368-1371.

13. Kovalev, O. B. (1989), "Physicomathematical Model of the Agglomeration of Aluminum in the Combustion of Mixed Condensed Systems", *Combustion, Explosion and Shock Waves,* Vol. 25, No. 1.

14. Boraas, S. (1984), "Modeling Slag Deposition in the Space Shuttle Rocket motor", *Journal of Spacecraft and Rockets,* Vol. 21, No. 1.

15. Babuk, V. A., Belov, V. P., Khodosov, V. V., and Shelukhin, G. G. (1985), "Investigation of the Agglomeration of Aluminum Particles During the Combustion of Metallized Composite Condensed Systems", *Combustion, Explosion and Shock Waves*, Vol. 21, No. 3.

16. Sambamurthi, J. K., Price, E. W., and Sigman, R. K. (1984), "Aluminum Agglomeration in Solid Propellant Combustion", *AIAA Journal*, Vol. 22, No. 8, pp. 1132-1138.

17. Tai-Kang Liu, Huey-Cherng Perng, Song-Ping Luh, and Fang Liu (1991), "Aluminum Agglomeration in AP/RDX/Al/HTPB Propellant Combustion", *AIAA-91-1870*. 11 p.

18. Kovalev, O. B., Petrov, A. P., and Fol'ts, A.V. (1987), "Simulating Aluminum Powder Aggregation in Mixed Condensed-System Combustion", *Combustion, Explosion and Shock Waves*, Vol. 23, No. 2.

19. Cohen, N. S. (1983), "A Pocket Model for Aluminum Agglomeration in Composite Propellants", *AIAA Journal*, Vol. 21, No. 5, pp. 720-725.

20. Dobbins. R. A., Strand, L., D. (1970), "A Comparison of Two Methods of Measuring Particle Size of Al_2O_3 Produced by a Small Rocket Motor". *AIAA Journal*, No. 9, pp. 1544-1550.

21. Bakhir, L. P., Levashenko G. I. (1973), "The Investigation of the size of alumina drops near the burning surface". *Combustion, Explosion and Shock Waves*, Vol. 9, No. 6.

22. Fedorov, B. N., Plechov, Yu. L., Timokhin E. M. (1982), "Study on Dispersion of Alumina Particles in Products of Combustion of Condensed Substances". *Combustion, Explosion and Shock Waves*, Vol. 18, No. 1.

23. Cofer, W. R., Lala G., G., Wightman, J. P. (1987), "Analysis of Midtropspheric Space Shuttle Exhausted Aluminum Oxide Particles". *Atmospheric Environment*, Vol. 21, No. 5, pp. 1187-1196.

24. Glotov, O. G., and Zyryanov, V. Ya. (1995), "The Condensed Combustion Products of Aluminized Solid Propellants. I. The Method of Quenching at Various Distances from Burning Surface for Studying the Evolution of Particles", *Combustion, Explosion and Shock Waves*, Vol. 31, No. 1.

25. Brooks, K. P., and Beckstead, M. W. (1995), "The Dynamics of Aluminum Combustion", *Journal of Propulsion and Power*, Vol. 11, No. 4, pp. 769-780.

26. Fedotova, T. D., Malachov V. V., Glotov, O. G., Kir'yanova, A. G. (1992), "Permanganatometric Determination of Metallic Aluminum in Condensed Combustion Products", *Siberian Chemical Journal*, No. 2, pp. 37-38 (in Russian).

27. Price, E. W., Sigman, R. K., Park C. J. (1982), "Behavior of Aluminum in Solid Propellant Combustion". *AFOSR-TR-82-0964*.

28. Kudryavtsev, V. M., Sukhov, A. V., Voronetskii, A. V., and Shapara, A. P. (1979), "High-Pressure Combustion of Metals (Three-Zone Model)", *Combustion, Explosion and Shock Waves*, Vol. 15, No. 6.

29. Grigor'ev, V. G., Zarko, V. E., Kutsenogii, K. P., Bobryshev, V. P., and Sakovich, G. V. (1981), "Model for the Agglomeration of Metal Powder in the Combustion of Composite Mixtures", *Doklady Akademii Nauk SSSR*, Vol. 259, No. 4, pp. 881-885. (in Russian).

30. Theory of Turbulent Jets (1984), Moscow, Nauka publ., 716 p.

31. Kraeutle, K. J. (1978), "Particle Size Analysis in Solid Propellant Combustion Research". In: *Experimental Diagnostics in Combustion of Solids*. Progress in Astronautics and Aeronautics Vol. 63, pp. 76-108.

32. Kuo, K. K. (1986), "Principles of Combustion". John & Wiley, Inc. 812 p.

33. Timnat, Y. M. (1987), "Advanced Chemical Rocket Propulsion", Academic Press. Harcourt Brace Jovanovich, Publishers.

34. Pokhil, P. F., Belyaev A. V., Frolov Yu. V., Logachev, V. S., and Korotkov A. I. (1972), "Combustion of Powdered Metals in Active Media", Nauka Publ., Moscow, USSR. (in Russian).

35. Gusachenko, E. I., Fursov, V. P., Shevtsov, V. I., Stesik, L. N., Zhitomirskii, B., M. (1982), "The peculiarities of Agglomerate Formation in Mixed Composition Combustion". In: *Physics of Air-disperse Systems*, Vol. 21, pp. 62-66. High School Publ., Kiev-Odessa. (in Russian).